2021

Understanding the Impact of Solvents in Oral Solid Dosage Formulation and Process Development

Matthew Kyle Defrese
University of Kentucky, matt.defrese@gmail.com
Digital Object Identifier: https://doi.org/10.13023/etd.2021.011

STUDENT AGREEMENT:

I represent that my thesis or dissertation and abstract are my original work. Proper attribution has been given to all outside sources. I understand that I am solely responsible for obtaining any needed copyright permissions. I have obtained needed written permission statement(s) from the owner(s) of each third-party copyrighted matter to be included in my work, allowing electronic distribution (if such use is not permitted by the fair use doctrine) which will be submitted to UKnowledge as Additional File.

I hereby grant to The University of Kentucky and its agents the irrevocable, non-exclusive, and royalty-free license to archive and make accessible my work in whole or in part in all forms of media, now or hereafter known. I agree that the document mentioned above may be made available immediately for worldwide access unless an embargo applies.

I retain all other ownership rights to the copyright of my work. I also retain the right to use in future works (such as articles or books) all or part of my work. I understand that I am free to register the copyright to my work.

REVIEW, APPROVAL AND ACCEPTANCE

The document mentioned above has been reviewed and accepted by the student's advisor, on behalf of the advisory committee, and by the Director of Graduate Studies (DGS), on behalf of the program; we verify that this is the final, approved version of the student's thesis including all changes required by the advisory committee. The undersigned agree to abide by the statements above.

Matthew Kyle Defrese, Student

Dr. Patrick Marsac, Major Professor

Dr. David Feola, Director of Graduate Studies

UNDERSTANDING THE IMPACT OF SOLVENTS IN ORAL SOLID DOSAGE FORMULATION AND PROCESS DEVELOPMENT

DISSERTATION

A dissertation submitted in partial fulfillment of the
requirements for the degree of Doctor of Philosophy in the
College of Pharmacy
at the University of Kentucky

By

Matthew Kyle Defrese

Lexington, Kentucky

Co- Directors: Dr. Patrick Marsac, Associate Professor of Pharmaceutical Sciences

and Dr. Younsoo Bae, Associate Professor of Pharmaceutical Sciences

Lexington, Kentucky

ABSTRACT OF DISSERTATION

UNDERSTANDING THE IMPACT OF SOLVENTS IN ORAL SOLID DOSAGE FORMULATION AND PROCESS DEVELOPMENT

The successful delivery of chemical compounds for the purpose of therapeutic treatments and prophylactics is a substantial undertaking in modern drug development. Notably, the adoption of high throughput screening techniques has led to the proliferation of poorly water soluble and/or highly potent molecules which further complicate development activities. Spray dried amorphous solid dispersions are an increasingly important formulation strategy to overcome solubility issues while wet granulation approaches are the method of choice for the preparation of highly potent APIs in oral solid dosage forms.

A common connection between these critical techniques is their reliance on solvent-based processing that can often result in unexpected outcomes on product quality and performance. Solvent choice has been shown to influence API form, habit, stabilizing interactions, and physical and chemical properties of drug product intermediates, which requires greater understanding. The objective of this dissertation is to provide a general overview and assessment of the role of solvents in the important methods of spray dried dispersions (SDDs) and highly potent compounds by wet shear granulations (HP-WSG) to address concerns related to poorly soluble and/or highly potent APIs.

Light scattering (LS) and dilute solution viscometry (DSV) techniques have been utilized to assess critical drug-polymer-solvent interactions in the solution state and explore the mechanisms by which solvent choice may influence SDD physical stability. Next, solid-state characterization techniques were leveraged to understand how the interplay between wet granulation processing parameters, API physical form, and environmental moisture may dictate chemical stability issues of a highly potent API. Conclusions and future work are presented with next steps that can be pursued in expanding our knowledge of complex multi-component solutions which are frequently encountered in pharmaceutical development.

KEYWORDS: spray dried dispersions, wet granulation, light scattering, rheometry, solvent processing, drug product development

Matthew Kyle Defrese

01/31/2021

UNDERSTANDING THE IMPACT OF SOLVENTS IN ORAL SOLID DOSAGE FORMULATION AND PROCESS DEVELOPMENT

By
Matthew Kyle Defrese

Dr. Patrick Marsac
Co-Director of Dissertation

Dr. Younsoo Bae
Co-Director of Dissertation

Dr. David Feola
Director of Graduate Studies

01/31/2021
Date

ACKNOWLEDGMENTS

There has been a multitude of people that have helped me throughout my graduate career that I greatly appreciate - from my mentors such as Dr. Mary Murray and Dr. Vikas Moolchandani who encouraged my interests towards graduate school, to the friends and family who have supported me throughout my journey.

My committee has been exceptionally helpful in their guidance; especially towards the end of my graduate studies in the face of the COVID-19 pandemic which added considerable uncertainty on how best to wrap up my studies. Dr. Pack was a great instructor during my graduate courses and challenged my fundamentals during my qualifying exams. This provided a strong appreciation for the difficulty in understanding phase change processes during solvent removal from drug products. Dr. Dziubla was kind enough to cut my teeth rotating through his lab early in my graduate career, while I was still learning the basic laboratory skills necessary to be useful. Likewise, he was a helpful and encouraging advisor during my tenure as an officer of the local ISPE student chapter. Dr. Munson was a steady and reliable voice who helped me from the beginning to the end of my studies, even though he left the university long before I defended. Initially, Dr. Munson was my initial motivation for applying to the College of Pharmacy at the University of Kentucky and I am very grateful for his support and during my time at UKY. Dr. Bae was a tremendous help in rigorously challenging me to explore my research in a new light and to ensure I was taking a well-defined path in addressing the problems I sought to solve. I am very thankful for how freely he allowed me to utilize his lab's light scattering equipment support of my research. I have left this experience with a profound appreciation and love for the experimental value of light scattering in understanding complex phenomena in multi-component solution state systems.

Lastly, I must express my appreciation for Dr. Patrick Marsac as my lead PI during this experience. He granted me the intellectual freedom and independence to pursue the questions that I held dear and trusted me to use these resources wisely. At heart I still find myself to have the inclinations of an engineer to tinker and play with toys, and the ability to engage and learn with the various processing technologies in the Marsac lab has been one of the most fulfilling experiences of my life, for which I am continuously grateful.

I would be remiss to not also acknowledge my graduate instructors, most especially Dr. John Anthony in the UKY Chemistry department and Dr. Brad Anderson from the College of Pharmacy. Dr. Anthony was by far the best organic chemistry teacher I have had the pleasure to learn from and I treasure the experiences I had in his class. Dr. Anderson demonstrated the high scientific ideals that I seek to fulfill in my own career. His values of scientific honesty, rigor, and depth of understanding have helped to shape me as a scientist in a way that I can only hope to justify. I greatly enjoyed our many discussions and will miss his friendship and guidance.

Support from the staff at the College of Pharmacy - specifically Catina Rossoll and Kristi Moore - was exceptional. Catina is a caring and helpful person without whom many a grad student would not have made it - I am no exception. Kristi keeps our labs running

safe and effective, like a well-oiled machine. I appreciate all her help and guidance throughout my time at the college. I also would like to thank Dr. Joe Chappell, our Chair of the Pharmaceutical Sciences department, as he helped our lab through these uncertain times with grace and understanding.

My lab mates deserve a medal for their patience and support during our time together in the Marsac lab. My time with Freddy Arce, Travis Jarrells, and Heather Campbell was an absolute privilege and I am excited to see where their futures will take them. They are each quality scientists who are sure to have an impact. I am proud to have worked with them and call them friends; I wish them the best in all their endeavors. Of course, I must also thank my good friend, Dr. Fahd Eisa, who was as kind and encouraging as anyone could be. I miss working with him in the lab, as he always made the day a great pleasure to be there. I must also express my appreciation for my time working with Dr. Amin Abedini and Amir Najarzadeh; I believe there is a bright future ahead for both of them. Much of the work in this dissertation was supported by an almost-army of undergraduates - though I must express my greatest thanks to Matthew Farmer, Yuhan Long, and Lucas Timmerman. Their efforts and eager attitudes kept me focused on getting the job done. I am indebted to each of them and I hope I was able to impart some value and learning to them as well.

Most importantly, I must thank and acknowledge my wife, Victoria Defrese, for her continuous support, patience, motivation, organization, planning, and `mad' technical skills that helped carry me across the finish line. Vicki and I had the unusual opportunity as husband and wife to work together in the lab, for which I am exceedingly grateful. Despite my initial trepidation, it was easily one of the best experiences of my life and I would trade it for nothing. The quality of her work was impressive and pushed me to do better in my own efforts, growing me into a better scientist in addition to all the other ways in my life in which she has made me a better person. My gratitude and love for her has no bounds.

Finally, good reader - my thanks to you! For rare is the dissertation that is read by anyone other than the author and their committee (sometimes). I hope the work in here may serve you well and should the need or desire ever arise, please reach out with any questions.

TABLE OF CONTENTS

LIST OF TABLES

LIST OF FIGURES

CHAPTER 1: CHALLENGES IN MODERN DRUG PRODUCT DEVELOPMENT

1.1 Making Molecules into Medicine

The successful delivery of chemical compounds for the purpose of therapeutic treatments and prophylactics is a substantial undertaking in modern drug development. In order to achieve the desired quality, safety, and efficacy of drug products, a variety of critical objectives must be met - including sufficient chemical and physical stability, manufactureability, patient acceptance and compliance, and the satisfaction of quality and regulatory requirements. The task of making molecules into medicines requires an extensive understanding and marriage of the target bio-performance metrics, material properties of the drug and functional excipients, as well as the processes by which these products are manufactured. Traditional approaches of simple drug-in-capsule formulations have increasingly become the exception rather than the rule. Development scientists are now expected to leverage an ever expanding toolbox of fundamental chemistry and materials science knowledge, techniques, and instrumentation in the design of pharmaceutical dosage forms.

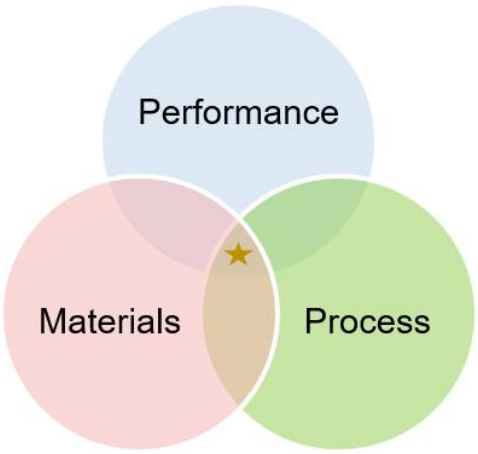

Figure 1.1: A successful drug product must fall within the overlap of formulation material properties, process capabilities, and performance requirements.

Notably, the adoption of high throughput screening techniques has led to the proliferation of poorly water soluble [1, 2, 3] and/or highly potent molecules [4, 5, 6, 7] which further complicate development activities. Approximately 90% of new chemical entities in the drug candidate pipeline are estimated to meet the criteria of the bio-pharmaceutical classification system (BCS) for poor aqueous solubility and/or permeability (Class II & IV compounds) [8]. While 20-30% of solubility issues might be addressed through screening for suitable salt forms or polymorphs [9], the majority of these compounds will require more advanced approaches to improve bioavailability. There are many enabling formulations techniques that can address these concerns, including cyclodextrins, self-microemulsifying drug delivery systems (SMEDDs), liposomes, micelles, co-crystals, and more - though one of the most effective and flourishing strategies is that of amorphous solid dispersions (ASDs) [10]. The unique solid state properties of ASDs provide enhanced dissolution rates, solubility, and permeability [11] which have made them an attractive option in the pursuit of increased bioavailability for BCS class II and IV molecules.

The formulation of highly potent molecules bring its own concerns and risks with

respect to ensuring product safety and efficacy. High potencies require much smaller dosages compared to conventional drug products, with low dosage forms typically considered to be those below 1 mg - though they may be as minor as 10-25 μg, as in the examples of levothyroxine [12] or Vitamin D. In these cases, the amount of excipients greatly exceeds that of the active pharmaceutical ingredient (API) which results in drug concentrations as low as 0.01% (w/w). Such minute amounts of drug substance can add substantial complexity to formulation and process development, including: difficulty in ensuring content uniformity of both drug product intermediates (DPIs) and dosage forms, low API recovery due to losses in manufacturing, and chemical instability which may be attributable to a range of sources such as increased relative surface exposure, physical transformations, and/or high ratios of excipient to drug amounts that may increase the likelihood of incompatibility [7]. Additional obstacles often present themselves in analytical development as it can be difficult to develop robust methods for the characterization of trace drug substance, impurities, physical form, and degradation products due to complexity in extraction from DPIs and dosage forms, maintaining drug stability during sample preparation, and the need to enhance method sensitivities [7].

In order to meet the challenges of these poorly water soluble and/or highly potent molecules, specialized formulation, process, and analytical strategies are often utilized to ensure successful product development. Spray dry processing has emerged as the leading processing method for the preparation of BCS class II/IV drugs as ASDs at commercial scale. This technique allows for the production of stable drug intermediates with readily tunable properties to facilitate ease of downstream processing. Wet shear granulation (WSG) is one of the oldest and best understood techniques in industrial pharmacy [13] and is considered the process of choice for dosage forms containing highly potent APIs (HP-API) [7]. This approach not only allows for the precise control of particle properties to aid downstream processing, but also provides a mechanism to ensure the uniform distribution of trace amounts of HP-APIs

throughout the formulation. Additionally, WSG helps to reduce worker exposure to potentially toxic materials during production through the minimization of dust generation compared to alternatives such as dry granulation techniques [7]. While spray drying and wet granulations are very distinct and disparate processes - one key aspect that they share in common, is the need for solvents during processing.

Solvents are essential and ubiquitous materials in pharmaceutical development and manufacturing practices, and are extensively utilized from early stage active pharmaceutical ingredient (API) synthesis and purification, to mid-stage intermediate processing such as spray drying and wet granulation, and late stage tablet coating processes. Generally, the role of solvents in mid-late stage processing has been under investigated in the pharmaceutical community, though there has been a growing awareness of the need to better understand their effects on both DPIs and drug products as more complex molecules and manufacturing methods have become more numerous. For example, solvent selection has been found to exhibit profound influence on API form, physical and chemical stability, particle size, porosity, uniformity, density and friability, flowability, compressibility, and dissolution performance of both SDD [14, 15, 16, 17, 18, 19, 20, 21, 22] and WSG [23, 24, 25, 7, 26, 27, 28, 29] products. The major complication in the interrogation of solvents in SDD and WSG formulation and processing is that these systems typically consist of several different materials, making it difficult to parse the mechanisms and interactions which govern product outcomes.

1.2 Spray Drying (SD)

Note: Much of this section is a modified reproduction of a portion of the paper by Defrese et al. (2020) [30], reproduced with permission.

The invention of the spray dryer can be traced to Samuel Percy and US patent US125406A, which was granted in 1872 [31]. While there have been many improvements to spray drying in the past 150 years, the fundamentals of this method have not

substantially changed. In brief, spray dry processing begins with the introduction of a liquid feed containing dissolved solids into the primary drying chamber. This liquid is then atomized into a fine spray of small droplets to provide a high surface area to volume ratio to facilitate a majority of solvent removal on the order of microseconds [32, 33]. Co-current hot process gas evaporates the carrier solvent which leads to subsequent particle solidification as the spray dried product.

These solid particles are then separated from the process gas stream through the use of gas-solid cyclone separator(s) which leverages differences in the centrifugal force experienced between the solid particles and gas due to variances in material densities. This effect causes the solids to separate from the gas stream and fall out the bottom of the cylcone for collection as the finished product. A bag filter is generally necessary after the cyclone(s) to collect residual 'fine' powders that are often prevalent in spray dry processing and difficult to separate by centrifugal force alone. Often, additional secondary drying of the collected product is required as significant amounts of residual solvents will remain. The filtered process gas stream is then either vented to the atmosphere (open-loop) or recirculated as needed to recover spent solvent and reconditioning of the process gas stream for continuous processing (closed-loop).

Though this process appears fairly straightforward on the surface, there are many process and formulation parameters that can exert substantial impact on the properties of the spray dried product that often requires extensive experimentation to understand and control [32, 33, 34, 35, 36, 37].

Atomization

The atomization process is an important step in spray drying, as the droplets generated can directly influence critical properties of the finished particles including size, shape, morphology, and uniformity [33, 38, 39]). There are four primary spray technologies that are utilized in pharmaceutical spray drying: rotary disc atomizers, pressure nozzles, bi-fluid (also known as pneumatic) nozzles, and ultrasonic nozzles.

Regardless of the atomization apparatus, all are impacted by the liquid feed physical properties (i.e. density, viscosity, surface tension, and solids concentration), though performance sensitivity to these factors may differ greatly.

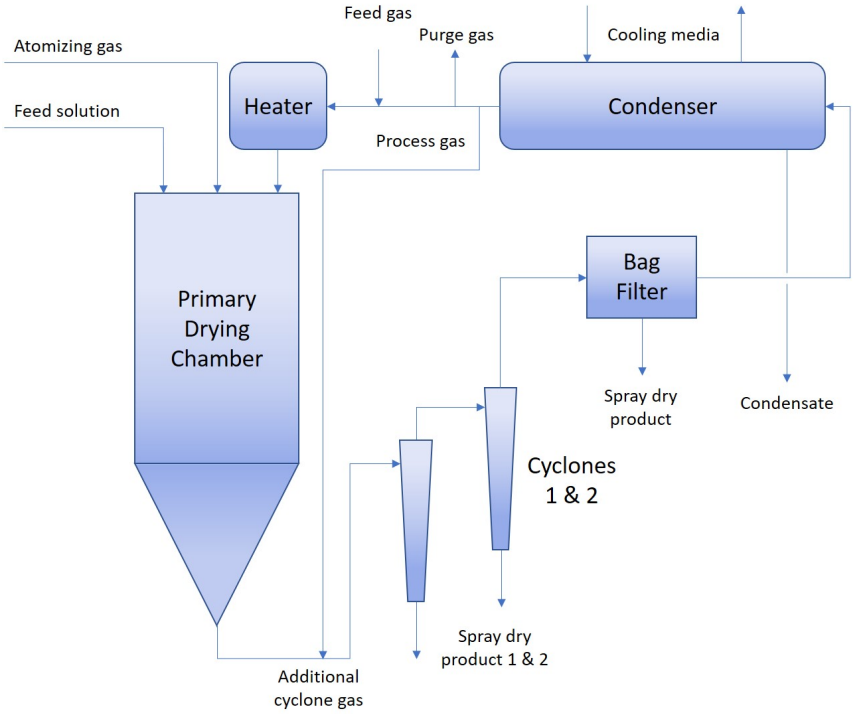

Figure 1.2: Schematic of a closed-loop spray drying process and equipment. Cyclone(s) may be used in series to help increase efficiency of particle separation and yields of finer particulates, though most commonly only one cyclone is used.

Rotary disc and pressure nozzle atomizers are generally restricted to use in commercial scale equipment due to processing realities that make these styles poorly suited for smaller instruments. Atomization via rotary discs is achieved by the introduction of a liquid feed to the center of a rapidly spinning disc at speeds in the range of 5,000 - 60,000 RPM (tip speeds of 100-200 m/s), causing the liquid to flow outward and breakup radially [40]. This necessitates the use of a large diameter chamber - otherwise a substantial amount of product may be lost due to deposition on the side walls of the equipment [41]. Rotary discs can produce a range of droplet sizes from 20-200 μm with a somewhat broad droplet distribution [42]. For pressure nozzles, atomization is produced by the tangential introduction of the liquid feed under high

pressures (typically 180-220 bar, up to a maximum of 450 bar), which generates turbulence within the nozzle head before vertically exiting through a narrow orifice as breakup begins due to capillary instability [40, 43]. Primary limitations of pressure nozzles are that the minimum required liquid mass flow rates are in excess of 5 kg/hr, which are incompatible with early stage development. Additionally, it is not possible to independently adjust the droplet size without changing the liquid feed flow rates - otherwise an alternate nozzle design is needed [39]. A key benefit of pressure nozzles is that they are able to produce droplet sizes ranging from 30-200 μm with more narrow distributions than those produced by both rotary discs and pneumatic nozzles [42].

At laboratory and pilot scales, bi-fluid and ultrasonic nozzles are the atomizers of choice. Bi-fluid nozzles, whereby pressurized air causes the breakup of the liquid feed into droplets, consist of two major configurations - external mixing nozzles which are the most commonly utilized, and internal mixing nozzles. For external mixing nozzles the air is introduced to the liquid feed after it has exited the nozzle, while for internal mixing designs, the air and liquid mix prior to exiting the nozzle orifice. Internal mixing nozzles have a more efficient atomization process which allows for a reduction in the required gas-liquid flow ratios to produce a target droplet size. This allows them to be better suited for greater throughput than the external mixing nozzles, though they are comparably more sensitive to changes in feed viscosity [39]. Both pneumatic styles are considered to be among the best options as they allow for simple direct control of droplet size by adjustment of the air pressure independently of the liquid feed [40]. However, these nozzles tend to produce both finer droplets (range of 5-75 μm) with less uniform distributions which can negatively impact downstream processing [39]. Ultrasonic nozzles leverage high frequency acoustic waves to produce very narrow droplet size distributions in the range of 20-100 μm, where higher frequencies produce smaller droplets [40]. Regrettably, each ultrasonic nozzle is limited to a single frequency which adds difficulty in exploring a wide range of droplet sizes

and in general have low throughput which currently restricts their use to small scales.

Evaporation & Particle Formation

As the atomization process completes and the fluid is converted to droplets, solvent evaporation and the liquid-solid phase transformation begins to take place. In most cases, except when spraying strong crystallizers, the evaporation rates are sufficiently high to produce amorphous materials due to the rapid vitrification and loss of mobility as the solvent is removed. Regardless, the particle formation process is highly complex and requires an understanding and control of the radial distribution of solution components within the drying droplet to ensure desired particle properties [33]. The radial composition during the drying process can be affected by a number of phenomena, though the most frequently considered are that of the surfactant activity of solutes [18, 44] and the Peclet effect, i.e. surface enrichment caused by the rapid reduction of the droplet radius with solvent evaporation occurring at rates much greater than solutes can diffuse to the center of the droplet [38].

Of these, the Peclet effect or number (Pe_i) for solute i, is most sensitive to the evaporation process and is a function of the solvent evaporation rate (κ) relative to the solute diffusivity (D_i) [33]:

$$Pe_i = \frac{\kappa}{8D_i} \tag{1.1}$$

Often the evaporation rate is approximated to be constant, which allows the lifetime of the droplet to be expressed as:

$$d^2(t) = d_0^2 - \kappa t \tag{1.2}$$

Where $d^2(t)$ is the droplet surface area as a function of time, d_0^2 the initial droplet surface area, and t is the drying time of the droplet. A simple rearrangement can then allow for an estimate of the required droplet drying time (τ_D) by setting $d^2(t) = 0$ and solving for time:

$$\tau_D = \frac{d_0^2}{\kappa} \tag{1.3}$$

Ideally, this value will be smaller than the residence time of the droplets in the dryer, which is generally estimated from the volume of the drying chamber and process gas flow rate, in order to ensure sufficiently low residual solvent content in the finished particles [45]. With knowledge of the evaporation rate and solute diffusivity, the extent of surface enrichment can be approximated with an accuracy of ± 1% by the following:

$$E_i = \frac{c_{s,i}}{c_{m,i}} = 1 + \frac{Pe_i}{5} + \frac{Pe_i^2}{100} - \frac{Pe_i^3}{4000} \tag{1.4}$$

Where E_i is the surface concentration of i ($c_{s,i}$) relative to the average concentration in the droplet ($c_{m,i}$). Knowledge of solute diffusivities can either be measured experimentally by methods such as dynamic light scattering, or modeled by appropriate methods [46]. Evaporation rates are primarily driven by the difference in solvent partial pressure at the surface of the droplet (Y_s) at the equilibrium temperature (T_e) relative to the partial pressure in the processing gas (Y_∞) and can be approximated by the following expression:

$$\kappa = 8D_g \frac{\rho_g}{\rho_l}(Y_s(T_e) - Y_\infty) \tag{1.5}$$

Where D_g is the diffusivity of the solvent in the gas phase, while ρ_g and ρ_l are the gas and liquid phase densities, respectively. This relationship is a good approximation as long as the droplet temperatures are much lower than the boiling point of the solvent, otherwise additional complexity will be introduced [33]. For a given feed solution, the primary mechanisms to control enrichment and particle morphology via the Peclet effect is by manipulation of evaporation rates through the adjustment of droplet size and processing gas temperature. Generally, dense, solid particles can be achieved with slower evaporation rates while light and hollow particles are formed at faster evaporation rates as the solutes are kinetically enriched at the surface (figure 1.3)

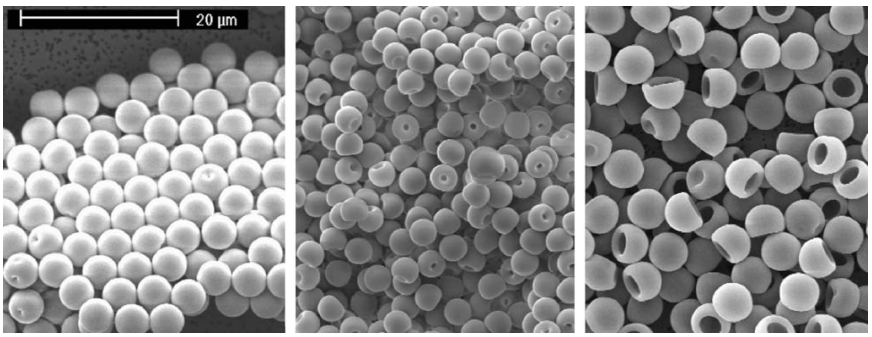

Figure 1.3: Morphology of mono-disperse glyco-protein particles produced at drying temperatures of 25, 50, and 125 °C, from left to right, corresponding to Peclet numbers of 2.7, 5.6, and 16.8;Reproduced with permission from [33].

Key considerations across production scales are the difference in evaporation capacities and residence times due to the size of equipment. The process gas flow rates control the relative rate of solvent that can be evaporated, assuming the same temperature and atomization conditions. Larger spray dryers are supported by larger air handler systems in order to support greater product throughput. Additionally, the larger drying chamber volumes relative to process gas flow rates can increase the residence time to facilitate enhanced solvent removal, which is desirable to potentially reduce the need for, or extent of, secondary drying processes. At all scales, common challenges include low yields arising from material deposition on the equipment sidewalls and/or insufficient solvent removal resulting in 'sticky' product at the chamber outlet. An understanding of material glass transition temperatures, residual solvent content, and target outlet temperatures are needed to prevent and control these complications.

Solids Separation

After exiting the drying chamber, the process gas containing the solid particles will then pass through a cyclone(s) and bag filter for removal and collection of the dried product. There are relatively few cyclone designs, with the most common being that of the Stairmand centrifugal cyclone with a geometrical ratio of the cone length to diameter of 4:1 [45]. Electrostatic particle separators are an emerging technology

which collect the solids from laminar process gas flow using an electric field generated along the side walls of the separator with high efficiencies ≥85 [47], though the fundamental operations are poorly understood and have not yet been scaled up to pilot and commercial scale applications [45].

For the Stairmand design, the particles are separated by the larger centrifugal forces experienced relative to the gas phase due to the presence of a vortex formed by the process gas within the cyclone. The larger, denser particles are separated most easily near the top of the cyclone and will fall out of the vortex along the boundary wall into the collection vessel due to gravity. Smaller, lighter particles are more likely to be retained within the vortex and will not separate until lower in the cyclone where the gas speeds are greater; or if sufficiently small, these fine particulates may stay entrained and exit the cylcone in the gas stream for separation at later stages (i.e. cyclone(s) &/or bag filters in series) or represent loss in yield for the remaining solids which are irrecoverable. An understanding of the separation process is necessary to ensure adequate yields which can be particularly important at laboratory and pilot scales where smaller size particles are often generated and result in reduced separation efficiencies. Differences in separation efficiency across scale can also cause varying product characteristics, as different ranges of the particle distribution may be collected based on cyclone designs and process conditions - even when the same particle distribution is able to be produced at all scales. The key parameters for cyclone performance are the pressure drop (ΔP_t) across the cyclone inlet and outlet (as captured by Euler's (Eu) number), and the collection efficiency (η) which is a function of the process gas properties (as captured by Reynold's (Re) number), and particle properties (as captured by Stokes' (St) number) [45]:

$$Eu = \frac{\Delta P_t}{0.5\rho_g \nu_i^2}, \qquad \eta = f(Re, St), \quad \text{where} \begin{cases} Re = \frac{\rho_g \nu_i d_i}{\mu_g} \\ \\ St = \frac{(\rho_p - \rho_g) d_p^2 \nu_i}{18 \mu_g d} \end{cases} \tag{1.6}$$

Where ρ_g is the gas density, ν_i the inlet gas velocity, d_i the cyclone inlet diameter, μ_g the gas dynamic viscosity, ρ_p the mean particle density, d_p the mean size particle diameter, and d the cyclone diameter. In general, increasing the Stokes' number up to 0.01 by reducing the cyclone diameter can improve efficiency while a more complex, process specific and non-linear relationship exists with respect to Re[45]. Optimization of solids separation and cyclone efficiency for spray dry processing is a growing area of interest. Recent work by Poozesh et al. includes the design of a multi-bin centrifugal cyclone for improved collection efficiency as well as partitioning the collected product by size according to the cyclone bins [48]. This valuable contribution provides the means to partition product by size during the powder collection event to allow for a better understanding of the drying and separation processes as a whole in support of continued improvement of spray drying processes.

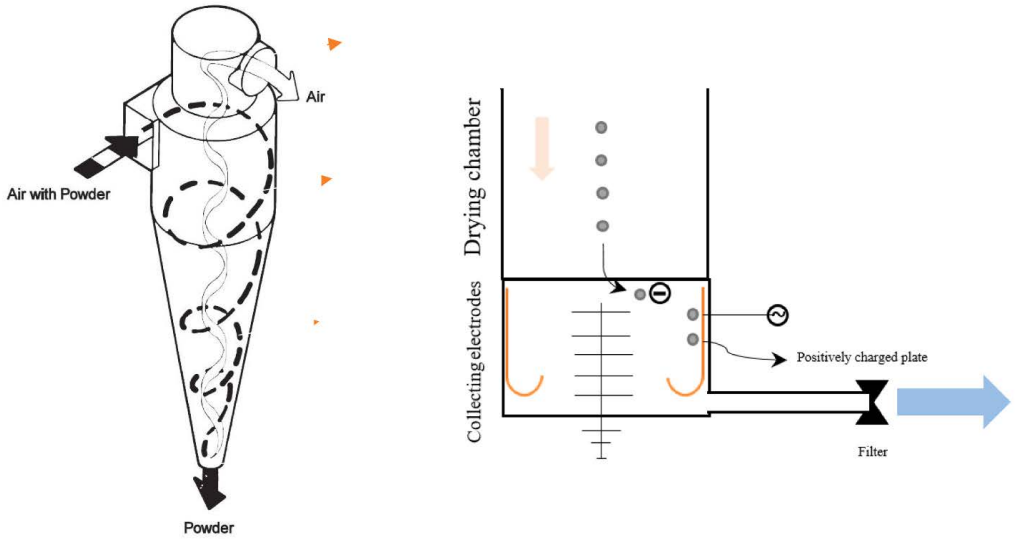

Figure 1.4: Two cyclones utilized in spray dry processing for the separation of particles from the processing gas steam. Left: Stairnmand or Vortex Cyclone; Right: Electrostatic Separator. Reproduced with permission from [45]

Secondary Drying

Secondary drying processes are usually required post spray drying due to relatively high residual solvents content. Residual solvent content is limited for safety and environmental reasons per International Council for Harmonization (ICH) guidance for industry *Q3C Impurities*: *Residual Solvents* with guidelines established for class 1, 2, and 3 solvents respectively. Class 1 solvents should be avoided at all costs in the pharmaceutical industry due to a high degree of toxicity and/or environmental hazard concerns. Class 2 solvents encompass those organic solvents which are suitable for use but should be limited when possible and must be carefully controlled and reduced to acceptable limits in the final drug product. For spray drying applications methanol, tetrahydrofuran (THF), and dichloromethane (DCM) are the class 2 solvents of greatest interest, with permitted daily exposure (PDE) limits of 30.0, 7.2, and 6.0 mg/day (or product concentrations of 3,000, 720, and 600 ppm), respectively. Lastly, there are the class 3 solvents which exhibit less toxicity with lower risks to human health such that no hazards are expected to be present from typical levels found in pharmaceuticals. These solvents should be limited by GMP or other quality-based requirements to PDE limits of 50 mg/day (corresponding to 5,000 ppm / 0.5% w/w) with additional strong justification should these targets not be realistically achievable. The solvents most applicable to spray drying in this class include acetone, most short chain alcohols (excluding methanol), acetic acid, methyl and ethyl acetates [34]. Water is also frequently utilized, especially in mixtures with miscible solvents to achieve the desired solubility of formulation excipients and API for spray drying efficiency and control of desired particle properties [34].

Spray dried powders tend to retain residual solvents of approximately 1-10 % w/w which necessitates additional solvent removal through a secondary drying process. Vacuum tray and fluid bed drying are the most common methods to reduce solvent content to acceptable levels. Notably, as novel APIs are increasingly poorly soluble 'grease-balls' or 'rocks;' stronger solvents may often be required for spray drying. As a

consequence, residual solvents may have very low acceptable limits per ICH guidelines and the secondary drying process may require exceedingly long times in tray drying or risk excess exposure of thermally labile products to heat in fluid bed granulation to reach target levels. Humid and/or solvent-assisted drying is a growing area of interest to address these complications. In assisted drying techniques, process gas is fed to the drying unit with varying levels of humidity and/or assisting solvent (typically methanol) to help remove less desirable residual solvents. The mechanism behind this approach is due to the plasticization effect that residual solvents have on glassy materials that are produced by spray dry processing - this plasticity increase the mobility and free volume of these materials which likewise increases the diffusion rate of the residual solvent, allowing it to more rapidly escape the particles in comparison to dry air or vacuum [49].

1.3 Spray Dried Dispersions (SDDs)

This section is a modified reproduction of a portion of the paper by Defrese et al. (2020) [30], reproduced with permission.

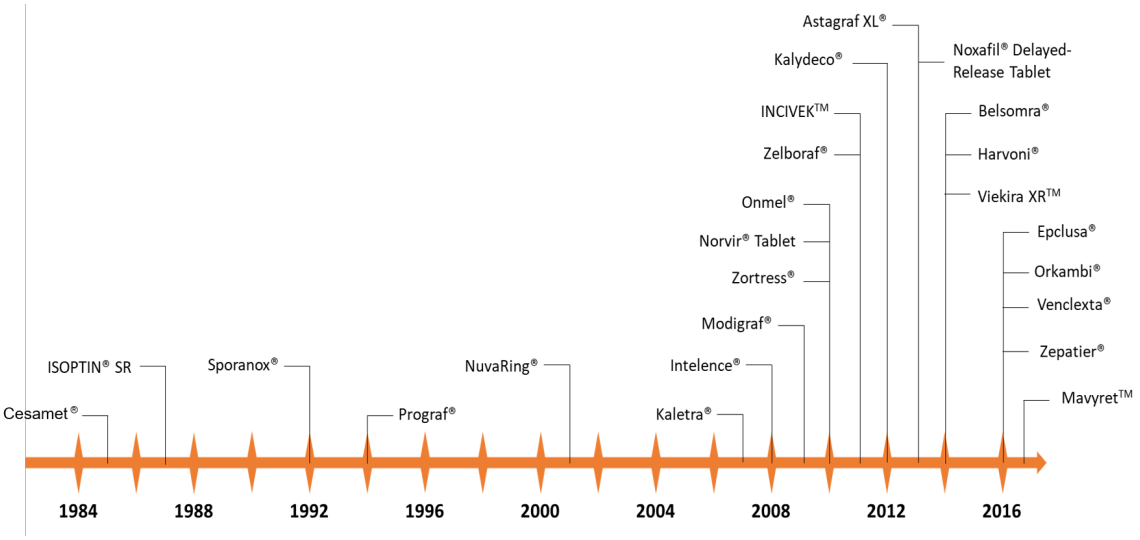

Figure 1.5: The increasing utilization of ASDs in FDA approved drug products in recent years. Reproduced with permission from [10]

As can be seen by the striking growth of FDA approved products since the turn of the century in figure 1.5, ASDs have become one of the most important and widely employed formulation strategies to address the insufficient bio-availability of poorly water soluble compounds [10]. They are manufactured by either melt or solvent-based techniques [35] to create uniform intimate mixtures between the drug and polymer. Of the various methods, spray drying is among the most popular at commercial scale owing to its economic feasibility, compatibility with thermally labile materials, and its ability to readily control desirable product attributes such as particle size, porosity, and wettability in comparison to alternatives such as hot melt extrusion [35]. In their simplest presentation, ASD intermediates typically consist of an amorphous drug incorporated into a homogeneous single-phase molecular dispersion within a polymeric carrier. In SDDs, this amorphous form is generated due to the rapid removal of solvent which preserves the isotropic disordered packing of the liquid state due to the loss of mobility from exponentially increasing viscosity experienced by the drug and polymer during the drying process as the glass transition temperature is approached. This produces a high energy metastable glassy state which increases the drug solubility 2-70 fold [11] relative to the crystal form by reduction of the energy barrier to dissolution through disruption of the crystal lattice [50, 51, 52].

Thermal History in Glasses

Notably, glasses are kinetically sensitive materials which are known to retain a 'thermal history' as the preserved molecular structure mirrors that of the starting conditions of the quench or drying process, with the glassy material exhibiting more similar characteristics of the liquid state as the quench rate is increased [53]. This can be understood with an enthalpy-temperature diagram demonstrating the potential glassy phase behaviors of an otherwise stable crystalline molecule at varying quench rates or exposure to annealing temperatures per figure 1.6a. At sufficiently rapid quenching rates, a liquid is unable to successfully re-orient its molecular packing to allow for

crystallization prior to the onset of vitrification as the glass transition temperature is approached. The quench rate reflects the initial disorder of the liquid state, where faster rates form amorphous phases that are less dense and more disordered (glass 1), whereas slower rates allow greater time for reorganization and densification resulting in a lower energy form (glass 2). This kinetic sensitivity is a key point - it suggests that the molecular interactions present in the solution and/or molten states must be closely related to those retained in the solid-state - and they are most similar for those conditions which provide the most rapid of vitrification processes. This has important and practical applications in understanding how solution state interactions may be tunable for the optimization of SDD properties, which will be explored in later chapters.

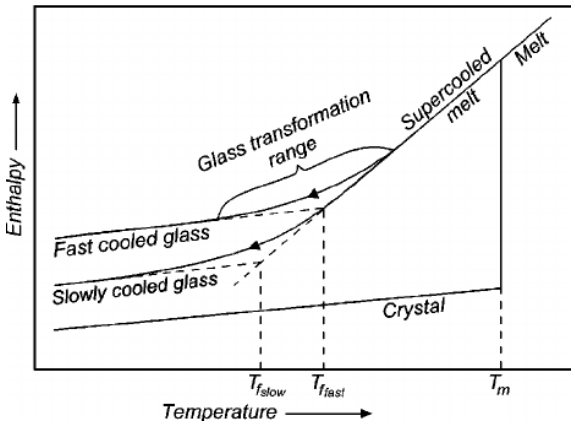

(a) Enthalpy-Temperature Diagram with glass transformations, reproduced with permission from [53]

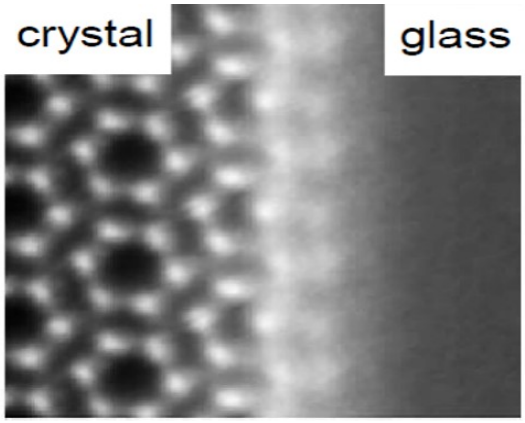

(b) Transmission Electron Microscope image of crystal/glass interface of Si_3N_4, reproduced with permission from [54]

Figure 1.6: Glass transformation & isotropic orientations relative to crystalline form

A natural consequence of producing kinetically restricted glassy materials is that ASDs are inherently in a non-equilibrium state which is undergoing constant relaxations and sampling of the local energy landscape to minimize free energy [55]. Due to the high energy state and chemical potential of the dispersed API, there often exists a thermodynamic driving force for phase separation and/or re-crystallization which can be prevented through sufficient mobility constraints and drug-polymer interactions in

the solid-state [56, 57, 58]. The suppression of these transitions in ASD products has been shown to be critical to the preservation of the desired stability, dissolution, and efficacy performance [59, 60, 61, 62]. Therefore, it is essential to understand and optimize the formation and maintenance of stabilizing drug-polymer interactions throughout the thermal and processing history experienced by these materials.

Impact of Solvents on SDD properties

The impact of solvent choice in SDDs has garnered increasing attention regarding its potential to influence key formulation properties such as homogeneity, physical stability, and dissolution performance [14, 15, 16, 18, 17, 63, 20, 21, 22, 44, 64, 65, 66]. Several rationalizations have been offered to explain solvent effects in SDDs which include changes in droplet size, kinetic effects arising from varying evaporation rates, and thermodynamic processes attributed to drug-polymer-solvent interactions prior to and during the drying event. For common bi-fluid nozzles, droplet size is chiefly determined by the physical properties of the liquid feed (e.g. viscosity, surface tension, and density), the atomizing gas to liquid mass flow rate ratios, and the nozzle size and/or design [67]. As such, any change in solvent will impact dissolution performance due to alterations in the droplet (particle) size when otherwise holding the remaining process parameters constant. This underscores the importance of conducting intrinsic dissolution studies to control for surface area when investigating solvent effects exclusive of their impacts on the atomization process.

Furthermore, different solvents will exhibit a range of volatility and phase behavior with drug and polymer solutes [22]. This can impact the evaporation rate as well as dictate exposure to regions of immiscibility, such as spinodal envelopes (i.e. the onset of spontaneous phase separation), that may be experienced during the solvent removal process. The rate of phase separation in the spinodal region is typically understood to be controlled by a combination of diffusivity and solute chemical potentials per the Cahn-Hilliard equation [68, 69]. This introduces a complex kinetic and thermo-

dynamic interaction that may present under varying solvent compositions, even after controlling for droplet size and evaporation rate effects. For example, slower evaporation rates have been shown by Purohit et al. (2017) to reduce homogeneity for systems that undergo phase separation during solvent removal [20].

Surface enrichment of either the drug or polymer has also been observed in SDDs. Enrichment of the polymer is generally attributed to a kinetic process via the Peclet effect [32, 33] which arises from dissimilarities in cosolute diffusion rates due to large differences in molecular weights of the drug and polymer. During the evaporation process, these differential diffusion rates result in a radial composition gradient within the dried particle, as the polymer diffuses much more slowly than the drug and builds up at the surface as the droplet collapses [38]. In contrast, the accumulation of drug has been shown to be due to surfactant-like behavior of dissolved drug, which rapidly migrates to the droplet surface after atomization and prior to completion of the evaporation event [18, 44]. Lastly, and the area of focus in later chapters of this work, initial solution-state drug-polymer interactions have also been proposed as additional drivers of SDD homogeneity and stability.

Polymers in solution demonstrate a variety of complex phenomena that change in response to their relative affinity for the solvent and cosolutes. Polymer conformation can expand or contract in the presence of good or poor solvent interactions, as the polymer adjusts to either swell and maximize its interactions with its environment or instead collapse and interact preferentially with itself. When applied to SDDs, it has been inferred that those conditions which produce an extended coil conformation allow for greater opportunity for stabilizing drug-polymer contacts to form, relative to the collapsed globular state [14, 15, 21]. Similarly, the presence of more elaborate solution-state polymer-drug assemblies in the liquid feed was found to be correlated with variations in SDD dissolution [63].

Dynamic light scattering (DLS) and dilute solution viscometry (DSV) are common techniques used to assess these conformational and structural changes, as char-

acterized by hydrodynamic and viscometric diameters and particle-particle interactions in solution. However, such studies must be cautiously executed to ensure accurate and reproducible results, especially for the selection of the appropriate data analysis/treatment, concentration regime, sample purity, and method suitability [70, 71, 72, 73, 74]. Our review of the existing SDD literature has found that such considerations in previous studies have been poorly examined and warrant further scrutiny.

Macromolecular solutions are biphasic systems consisting of the pervaded volume of the macromolecule and the bulk solution [75]. Multi-component macromolecular solutions exhibit preferential solvation behavior, whereby cosolvents/solutes with favorable net interactions tend to be sorbed within the local environment of the macromolecule, while those that are unfavorable will be excluded [76]. SDD liquid feeds contain a minimum of three components (drug, polymer, solvent) and often more - as cosolvents and/or formulation adjuvants are increasingly employed to address solubility, processability, performance, safety, and environmental concerns [34]. The relative affinity to or repulsion of drug cosolutes from the pervaded volume of the polymer may play a significant role in the formation of stabilizing drug-polymer contacts that are necessary to preserve the amorphous character in the finished product. It should be noted that this argument relies on the maintenance of these interactions throughout the spray drying process, though this seems reasonable as such outcomes were observed for the solution-state assemblies investigated by Dalsin et al [63]. As the importance of cosolute preferential solvation/adsorption in protein formulation stability has already been well established [77, 78], it is proposed that the solution-state organization of spray drying liquid feeds will be likewise influential to successful SDD development. These questions are further explored in chapters 2 and 3.

1.4 Wet Granulation (WG)

Wet granulation approaches are among the oldest of particle engineering techniques utilized in the manufacture of pharmaceutical tablets [7]; of which high shear wet granulation (HSWG) is the most extensively employed in modern drug development [79]. It is one of the many methods used to combine a variety of powdered formulation materials through the agglomeration of smaller, primary particles with a liquid solvent and/or binder into larger units known as granules. These granules must exhibit suitable flowability, density, and compressibility for use in high speed tableting processes [79]. Modern tableting equipment requires free flowing product that is able to flow into and fill a small die cavity uniformly by volume at time scales on the order of single microseconds [80]. Often, API powders consist of sub 50 μm, cohesive particles with low density and poor or nonexistent flowability. High dose APIs will typically form the bulk of the tablet formulation (i.e. ibuprofen and acetaminophen), which means intermediate processing techniques such as granulation are needed to enhance flowability and compressibility of the API to ensure a successful tablet can be produced [79]. In addition to flow and compressibility, granulations also serve to improve content uniformity, reduce segregation through the generation of narrow particle size distributions, improve tablet strength due to incorporation of binder excipients in the granules, increase powder density, reduce dusting, and improve dissolution of the drug product [7].

The HSWG process typically begins with the preparation of a well-mixed powder bed, either by blending before granulation or more commonly, by mixing directly in the granulation bowl prior to adding the granulating fluid. Liquid binder and/or wetting agents are often dissolved in a granulating solvent; this solution is then atomized into droplets onto the powder bed, which is being simultaneously mixed with a large spinning impeller at 100-500 RPM and granulated/densified with a small rapidly spinning chopping blade operatin in the range of 1000-3000 RPM [7]. This mixing and

chopping facilitates distribution of the binder/cosolutes and generates a 'wet mass' product. Once all of the liquid solution has been added the process continues to mix and chop until the granulation end point is reached. The granulation will then often be wet milled and dried in a fluid bed dryer until the target residual solvent or moisture content is achieved [7]. Low shear wet granulation (LSWG) processes are similar in concept and execution to HSWG, though instead the granulation is achieved using a single low-speed mixing blade, often resulting in less dense, uniform, and robust granules [81]. LSWG also tends to require 30-40 % more liquid binder relative to HSWG to achieve comparable granules [7]. The types of processes which have been determined to be fundamental in understanding wet granulation performance consist of (1) wetting and nucleation, (2) consolidation and coalescence, and (3) breakage and attrition [82] (figure 1.7).

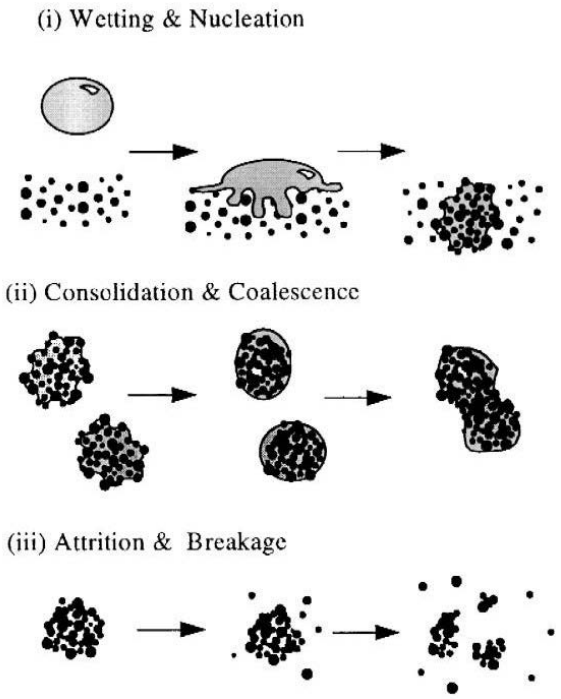

Figure 1.7: Schematic of key wet granulation processes which dictate granule properties. Reproduced with permission from [82]

Wetting and Nucleation

The process of wetting and nucleation is the act of bringing the liquid solution into contact with the dry powder bed through which nuclei granules are formed due to the liquid and powder interactions [82]. The atomization of the liquid feed is a critical step in the wet granulation process as it can impact the granule size and uniformity due to the droplet size distribution and spray pattern generated [83]. The initiation of granule formation is typically understood via the 'immersion nucleation' mechanism whereby the atomized droplets are much larger in size than the powder materials such that the liquid binder permeates through the powder bed via capillary actions to bind the loose particles together as the starting granule [83]. The key parameters in understanding and scaling up this stage of the granulation process are the droplet penetration time and the dimensionless spray flux. The droplet penetration time (t_p) into a loosely packed powder bed is a complex relationship dependent on the chemical and physical properties of the liquid solution, the granulation powder bed, and their relative affinity [83]:

$$t_p = 1.35 \frac{V_d^{2/3}}{\epsilon_{eff}^2 R_{eff}} \frac{\mu}{\gamma cos\theta} \tag{1.7}$$

Where V_d is the volume of the droplet size, ϵ_{eff} and R_{eff} are the effective bed voidage and average pore size available for capillary flow, μ and γ are the liquid binder viscosity and surface tension, and θ is the contact angle formed between the liquid binder solution and the surface of the granulation bed. Of these properties, μ generally has the greatest effect on granule properties as the liquid viscosity can easily vary within several orders of magnitude depending on the solids concentration and/or binder material that is used [83]. From the perspective of the powder properties, reducing the initial powder particle size increases the penetration time due to reduced packing efficiencies reflected in ϵ_{eff} and R_{eff}. In the case of very fine and cohesive powders, equation 1.7 becomes less accurate and experimental tests are instead recommended to support scale up activities [83]. The droplet penetration process can be visualized

in figure ().

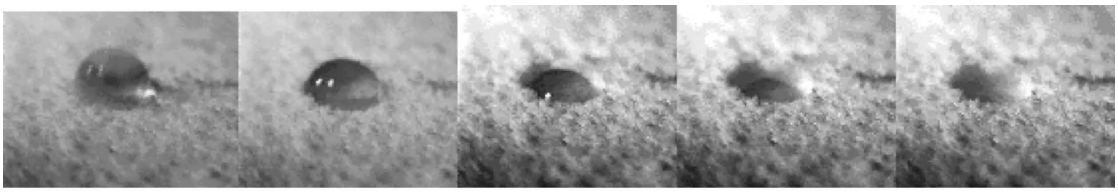

Figure 1.8: Water droplet penetrating into lactose powder at (a) impact; (b) 0.23s; (c) 0.9s; (d) 1.4s; and (e) 2.3s. Reproduced with permission from [83]

The dimensionless spray flux (Ψ_a) is defined as "the ratio of the rate at which wetted area ($\dot{a}$) is created by the incoming droplets compared to the total area of dry powder ($\dot{A}$) passing through the spray zone" and is a measure of the density of the liquid droplets striking the powder bed [83]:

$$Psi_a = \frac{\dot{a}}{\dot{A}} = \frac{3\dot{V}}{2\dot{A}d_d} \tag{1.8}$$

$\dot{A}$ may also be considered as the dynamic spray zone, which is a function of not just the area of the spray pattern generated from the atomization process, but also incorporates the rate of mixing and surface turnover of the powder bed. As the powder mixing rate increases while holding the atomization process constant, then Ψ_a will decrease as the fraction of the total powder bed area covered ($f_covered$) by the liquid droplets reduces. If instead one holds the powder mixing rate constant while increasing the liquid mass flow rate, then Ψ_a will increase as a greater proportion of the powder surface is wetted. At values of $\Psi_a \leq 0.01$, most of the spray droplets are expected to form individual granules that reflect the droplet size distribution.

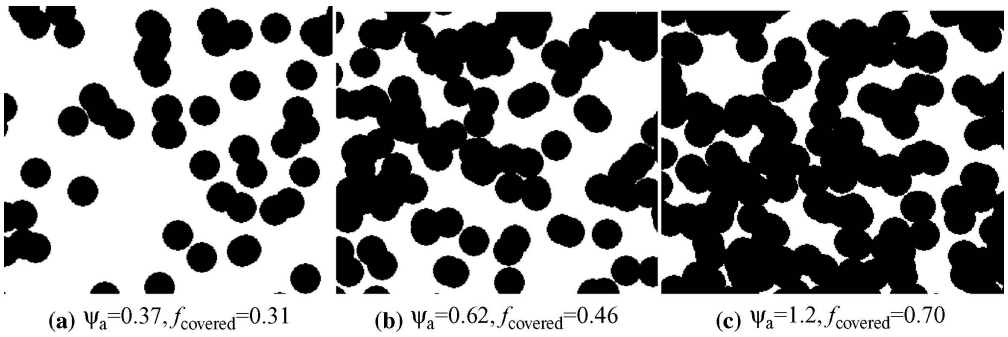

Figure 1.9: Monte-Carlo simulation of spray flux. Reproduced with permission from [83]

However, as Ψ_a increases, the droplets will begin to overlap and coalesce together at the surface of the powder bed, eventually forming an almost continuous sheet of liquid in the spray zone (figure 1.9). As the powder is moved and dispersed due to the rotations of the impeller and chopper blades, the sheeting of liquid is mechanically dispersed into the powder bed and where it can bind with other particles or droplet regimes to form a nucleus; rather than being formed purely due to the spray droplet penetration process. The relative extent of this effect can be explored with the dimensionless ratio (τ_p) of the droplet penetration time to the powder circulation time (t_c) back into the spray zone [83]:

$$\tau_p = \frac{t_p}{t_c} \tag{1.9}$$

Mechanical dispersion processes dominate under conditions of slow droplet penetration, fast powder re-circulation, and high spray flux ($\tau_p, \Psi_a \geq 1$)); while droplet nucleation dominates under the opposing conditions ($\tau_p, \Psi_a \leq 0.1$)), with intermediate regimes consisting of substantial activity from both nucleation mechanisms between these ranges (see figure 1.10). Droplet nucleation will tend to produce more uniform granule distributions proportional to the droplet size distributions from the atomization process, while mechanical dispersion will be more broad. More often than not, most granulators will operate within the mechanical dispersion regime due to both

slow penetration times and rapid re-circulation times resulting in the agglomeration of wet liquid regions [83].

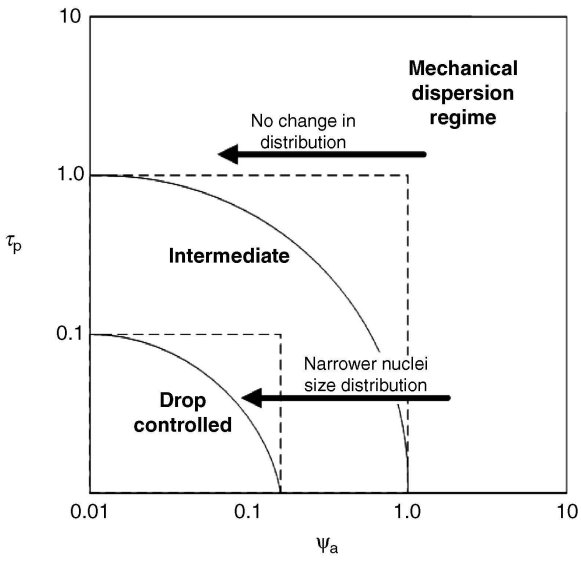

Figure 1.10: Nucleation mechanism regime map as a function of τ_p and Ψ_a, with droplet controlled dominating in the bottom left region, mechanical dispersion in the upper right regions, and between a intermediate region where both mechanisms are active. Reproduced with permission from [83]

Consolidation and Coalescence

The processes of granule consolidation and coalescence are the result of collisions between granules, granules and the powder bed, or the granules and the equipment which results in densification and growth [82] - as long as the binder solution is still liquid; once dried, consolidation is no longer possible and instead attrition will occur [83]. The granules first formed in the nucleation process are generally smaller with low density and significant volumes of void space which results in weak granules that are not appropriate for downstream processing. During the granulation process, the granules grow and increase in size over time as dry particles adhere to wet granules (layering [82]) and/or wet granules agglomerate to one another (coalescence [82]) with increasing liquid addition. As these granules are exposed to shear forces caused by the impeller and chopper blades, the granules are compressed and densified, resulting in less porous and stronger granules [83]. Should densification continue too

far, the majority of the void space will be removed with increasing compaction such that the relative saturation of the granules increases until the liquid fills all internal voids and is then squeezed to the outer surface of the granule. This effect results in rapid coalescence of granules such that a run away growth of granule size is observed which is characteristic of the onset of induction granule growth behavior and/or 'over-granulation' [83] which correlates with a broader granule size distribution and poor compactibility. An additional consequence of the lack of sufficient porosity can lead to difficulties in dispersion and dissolution due to the loss of available surface area to facilitate adequate release of an API [82].

Attrition and Breakage

The process of granule attrition and breakage is due to the fracture of 'wet' granules attributed to impact, wear, and compaction in high shear wet granulation equipment or in later product handling and downstream processing of 'dry' granules [82]. Notably, the mechanisms which govern the breakage and attrition of wet granules differs substantially from dry granules such that they must be addressed separately. For wet granules, deformation typically exhibits either plastic or semi-brittle behavior and is only considered significant within high shear granulation processes (i.e. not LSWG or fluid bed granulations) [83]. Plastic deforming wet granules are damaged due to the extensive shear and extensional flow experienced in the granulator which can often be confirmed due to the presence of smeared granules along the granulator walls or the development of a paste instead of granules [82]. In contrast, semi-brittle behavior is attributed to crack propagation initiated by impacts within the impeller zone and is more likely to be observed for non-spherical granules [83]. Increases in impeller speeds have been shown to consistently reduce granule size distributions attributed to brittle breakage in HSWG processes, such that the larger granules are expected to be broken preferentially to smaller granules [82]. The breakdown of granule properties are associated with the onset of over-granulation which is often monitored by tracking the

the rapid loss in power consumption over the course of the wet granulation process (figure 1.11) [79].

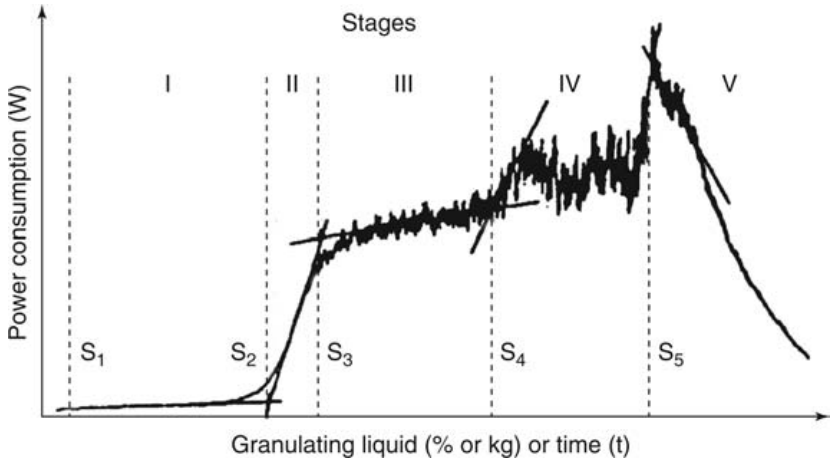

Figure 1.11: Power consumption profile of a high shear wet granulation process. Onset of over-granulation indicated by rapid loss in power consumption. Reproduced with permission from [79]

Attrition and breakage in dry granules is less well understood, though they are known to fail in a brittle or semi-brittle fashion ascribed to a complex crack propagation process. The robustness of dry granules has been successfully correlated with empirical three-point bend tests which are conducted by first forming solid bars of out of wet granules with notches of known size, letting them dry fully and measuring the force displacement required to fracture the bars [82]. The two primary proposed mechanisms for dry granule breakage are fragmentation and wear or attrition. Fragmentation typically occurs when the size of the initial crack propagation site, or process zone, is small relative to the granule size; this leads to the fracture of the granule into multiple large pieces. In contrast, the attrition mechanism occurs when the process zone size is on the order of the size of the granule and instead fine dust is generated due to diffuse micro-cracking [82].

Post Wet Granulation Processes

After completion of the wet shear granulation, multiple additional steps are generally employed to prepare the drug product intermediate for further downstream processing activities. The first step is wet milling or screening, where the still wet granulation is passed through a screen of specific size to break down the largest granules to ensure a more uniform size distribution with faster drying kinetics to minimize thermal exposure of the granulation [7]. Wet milling may not always be necessary and is typically dependent on the quality of the prepared granulation. Removal of residual liquid from the granules is accomplished most often by either fluid bed or vacuum tray dryers, similar to those discussed previously in the spray dry processing discussion in section 1.2.4. Moisture content is an important parameter as it can have significant impact on compactibility in tablet compression processes [7]. Lastly, dry milling or sizing is performed after drying using conical screening and hammer mills to reduce and control the final granule size distribution [7].

1.5 Wet Granulation of Highly Potent APIs (HP-APIs)

The primary benefits in the processing of HP-APIs by wet granulation is to ensure content uniformity (CU) of the drug compound within the formulation as well as the preparation of particles with acceptable flow and/or compression properties suitable for downstream processing [82, 7, 83]. An additional goal is the reduction of 'dusting,' i.e. the ability for formulation materials to become easily airborne, which adds risks to worker health due to the high potency nature of the APIs [7]. Densification and particle agglomeration minimizes the risk of powder inhalation by preventing the generation of airborne particles during handling and processing of the formulation materials.

Content Uniformity

As HP-APIs are typically in the range of 0.01-1 w/w% of the final formulation, it may often be difficult to mitigate the many potential causes of heterogeneity and/or potency loss. While its is commonly appreciated that the API tends to reside preferentially in the smallest particle class size (i.e 'fines') both before and after granulation due to small initial API particle size and resulting segregation [84, 85, 86], this can still be a concern even when the API is previously prepared with a larger particle size prior to granulation for the purpose of reducing this risk [87]. Another cause of granule heterogeneity has been shown to be due to differences in the wetting properties of the excipient and API powders, such that the liquid binder interacts favorably with the excipients which will form larger granules while the API may be repelled or settle at the bottom of the granulation bowl to avoid the solvent [85]. This is expected to be particularly relevant when the liquid binder solvent is water and the API is a poorly water soluble compound resulting in limited API wettability. Extending the wet massing granulation time has been shown to improve CU [86], though this may not always be an acceptable solution as the granule physical properties are sensitive to granulation time and there is an increased risk for the onset of over-granulation as time increases [83].

A common technique to mitigate CU issues with HP-APIs is to incorporate the drug compound into the liquid binder solution to facilitate the distribution of the API onto the granule bed more evenly [88, 89]. This requires adequate atomization of the liquid solution to ensure uniform dissemination, where slower liquid flow rates, with narrow droplet size distributions and a broad spray zone would be preferred. Notably, the properties of the atomization plume and liquid addition rate also affect the granule properties per the previous discussion, which must be taken into consideration. However, this approach is not without its downsides as well. When water is utilized as the liquid solvent, the API may be susceptible to hydrolysis, such as lofexidine which will be discussed in chapters 4 & 5 of this dissertation. Most

HP-APIs are likewise poorly water soluble and may require strong organic solvents to dissolve these compounds which bring concerns with respect to adequate solvent removal, similar to those addressed previously with respect to secondary drying post-spray dry processing. Potency loss may also occur as drug may adsorb to various process equipment surfaces instead of becoming incorporated within the granulation. This effect is usually negligible at traditionally higher levels of API content; but for highly potent compounds, this loss can be substantial relative to the label claim and may require an overage to account for processing induced losses[90].

Impact of Solvents in Wet Granulated HP-APIs

The solid state phase of the API has long been recognized to influence the stability and performance of a drug product. An API may express a substantial range of physical phases due to exposure to wet granulation processes including the transformation to various polymorphs[91, 92, 93], solvates/hydrates [94, 95, 96, 97], salt disproportionation [98, 99], co-crystals, and/or amorphous forms [100, 101] which can each exhibit substantially different dissolution behaviors and physical and chemical stability. Interactions between the API, solvent(s) [94, 91, 92], formulation excipients [95], and process parameters [92, 96] serve to further exacerbate the many possible outcomes on physical form. Particularly problematic in the case of HP-APIs is that the low drug concentrations in the formulation severely limit the ability to identify which physical phase(s) of the API are present, and in what relative amounts. For example, the most commonly utilized techniques to quantify the solid-state phase percentage of pharmaceutical materials are powder x-ray diffraction (pXRD), Raman spectroscopy, and differential scanning calorimetry (DSC), which are recognized to have detection limits for crystal forms from 0.2-5% [102, 103, 104] and for amorphous forms from 1-10 % [105, 106, 104] of the total sample weight. With API amounts as low as 0.01 w/w % in a formulation, it is often unreasonable to accurately quantify the phase composition of HP-APIs in a given drug product.

As HP-APIs are frequently dissolved in the liquid binder solution to aid distribution, a range of physical forms can be expected due to preference for varying polymorphic forms when precipitating from different solvents or generation of a glassy state due to co-dissolution of granule bed excipients (i.e polymers/binder) which stabilize the amorphous form. If the amorphous phase dominates, then a loss in chemical stability is expected due to the higher energy state of the glassy form. These effects can be screened by creating films of the solvent, API, with or without co-dissolved excipients of interest at high drug-excipient weight ratios to explore the tendency of the possible physical forms which may precipitate during processing. While this approach can overcome analytical limitations for assessing physical form, it may not be representative of how the drug will behave at low drug amounts in the true formulation and should be applied with caution. Additionally, the API will be preferentially distributed on the surface of the granules which will result in greater surface energy effects as well as increased environmental exposure than if it was sequestered within the interior of the granules/particles. Hydrolysis/solvolysis during solution preparation and the spraying process are additional risks to product stability due to the faster degradation occurring in the liquid state relative to solid-state kinetics coupled with exposure to the solvent(s) and any cosolutes. It is clear that an understanding of API-solvent interactions from both physical and chemical perspectives are necessary to facilitate the successful development of a wet granulated HP-API product.

1.6 Objectives

The objective of this dissertation is to provide a general overview and assessment of the role of solvents in the important methods of spray dried dispersions (SDDs) and low dosage wet granulations to address concerns related to poorly soluble and/or highly potent APIs. Light scattering (LS) and dilute solution viscometry (DSV) techniques have been utilized to assess critical drug-polymer-solvent interactions in the solution state and explore the mechanisms by which solvent choice may influence

SDD physical stability. Next, solid-state characterization techniques were leveraged to understand how the interplay between a WSG processing parameters, API physical form, and environmental moisture may dictate chemical stability issues. These learnings then inform the formulation and process statistical design of experiment (DOE) strategies in the creation of an optimal controlled-release tablet to satisfy the target dissolution and chemical stability performance requirements. Conclusions and future work are presented to outline next steps that can be pursued in expanding our knowledge of complex multi-component solutions which are frequently encountered in pharmaceutical development.

CHAPTER 2: APPLICATION OF LIGHT SCATTERING TO ASSESS SOLUTION-STATE INTERACTIONS IN SDD LIQUID FEEDS

This chapter is a modified reproduction of a portion of the paper by Defrese et al. (2020), reprinted (adapted) with permission [30]. Copyright (2020) American Chemical Society.

2.1 Introduction

It is well established that polymers adopt a range of conformations and solution state organization in response to varying solution environments, though very little work has been done to understand how these effects might impact the physical stability and bioavailability of spray dried amorphous dispersions (SDDs). Potentially relevant solution state polymer-solvent/cosolute interactions include preferential solvation, hydrodynamic size (i.e. polymer swelling or collapse), and solvent quality indicators (i.e. attractive or repulsive self-interactions). Of particular interest is the investigation of preferential solvation, defined as the relative attraction or rejection of a cosolvent and/or cosolute from the local environment of a solvated macromolecule, which often occurs in multi-component macromolecular solutions. As spray drying and other solvent-based dispersion processing necessitates the use of complex media consisting of at least three or more components (drug, polymer, solvent(s), and other possible excipients) - the prevalence of this phenomenon is likely.

This chapter characterizes largely unexplored solution-state properties in model spray dried dispersion feed solutions using both dynamic and static light scattering techniques to add greater context and guidance in studying these information rich

materials. These systems are found to exhibit complex non-intuitive behavior which serve to highlight the potential utility of preferential solvation in spray dried dispersion processing and stability. It is hypothesized that solution-state organization of the liquid feed can be engineered and translated to the solid-state for the optimization of SDD properties.

2.2 Theoretical Background

Dynamic Light Scattering (DLS)

DLS is a powerful technique with broad application in the polymer, nanoparticle, and biomedical sciences as evidenced by its widespread utilization to provide detailed sample characterization including particle size [71], shape [107, 108, 109, 110], particle-particle interactions [111, 112, 113], colloidal stability [114, 115, 116], aggregation [117, 107, 118], phase separation [119, 120, 121], and translational and rotational diffusion coefficients [122, 123, 124].

Alongside the prevalent use of DLS methods, many researchers have highlighted the need for careful appreciation of inherent differences in data treatment [71, 125, 73] and experimental sensitivity to seemingly negligible amounts of impurities [70, 72]. For example, Franks et al. determined that the different common algorithms used for data treatment (cumulants, non-negative least squares (NNLS), constrained regularization method for inverting data (CONTIN), and frequency) often return non-equivalent results. It was noted that the cumulants method appeared to provide a minimal amount of variance for monomodal distributions while the conversion of intensity distribution data to volume distributions can add significant variation to DLS results [73]. It was suggested that researchers state the evaluation algorithm used in any analysis and to be hesitant in determining size based on volume distributions, and instead should rely on intensity-based size results. However, they also noted that volume distributions are still useful for assigning approximate mass proportions for

samples with non-monomodal distributions.

Additional considerations in algorithm selection are the expected properties of the measured sample, the analyte of interest, and its sensitivity to transient species (i.e. phase separation, agglomeration) or 'dust' impurities (i.e. trace insoluble contaminants arising from sample and/or consumable manufacturing processes or aerosols introduced from the laboratory environment). For example, the cumulants method is very sensitive to minor amounts of larger particles which can skew the reported overall diffusion coefficient [71]. In some cases this can be quite useful, as in the ability to readily detect changes due to small amounts of aggregated protein; while in other cases this may be detrimental as for small particle size analytes ($\leq$ 20 nm) that can be rapidly obscured due to the comparably strong scattering of trace impurities - especially at lower concentration regimes and smaller scattering angles [70].

For non-Gaussian monomodal distributions, NNLS algorithms are preferred due to their lack of innate assumptions of sample distributions which makes them better suited for expected polydisperse materials [71], such as synthetic polymers or complex multi-component systems comprising mixtures of drug, polymer, and multiple solvents as explored in this study. Furthermore, sensitivity to dust can be minimized by providing resolution of the analyte peak from apparent contaminants or transient species that are not of primary interest [126]. For these reasons, and also to allow comparison with prior literature results of interest, we have selected the NNLS algorithm for analysis in this work. For a more detailed overview of the mathematics governing time auto-correlation functions, DLS intensity data analysis, and light scattering in general, we refer the interested reader to summaries in the literature [127, 128, 129, 130, 71].

Critical to the study of hydrodynamic size of dilute macromolecule solutions by DLS is the apparent diffusion coefficient D_{app} as determined from the intensity fluctuation data (with higher order virial expansions truncated) [128]:

$$D_{app}(q,c) = D_{z,0}[1 + CR_g^2q^2 + ...][1 + k_Dc + ...] \tag{2.1}$$

Where $D_{z,0}$ is the intensity-weighted translational diffusion coefficient extrapolated to zero concentration and scattering angle, C a characteristic coefficient of the macromolecule, R_g the radius of gyration, q the wave vector, k_D the dynamic interaction parameter, and c the macromolecule concentration. Notably for isotropic Rayleigh scatterers (i.e. those particles which are less than $\approx 1/20$ the size of the wavelength (λ_0) of the incident laser in a vacuum), $CR_g^2q^2$ is $<< 1$ and the effect of angle becomes negligible on the observed diffusion coefficient:

$$D_{app}(c) = D_{z,0}(1 + k_D c) \tag{2.2}$$

This result demonstrates that the concentration of Rayleigh scatterers can impact the determination of the apparent diffusion coefficient as measured by DLS when $\mid k_D c \mid$ is not sufficiently small. This parameter arises from non-ideal repulsive or attractive inter-particle interactions and is often utilized as an indicator of protein or colloidal stability in formulation development [111, 112, 113]. At positive k_D, particles are considered stable as they repel one another and move rapidly apart, increasing their mobility and the observed diffusion coefficient. When k_D is negative, the particles are unstable as they become attracted together, slowing their mobility while potentially forming complexes or aggregates and demonstrating reduced diffusion coefficients.

This parameter is also related to the osmotic second virial coefficient, B_{22}, a characteristic thermodynamic factor which describes the relative particle-particle to particle-solvent interactions [127]:

$$k_D = 2B_{22}M_w - \zeta_1 - 2\overline{v} \tag{2.3}$$

where M_w is the molecular weight of the macromolecule, ζ_1 a frictional factor, and $\overline{v}$ the specific volume of the macromolecule.

Both k_D and B_{22} are solvent quality factors which describe the relative strength of polymer-polymer interactions compared to polymer-solvent interactions. Solvent quality is an important concept in polymer science which arose from the derivation of

the 'theta' solvent concept per Flory-Huggins solution theory - i.e. a solvent condition whereby the net excluded volume and excess chemical potential of mixing of a polymer in a solvent is equal to zero [75]. In theta solvents ($B_{22} = 0$), the steric repulsion of the monomers in the polymer chain are balanced exactly with solvent-mediated attraction between the monomers and the polymer adopts ideal chain conformations. Conditions in which the polymer-solvent interactions are stronger than polymer-polymer interactions are known as 'good' solvents ($B_{22} > 0$) and causes the polymer conformations to swell and increase in size relative to theta solvents. Conversely, solutions where polymer-polymer interactions dominate are known as 'poor' solvents ($B_{22} < 0$), leading to a reduction in size as the polymer contracts due to stronger polymer self-interactions in comparison to polymer-solvent interactions. The range of these descriptions from 'poor' to 'theta' to 'good' is known as solvent quality. As solvent quality increases, more polymer-solvent contacts are made, and the polymer swells - whereas decreasing solvent quality implies the opposite.

The Stokes-Einstein equation (2.4) describes the relationship between the Brownian translational diffusion coefficient $D_{z,0}$ (i.e. the random translational motion of particles suspended in a fluid arising from collision theory) and particle size via the hydrodynamic radius (R_H), modeled as that of an equivalent sphere that diffuses at the same rate as determined under infinite dilution:

$$D_{z,0} = \frac{k_B T}{6\pi\eta_s R_H} \tag{2.4}$$

where k_B is the Boltzmann coefficient, T the absolute temperature, and η_s the dispersant or solvent viscosity.

Best practice for determination of an accurate hydrodynamic radius requires measurement of a dilution series that is extrapolated to infinite dilution to satisfy the assumption of random Brownian motion [71]. This assumption is violated when $\mid k_D c \mid$ is not $<< 1$, as the repulsive/attractive interactions cause changes in mobility that are no longer random in nature. Only in those cases where particle-particle interactions are known to be negligible is it acceptable to determine the hydrodynamic radius

from a single concentration; though it is still necessary to correct for changes in the sample viscosity unless likewise sufficiently dilute to have minimal impact to diffusion processes. This chapter will highlight the importance of the dynamic interaction parameter and its relation to static light scattering measurements in understanding the solution state properties of relevant spray dried dispersion feed stock solutions.

Static Light Scattering (SLS)

SLS is an experimental method which has long been applied to macromolecular solutions to characterize properties such as the molecular weight (M_w), size (via the radius of gyration - R_g), shape (via the Perrin form factor - $P(\theta)$), and thermodynamic behavior (via the osmotic second virial coefficient B_{22}). Radiative scattering methods, including X-rays, neutrons, and light scattering, all rely on measurements of the time-averaged excess intensity of the scattering contrast arising from the particles of interest relative to the background intensity [75]. Determination of these properties are typically conducted through a Zimm plot analysis as constructed from the averaged intensity data measured at multiple scattering angles and concentrations, which is then extrapolated to zero angle and concentration (with truncation of the higher order virial expansion terms as before):

$$\frac{Kc}{R(q,c)} = [\frac{1}{M_w} + 2B_{22}c + ...][1 + CR_g^2q^2 + ...] \tag{2.5}$$

where $R(q,c)$ is the angle and concentration-dependent Rayleigh ratio, and K the optical constant:

$$K = \frac{4\pi^2 n_0^2}{\lambda_0^4 N_A}(\frac{dn}{dc_2})^2_{\mu_{i\neq 2}} \tag{2.6}$$

where n_0 is the refractive index of the solvent, N_A Avogadro's constant, and $(\frac{dn}{dc_2})_{\mu_{i\neq 2}}$ the differential refractive increment (DRI) at constant chemical potential for all components except the macromolecule, component 2. Simplifying for application to Rayleigh scatterers results in the following:

$$\frac{Kc}{R(c)} = (\frac{1}{M_w} + 2B_{22}c) \tag{2.7}$$

Typically, equation 2.7 is truncated to the dilute linear region captured by first two terms, as the higher order terms are often experimentally inaccessible. It is important to consider a few aspects regarding the DRI parameter with respect to SLS. As the source of the measured excess scattering intensity arises from the difference of the analyte refractive index with respect to the reference solution - the greater the disparity in refractive indices between the macromolecule and the reference solution, the stronger the signal observed and lower the concentrations that can be accurately analyzed (and vice versa) [130]. As $\frac{dn}{dc}$ is squared in the optical constant, any relative error in its determination will be doubled in the errors of M_w and B_{22} [127, 130]. To minimize systematic errors, measurements should ideally be conducted at an equivalent temperature and wavelength as the light scattering conditions.

Preferential Solvation

In multi-component solutions, such as in the case of mixed solvent systems or in the presence of dissolved cosolutes as is necessary in spray dried dispersion processing, the DRI parameter can also be affected by preferential solvation of the polymer by the various species in solution (adapted from [131, 132, 133]):

$$(\frac{dn}{dc_2})_{\mu_{i\neq 2}} = (\frac{dn}{dc_2})_{\theta_i} + \sum_{i\neq 2}^{n} \lambda_i (\frac{dn}{d\theta_i})_{c_2=0} \tag{2.8}$$

where $(\frac{dn}{dc_2})_{\theta_i}$ is the observed polymer DRI at constant volume composition (θ_i), λ_i the preferential solvation coefficient of the i^{th} component, $(\frac{dn}{d\theta_i})_{c_2=0}$ the DRI with respect to the i^{th} component, holding all other species constant as the concentration of the macromolecule approaches infinite dilution.

Preferential solvation is a phenomenon which originates from the relative net favorable or unfavorable cosolute-macromolecule local interactions resulting in either the excess sorption (favorable) or exclusion (unfavorable) of cosolutes to or from the pervaded volume of the macromolecule. As this pervaded volume, or the volume of solution spanned by the macromolecular chain, is orders of magnitude larger than its

occupied volume, the macromolecule can inhabit a substantial volume fraction of the solution even at low weight concentrations and can thus readily impact the composition of the bulk solution. When present, this phenomena can affect the refractive index of the bulk and pervaded volumes due to changing concentrations which shifts the strength of the signal arising from the refractive index contrast (i.e DRI) during the static light scattering experiment. λ_i is defined as the rate of change in the bulk volume fraction of the i^{th} species with respect to macromolecule concentration and conceptually may be understood as the excess number of i^{th} molecules (γ_i) of partial molar volume (V_i) that are preferentially adsorbed within the local environment of the macromolecular chain:

$$\lambda_i \equiv (\frac{d\theta_i}{dc_2})_{\mu_i, c_2=0} \equiv -\frac{\gamma_i V_i}{M_w} \tag{2.9}$$

By convention, a positive value indicates exclusion from the pervaded volume while negative values represent preferential adsorption within. Dialysis can correct for these effects by allowing for the exchange of solutes to re-establish the initial bulk volume fractions; though this is often tedious and prohibitively expensive for materials such as therapeutic proteins and/or drug cosolutes. In the absence of dialysis of multi-component systems, the observed or apparent M_w^* and B_{22}^* can become distorted due to the effects of preferential solvation. While an experimental static light scattering approach for determination of λ_i is generally not feasible for systems in excess of three components, Benoit and Strazielle developed an accessible relation for ternary systems, provided the true molecular weight is known or previously measured from a single solvent system [134]:

$$\lambda_3 = [(\frac{M_w^*}{M_w})^{0.5} - 1]\frac{(dn/dc_2)_{\theta_{1,3}}}{(dn/d\theta_3)_{c_2=0}} \tag{2.10}$$

$$B_{22} = B_{22}^*(M_w^*/M_w) \tag{2.11}$$

where subscript 1 denotes the primary solvent, 2 the macromolecule, and 3 the cosolvent or cosolute.

For mixed liquid systems, the volume fractions and $(dn/d\theta_3)$ can be either computed or measured directly from solution preparations; while for otherwise solid cosolutes such as drug compounds, which are prepared and measured on a mass concentration basis, the conversion to volume fraction is needed. To address this, the (dn/dc_3) in the dilute regime can be measured and the Gladstone-Dale equation [135] used to find the partial specific volume $\overline{v}$ of the dissolved cosolute in the pure solvent to convert concentrations to volume fractions for determination of $(dn/d\theta_3)$:

$$\overline{v}_3 = \frac{(dn/dc_3)}{n_3 - n_1} = \frac{\theta_3}{c_3} \tag{2.12}$$

where n_1 and n_3 are the refractive indices of the pure solvent and cosolute, respectively.

2.3 Materials and Methods

Polyvinylpyrrolidone K25 (PVP) was gifted from Ashland Global Specialty Chemicals Inc. (Covington, KY). The polymer was held at 40 °C under vacuum for at least 24 hours prior to use for removal of residual water content to ensure accurate polymer mass for solution preparations, as PVP is known to sorb substantial moisture even at ambient conditions [136]. (S)-(+)-2-(6-Methoxy-2-naphthyl)propionic Acid (i.e. Naproxen (NAP)), $\geq$ 99.0% purity was sourced from TCI America (Portland, OR) and purchased through VWR International (Radnor, PA) and used as received. HPLC grade Methanol and Acetone with maximum specifications of 0.03% (w/w) and 0.2 % (w/w) water content were purchased from VWR International and used as received. 0.02 um Whatman Anotop Syringe Filters were sourced from GE Healthcare (Chicago, IL), purchased though VWR International and used as received. The chemical structures of PVPK25 and Naproxen are shown in Figure 2.1.

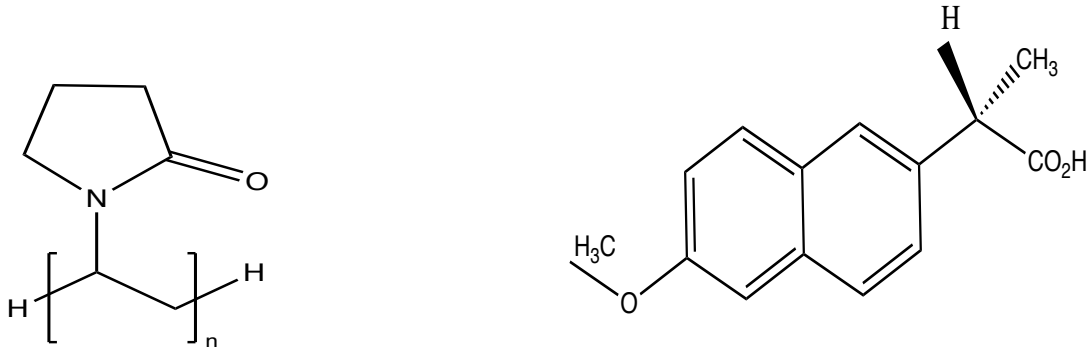

Figure 2.1: Chemical structures of a) PVP and b) Naproxen

Solution Preparation

All solvent mixtures and solutions were prepared by mass under room temperature conditions. Concentration series of polymer solutions were prepared independently in volumetric flasks using a previously prepared reference solvent mixture or drug solution for each selected cosolute/solvent composition. Each solution was allowed to equilibrate a minimum of 12 hours and sealed with parafilm to inhibit evaporation. Solutions were then filtered 3-6 times as necessary to remove impurities prior to characterization. All samples were visually transparent and uniform. No analyte was observed to be lost due to the filtration process.

Light Scattering

All light scattering data were collected with a Malvern Zetasizer Nano ZS at 25.0 °C with 5 minutes equilibration time using a low volume quartz cuvette cell. The cell was pre-rinsed 2 times with filtered sample before final sample loading and cleaned with a standard washing protocol between samples. Measurements were conducted at an angle of 173°and averaged from manual settings of 7 measurements consisting of 60 runs of 5 second duration each, at a position of 4.2 with automatic attenuator selection. The refractive index and absorption values used for PVP were 1.525 and

0.002 [137]. The data was processed using the 'General Purpose' NNLS algorithm. Dispersant (i.e. reference solution) viscosity and refractive index measures needed in support of light scattering were determined as described below. 20 nm filtered toluene was used as a reference standard with scattering intensity measured at each applicable attenuator.

The intensity diffusion coefficient for the primary polymer peak was extracted for dynamic light scattering analysis (DLS) while the mean intensity count rate was extracted for static light scattering (SLS) analysis. Intensity peak analysis was used to minimize noise from errant dust particles and to distinguish between drug and polymer diffusivity peaks where applicable. No observations of temporal effects or in-homogeneity, such as increasing phase separation or agglomeration (i.e. no trending increase of scattering intensity, DLS polydispersity index (PDI), and non-monomodality or peak size over the time span ($\approx$ 40 min.) of measurements) were observed during this study.

Viscometry

The viscosity of all solvent mixtures (i.e. without dissolved solutes) were measured using a Rheosense microVisc Viscometer with A05 chip and temperature controller, conducted at 25.00 (+/- 0.04) °C with an equilibration time of at least 3 minutes for each new pipette, with 150 uL prime and 60 uL measurement volumes. Each solvent mixture viscosity was averaged across at least 6 measurements using 2 disposable pipettes, with at least 3 measures per pipette. If large differences between averaged pipette measures were observed (> 0.015 cP), a third pipette with at least 3 additional measures was conducted and averaged to reduce variance attributable to deviations in pipette dimensions.

Refractometry

Refractive index (RI) measurements in support of light scattering studies were conducted using a Carl Zeiss Abbe Refractometer with wavelength of 589 nm at room temperature conditions. Each sample was measured twice and averaged for use in the determination of differential refractive increments (DRIs).

Residual Water Assessments

To assess the potential impact of residual water on the static light scattering measurements, 20% (w/v) 3Å activated molecular sieves were added to the as received HPLC grade acetone and methanol solvents with maximum specifications of 0.2% (w/w) and 0.03 % (w/w) water content. After both 24 and 48 hours exposure to the molecular sieves, mixtures were prepared from the solvents at 0-88% (θ_{ACE}), consistent with ratios evaluated in the light scattering studies with the polymer, with RI measurements conducted as previously described.

Data Analysis and Presentation

Statistical analysis and graphs prepared in excel with visualization aided by Daniel's XL Toolbox addin for Excel, version 7.3.2 [138]. All error bars represent 95% confidence intervals as determined by regression analysis unless stated otherwise. Data Thief was used for the extraction of data from graphs in the literature for comparison and analysis [139].

2.4 Results and Discussion

Dynamic Light Scattering

In order to characterize diffusion interaction parameters and hydrodynamic diameters for comparison to prior literature results, we evaluated several concentration series of polymer solutions by DLS ranging from 2-50 mg/mL at dispersant compositions

of naproxen in methanol at 4.7% θ_{NAP} (i.e. 50 mg/mL) and solvent mixtures of acetone in methanol ranging from 0-88% θ_{ACE}. For each solvent or reference solution condition, the peak apparent diffusion coefficient was extracted and plotted against concentration for determination of the diffusion coefficient at infinite dilution from the extrapolated intercept and the diffusion interaction parameter from the linear slope according to equation (2.2) (figure 2.2).

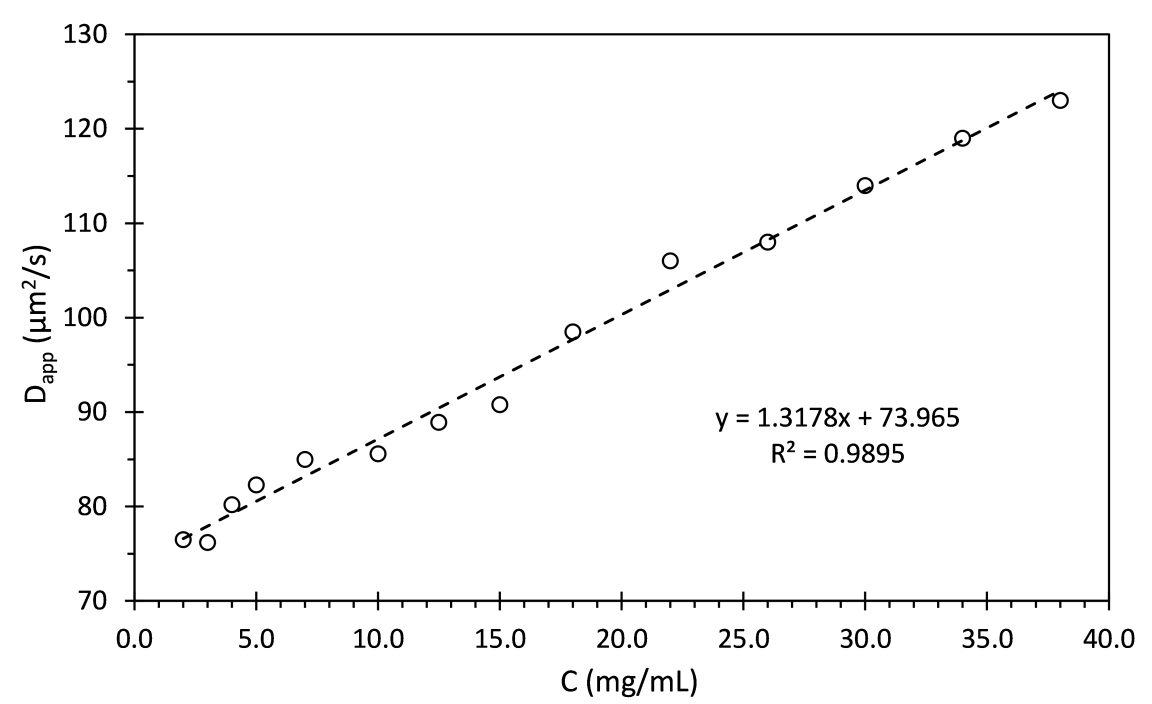

Figure 2.2: Example plot of D_{app} vs. C for PVP in methanol with linear regression fit.

The fitted diffusion coefficients and interaction parameters from the DLS data at each solvent condition are compiled in figure 2.3 and plotted against the acetone volume fractions in methanol (or the single solution of θ_{NAP} in methanol, respectively). Focusing first on the diffusion coefficients, we can observe that polymer mobility increases substantially with rising acetone content as indicated by a near doubling over the range of investigated solvent mixtures. In contrast, a somewhat more restricted movement is observed in the presence of naproxen as indicated by a loss in diffusivity compared to the pure methanol system. These mobility differences are primarily

attributable to the range of dispersant viscosities explored, despite seemingly small differences of at most ≈ 0.3 cP between all systems with a span of 0.313-0.630 cP. This highlights the sensitivity of the diffusion coefficients and thus hydrodynamic diameters to accurate viscosity measurements, which can be experimentally difficult at such low absolute viscosity values. The implications of errors in viscosity measurements on DLS data will be addressed in greater detail in following discussions.

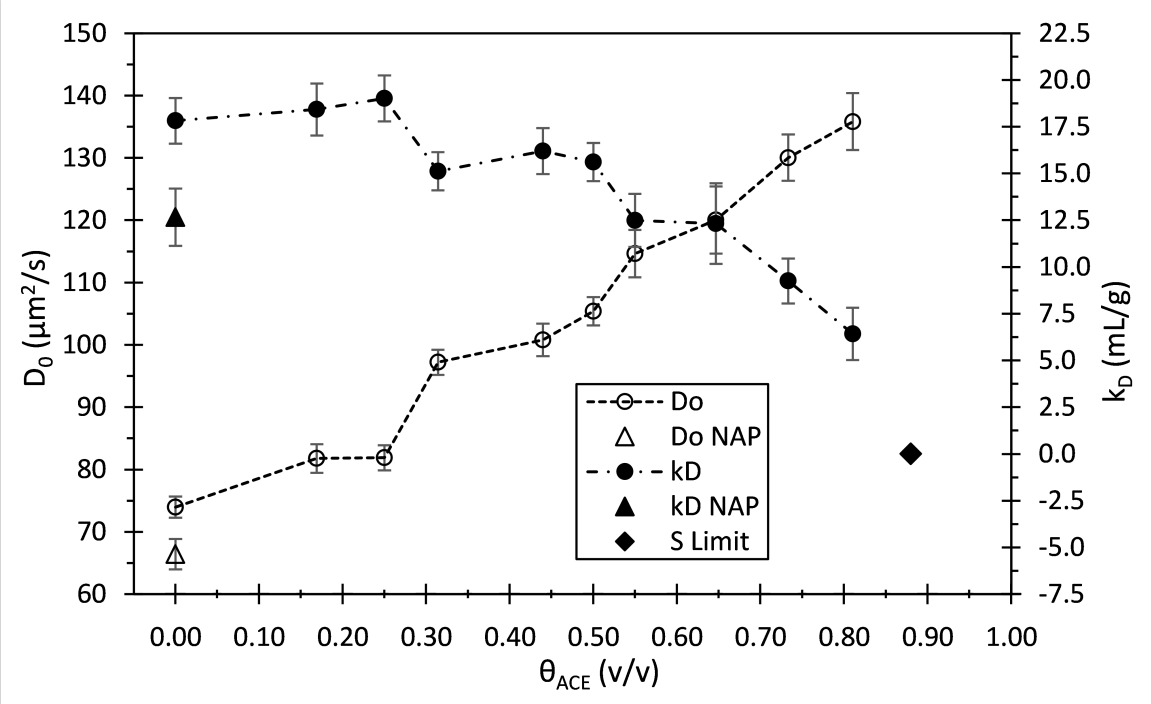

Figure 2.3: DLS Summary plot: D_0 (○) and k_D (●) vs θ_{ACE}. Mobility (D_0) increases while solvent quality (k_D) is reduced with additional acetone content. Both mobility and solvent quality are reduced in the presence of naproxen in methanol. ♦ represents the θ_{ACE} found to be at or near the solubility limit (S Limit) of PVP, with a k_D value of 0 included to describe continuing loss of solvent quality. △ and ▲ are the results for PVP in the presence of 50 mg/mL NAP in methanol. Trace lines are included as an aid to the eye. Error bars are 95% confidence intervals.

The larger, positive diffusion interaction parameters that persists until ≈ 30% θ_{ACE} demonstrate strongly repulsive polymer-polymer interactions which is indicative of a 'good' quality solvent where polymer-solvent interactions are preferred. This self repulsive behavior begins to decay with increasing acetone content as the polymer approaches its solubility limit near ≈ 88% θ_{ACE}, as deduced by the positive k_D value

approaching 0 with increasing θ_{ACE} (figure 2.3). The diamond symbol marks the θ_{ACE} at which PVP solubility was observed to be insufficient to allow for DLS analysis (i.e. precipitate formed during sample handling and filtration), from which it can be inferred that k_D must be ≤ 0. The trending loss of solvent quality with increasing θ_{ACE} is expected due to the known 'poor' solvent character of PVP in acetone rich solvent conditions [22]. It is possible that critical transition points may exist near 30 and 50% θ_{ACE} where the trends of D_0 and k_D appear to change most sharply is response to changing solvent composition. Notably, there is also a substantial drop in k_D in the presence of naproxen, which indicates that 'solvent'-polymer contacts are less favored in comparison to the drugs absence. As naproxen is a carboxylic acid which is known to adopt stable dimers[140], this change in polymer behavior may be due to preferential naproxen-naproxen self-interactions or the formation of similarly strong methanol-naproxen contacts such that the polymer is less able to maintain stable solvent connections.

After converting the diffusion coefficient to the hydrodynamic radius via equation (2.4) and plotting vs. θ_{ACE} alongside prior literature results [15], we see behavior that is more consistent with the k_D results. The polymer size appears to swell up to $\approx$ 25% θ_{ACE}, before contracting at $\approx$ 30% then staying relatively constant or possibly trending with a slight rise then decrease as the amount of acetone increases (figure 2.4). R_H was also determined in the presence of 50 mg/mL NAP in methanol, with no meaningful change in comparison to pure methanol; in contrast to the initial diffusivity and interaction parameter results. This discrepancy with the diffusion coefficient can be attributed to the increased dispersant viscosity arising from the dissolved naproxen rather than any difference in R_H, though the change in k_D due to naproxen appears significant and indicates a meaningful loss of solvent quality with co-dissolved drug in methanol.

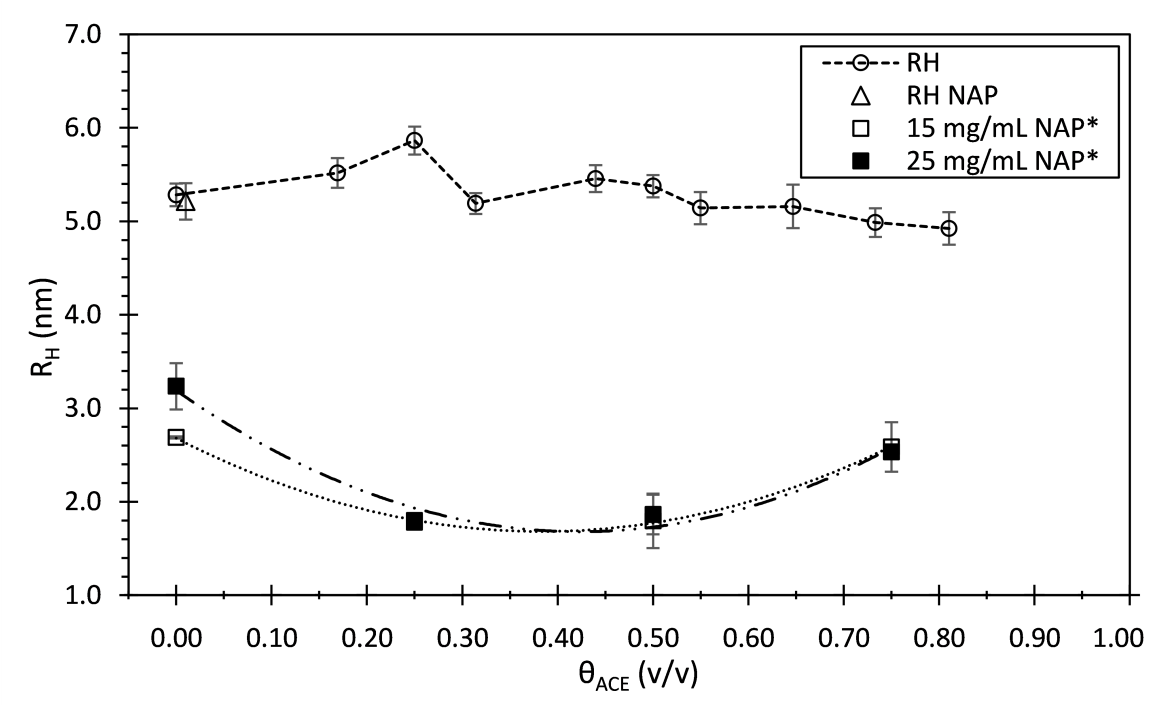

Figure 2.4: R_H vs. θ_{ACE} in the absence (○) and presence (△) of 50 mg/mL NAP in methanol from this work. Data extracted from reference [15] measured at conditions of 35 mg/mL PVP in the presence of 15 mg/mL NAP (□) and 25 mg/mL PVP in the presence of 25 mg/mL NAP (■) respectively. Lines are a trace for this work with 2^{nd} order polynomial fits for literature data, included as an aid to the eye. The results from this work differ significantly from reference [15]. Error bars from the literature data are standard deviations while those from this work are 95% confidence intervals.

When assessing the outcomes between R_H and k_D, it appears that the diffusion interaction parameter may be the more sensitive indicator of solvent quality and/or polymer-cosolute interactions. For example, at higher acetone content and also with co-dissolved naproxen, it can be seen that the reduction in k_D is much more rapid and apparent in comparison to R_H (figures 2.3 and 2.4). Overall, both parameters agree fairly well with each other, increasing in hydrodynamic size along with increasing solvent quality behavior with an R^2 of 0.755 determined from a linear correlation plot of R_H vs k_D (figure 2.5). These results demonstrate the value of additional context and supporting information that an assessment of a dilution series provides in comparison to single concentration DLS measurements.

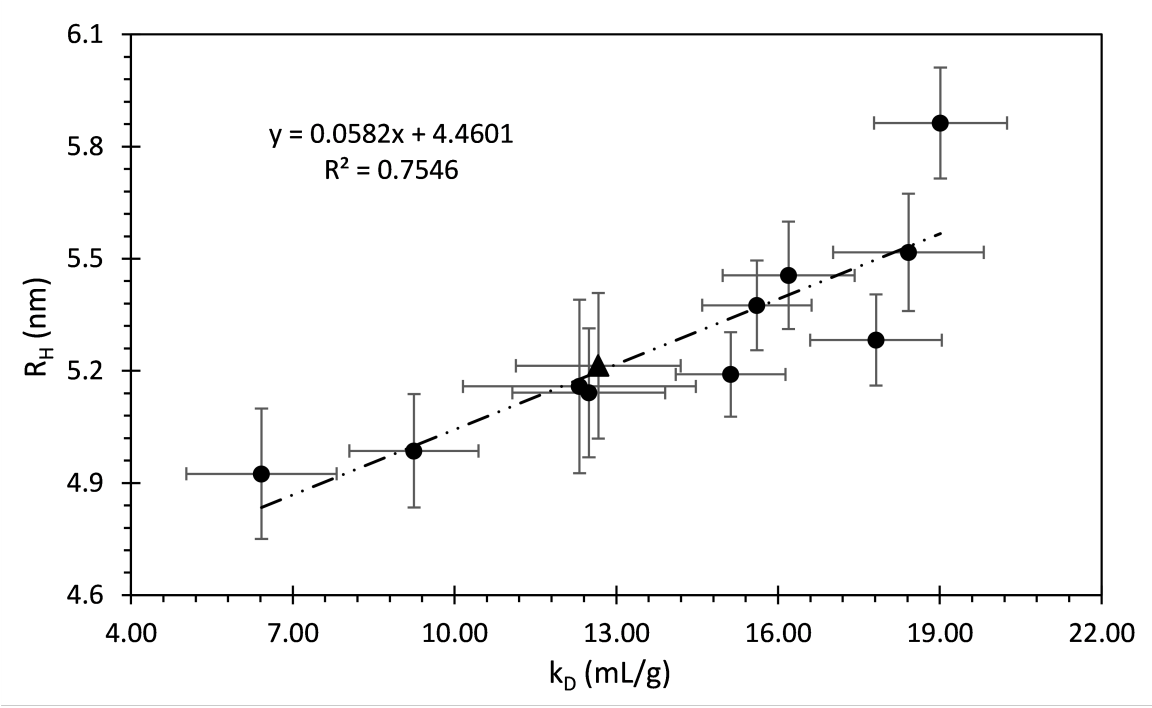

Figure 2.5: Correlation plot of the Stokes' R_H vs k_D, with equation and R^2 of the linear fit. (●) is PVP in the methanol-acetone solvent mixtures and (▲) is in the presence of 50 mg/mL NAP in methanol. The greater change of k_D in comparison to R_H highlights the potential of k_D as a more sensitive parameter to assess solvent quality and/or cosolute-polymer interactions. The relatively strong R^2 indicates internal consistency between the parameters in describing the behavior of the polymer in solution. Error bars are 95% confidence intervals.

It is also important to describe how and why our results differ significantly from prior literature [15], where values of R_H were found to range from $\approx 1.8 - 3.2$ nm, in comparison to this work which falls within a range of $\approx 4.9 - 5.9$ nm for the same systems (figure 2.4). The literature values are surprisingly smaller than would be expected for a polymer of this molecular weight and contain an apparent minimum occurring between 25-50% θ_{ACE} before increasing in size at 75% [15], contradicting the typical expectation of polymer collapse as the solubility limit is approached. It should be noted that the literature work presented was carried out at either constant concentrations of 35 mg/mL PVP in the presence of 15 mg/mL NAP or 25 mg/mL PVP in the presence of 25 mg/mL NAP respectively at varying θ_{ACE}. In this work, we have first extrapolated to zero concentration and primarily conducted measurements

in the absence of naproxen, except for the pure methanol solvent system which was also evaluated with co-dissolved 50 mg/mL NAP in methanol.

These discrepancies can be explored further in additional related work [16] where the hydrodynamic size was evaluated at a constant combined 20 w/v% (i.e. 200 mg/mL of total solids) of NAP and PVP at varying drug and polymer fractions. If the presence of naproxen has a minor or negligible effect on hydrodynamic size of PVP in methanol as found in this work, then these data may be treated as a pseudo-dilution series for extrapolation to the Stokes' radii (figure 2.6). From this treatment of the data, we demonstrate a Stokes' radii of $\approx 5.5 - 6$ nm, similar to our findings of ≈ 5.25 nm when in the presence of 50 mg/mL naproxen and much greater than the results published in the initial reference[15]. We should note that this is only an approximation as a proper dilution series for extrapolation should be conducted in a specific reference solution, i.e. at a constant naproxen concentration, where in the reference source the drug amount is varied due to holding % solids in solution constant.

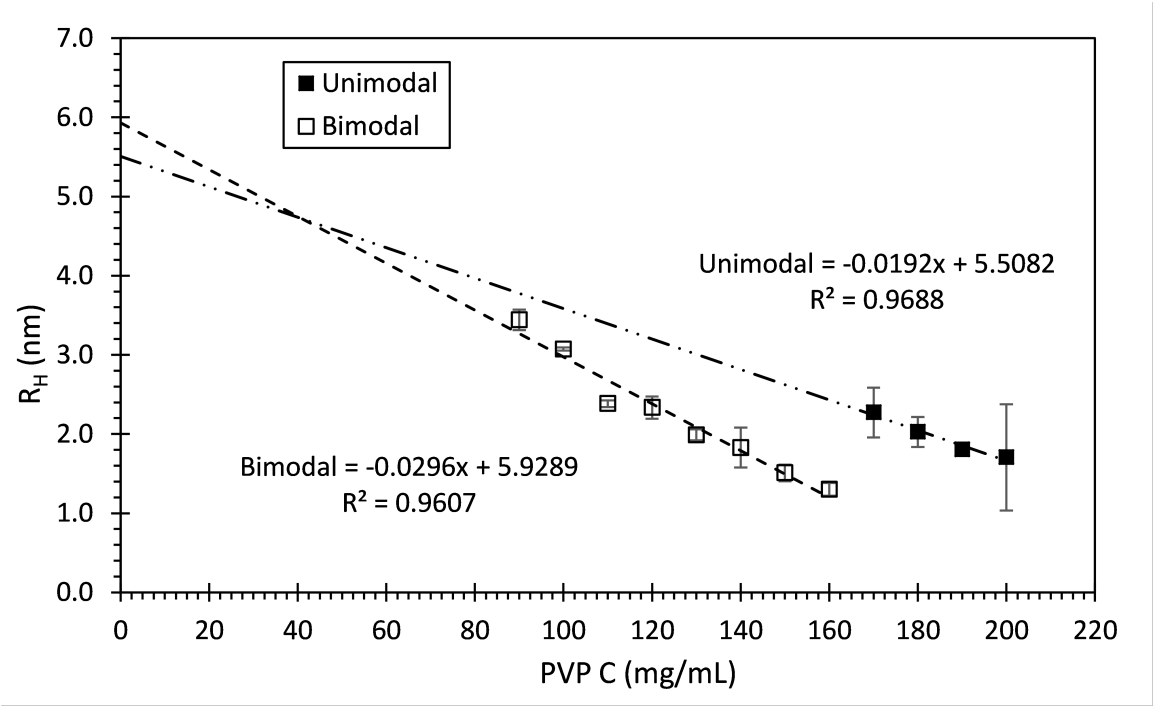

Figure 2.6: Hydrodynamic radii (R_H) vs. PVP concentration with varying NAP amounts as extracted from the bimodal (○) and unimodal (●) distributions respectively, per reference [16]. When a dilution series and extrapolation is applied to the literature data, similar R_H of ≈ 5.5 and 5.9 nm are found which are comparable to results from this work (5.3 nm with 50 mg/mL NAP in methanol). Linear regression fits and trend lines included to demonstrate extrapolated size from the intercepts. Error bars are standard deviations.

Per this study [16], development of a bimodal distribution was observed at lower polymer/higher drug content where the larger population grows in size as naproxen concentration increases - this was considered a 'remarkable' observation, yet we believe the explanation is straightforward. We suggest that the generation of the bimodal distribution with increasing naproxen content is likely due to phase separation and/or crystallization of the drug as the solubility limit of naproxen in methanol has been previously determined to range between ≈ 50 and 85 mg/mL [141, 142, 143], while the reference data assessed concentrations of NAP up to 110 mg/mL.

Table 2.1: Literature viscometry data per reference [15]

	S_0	S_1	S_2	S_3
PVP (mg/mL)	0	22.5	35	50
NAP (mg/mL)	0	27.5	15	0
θ_{ACE}	η_0	η_1	η_2	η_3
0	0.58 ±0.002	0.56[a]	0.63	1.09
0.25	0.69 ±0.002	0.48[a]	0.49[a]	0.76
0.50	0.58 ±0.005	0.39[a]	0.44[a]	0.65
0.75	0.46 ±0.005	0.30[a]	0.34[a]	0.61

Unexpectedly low viscosity with added solutes in comparison to the pure solvent mixtures, all table values in centipoise (cP)
S_0: pure solvent mixture viscosities with standard deviations from n=3 measures
S_1: solutions of 50 mg/mL PVP & 0 mg/mL NAP
S_2: solutions of 35 mg/mL PVP & 15 mg/mL NAP
S_3: solutions of 22.5 mg/mL PVP & 27.5 mg/mL NAP

Additionally, the viscometry data sourced from reference [15] used to calculate R_H appears to be inaccurate, as captured in Table 2.1. In some cases, the measured viscosity of the solutions containing dissolved PVP and NAP are less than that of the pure solvents, which should not occur. Furthermore, the viscosities of the pure methanol-acetone solvent mixtures are neither consistent with our results nor prior work in the literature [144], which agree well with each other (figure 2.7). It is clear that per equation (2.4), any error in the measured viscosity will likewise translate to a similar error in the reported R_H. From this, it is clearly demonstrated that the discrepancy between our hydrodynamic sizes and those in reference [15] (and even the differences in size due to naproxen content within that same work) are likely due to both polymer concentration effects attributable to the k_D interaction parameter as well as inaccurate viscometry measurements. Overall, these outcomes illustrate the importance of conducting a dilution series alongside accurate viscosity measurements for the correct interpretation of DLS data while also highlighting the value in determination of the diffusion interaction parameter in understanding solution state behavior of polymer-drug interactions.

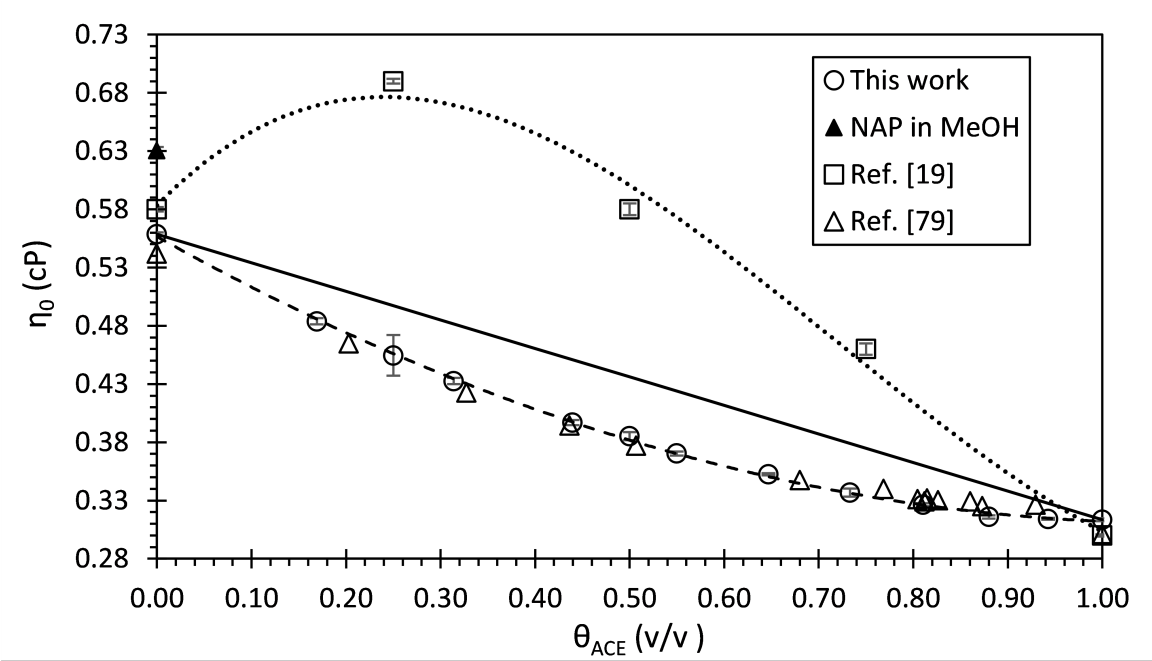

Figure 2.7: Comparison of solvent mixture viscosities vs θ_{ACE} from reference [15] (□), this work (○), and reference [144] (△). Viscometry results of pure solvent mixtures from this work are well behaved and align well with reference [144] in comparison to reference [15]. Dashed line is 2^{nd} order polynomial fit from this work; dotted line is 3^{rd} order polynomial fit of reference [15], solid line represents predictions from ideal viscosity of mixing. Error bars represent standard deviations for all data sets.

Static Light Scattering and Refractometry

In order to characterize the true molecular weight, osmotic second virial coefficients, and preferential solvation parameters of naproxen in methanol and acetone in methanol at varying θ_{ACE}, the same solutions were also evaluated by SLS and refractometry techniques. For each solvent or reference solution condition, the time-averaged scattering intensity was extracted from the light scattering data for determination of the true (and apparent) molecular weight M_w (M_w^*) and osmotic second virial coefficient B_{22} (B_{22}^*) from the extrapolated intercept and slope of the linear dilute region of KC/R_θ vs. concentration according to equation (2.7).

However, before moving forward with SLS and related RI measures, the potential effects of trace residual moisture on the refractive index measurements in the HPLC grade solvents need to be considered. It is expected that the measurements expected

to be most affected due to trace water are the preferential solvation parameters. These are the most susceptible to misinterpretation due to limitations of SLS analysis for multi-component systems in excess of 3 components. The presence of 4 or more components makes it difficult to discern which component is causing the distortion of the molecular weight in mixed solvent conditions arising from the changes in refractive indices per equation 2.8.

To address this concern, we have conducted both a theoretical and empirical assessment to explore the maximum potential impact of residual water content on the refractive index of the solvent mixtures at the maximum specification of the HPLC grade solvents. We searched the literature for experimental data[145] of the refractive indices of acetone, methanol, and water mixtures to calculate the expected change in refractive index due to the presence of residual water, with model parameters from [145] in terms of mole fractions of the solvent mixtures explored in this work, as contained in table 2.2 below:

Table 2.2: Ternary RI Model Coefficients for Acetone, Methanol, & Water mixtures [145]

	Coefficients by Polynomial Order			
Solvent	1	2	3	4
ACE	1.4306	-0.2059	0.2263	-0.0963
MeOH	1.3503	0.0757	-0.1094	0.0554
H2O	1.3573	-0.0093	0.0393	-0.0542

We calculated the refractive indices of the mixtures both with (column 6, assume x_{H_2O} at max spec limits) and without (column 7, assume $x_{H_2O} \approx 0$) the presence of water in the solvents and took the difference between these results (column 8) per table 2.3. In all cases, the presence of water would be expected to reduce the observed refractive index in the range of 3.86E-06 to 8.32E-05 RI units, with a trend of greater reductions with increasing acetone content. These effects would be expected due to the maximum of 0.2 % residual water in acetone vs 0.03 % in the case of methanol, as well as the larger relative difference in the refractive indices between acetone and

water, in comparison to those differences between methanol and water, which are much closer in value.

However, there are several key points to recognize why this would not be expected to affect our results. The maximum expected change in refractive index is very minor and is almost an order of magnitude below the rated sensitivity limits of our refractometer (2E-04), which is thus expected to be below the limits of detection in our experiment. Additionally, this example assumes the worst case conditions – specifically, that the water content was at or near the specified maximum within the solvents, and that the water must be partitioned fully in one phase or the other to maximize the change in refractive index on the impact to the preferential solvation parameter. This is highly unlikely as water interacts favorably with all components in solution (acetone, methanol, PVP), with the exception of naproxen – though naproxen is present in limited amounts and only present as a cosolute in methanol, which had the least expected water content. This analysis indicates that we should not expect any meaningful impact on this study due to residual moisture.

Table 2.3: Comparison of theoretical RI differences with and without the presence of residual water for the studied solvent mixtures

Assume $X_{H_2O} = 0$		Assume X_{H_2O} at max			Refractive Index Results		
X_{MeOH}	X_{ACE}	X_{MeOH}	X_{ACE}	X_{H_2O}	w/ H_2O	w/o H_2O	Δn_D
1.000	0.000	0.99947	0.00000	0.00053	1.32700	1.32700	-3.86E-06
0.900	0.100	0.89914	0.09973	0.00112	1.33391	1.33390	-7.00E-06
0.845	0.155	0.84404	0.15451	0.00145	1.33686	1.33685	-1.39E-05
0.800	0.200	0.79890	0.19939	0.00171	1.33893	1.33891	-2.10E-05
0.700	0.300	0.69874	0.29895	0.00230	1.34260	1.34256	-3.82E-05
0.645	0.355	0.64381	0.35356	0.00263	1.34420	1.34415	-4.70E-05
0.600	0.400	0.59867	0.39844	0.00289	1.34535	1.34530	-5.33E-05
0.500	0.500	0.49868	0.49783	0.00348	1.34752	1.34746	-6.41E-05
0.400	0.600	0.39878	0.59715	0.00407	1.34936	1.34928	-7.20E-05
0.300	0.700	0.29896	0.69638	0.00466	1.35101	1.35093	-8.32E-05

To support these theoretical outcomes with experimental confirmation, we next dried the methanol and acetone solvents using freshly activated 3Å molecular sieves

added at 20% m/v ratios and measured the refractive indices of the solvent mixtures after 24 and 48 hours exposure for comparison to the as received solvents (i.e. 'wet'), with results below:

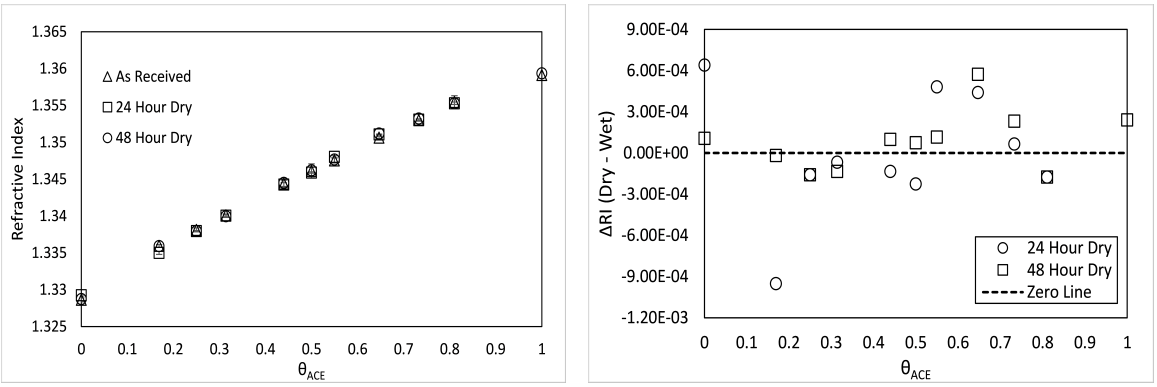

(a) **(b)**

Figure 2.8: Refractive index results from a) the as-received solvents, and after 24 and 48 hours exposure to 20 % w/v 3Å molecular sieves and b) changes in refractive index in comparison to the as-received solvents

Per a) in figure 2.8, we can observe no obvious change in the refractive indices after exposure to molecular sieves for 24 and 48 hours. To explore any potential differences more closely, the observed changes in refractive indices after 24 and 48 with respect to the as received solvents were plotted in panel b). There is no negative trend with acetone content as would be expected from the theoretical analysis ; nor is there otherwise any meaningful differences in general with respect to exposure time to the molecular sieves. Taken together, we believe these data demonstrate that any potential effects of residual moisture are negligible and below the limits of detection in this study. As such, evaluation of these systems by SLS and related refractometry results follow in figures 2.9, 2.10, 2.11, and 2.12.

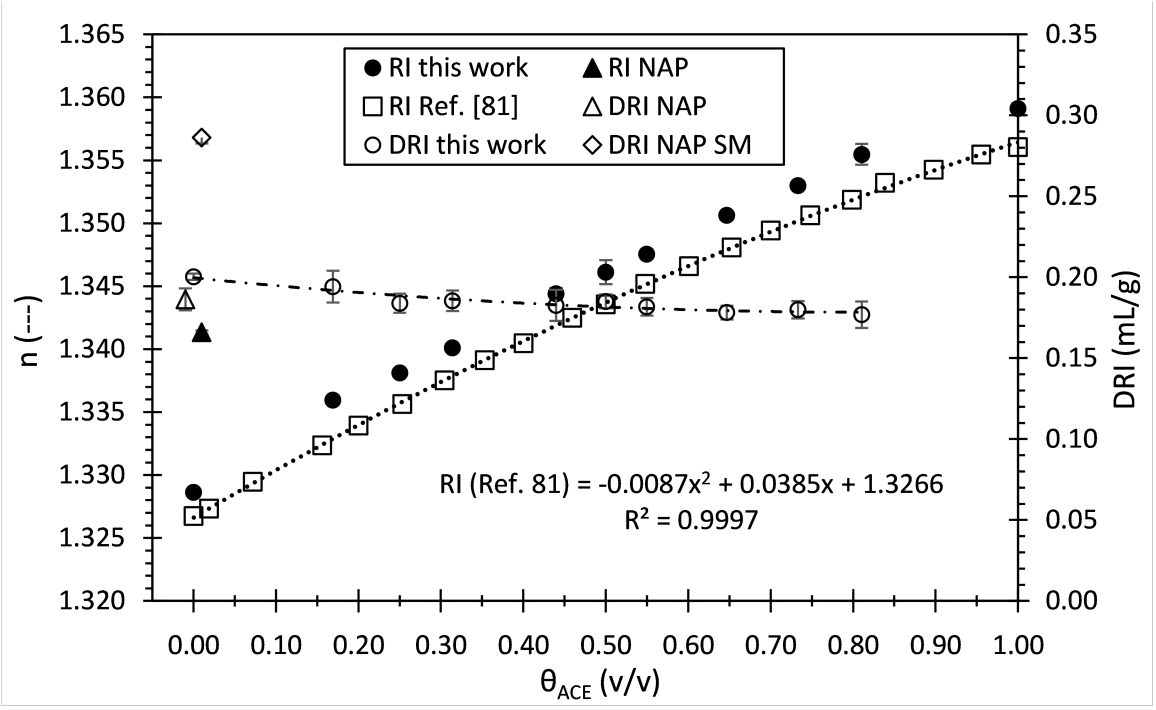

Figure 2.9: RI results of NAP in methanol without PVP (▲), and acetone-methanol solvent mixtures from this work (●), in which the trends agree well, though elevated in comparison to reference [146] (□). The RI differences observed are attributable to conducting measurements at room temperature rather than 25 °C, due to lack of temperature controls on the RI instrument. DRI results of NAP in methanol without PVP (⧫), PVP solutions at varying θ_{ACE} content (○), and PVP in the presence of NAP in methanol (△). Error bars are standard deviations for RI measurements and 95% confidence intervals for DRI results.

The DRI of PVP in the reference solution and of NAP in methanol were determined from the slopes of the refractive index (RI) vs. concentration plots. The DRI of acetone in methanol as a function of θ_{ACE} was extracted from data in reference [146] due to the greater precision of their measurements. Per figure 2.9, the refractive index trends of acetone-solvent mixtures aligns well with prior literature results from reference [146], though our absolute values are somewhat elevated. This is most likely from conducting measures at room temperature conditions of ≈ 21°C instead of 25°C due to lack of available temperature control instrumentation. This is not expected to have a substantial impact on the DRI measures (i.e. slopes) required for determination of preferential solvation effects and the relative % errors achieved ranged within

an acceptable 0.97-5.27 %. The DRI of PVP decreases with increasing acetone and naproxen content which is expected as both have refractive indices closer to PVP than that of methanol such that the addition of polymer has less of an impact on the overall solution refractive index. Despite this loss in scattering contrast, the polymer DRIs are all well above the minimum recommendation of 0.100 ml/g required for good signal to noise in support of SLS studies. [130].

An example SLS plot of PVP in methanol is shown in figure 2.10. Notably, the M_w and B_{22} parameters must be derived from only the dilute linear portion of the SLS plot per the truncated form of equation 2.7:

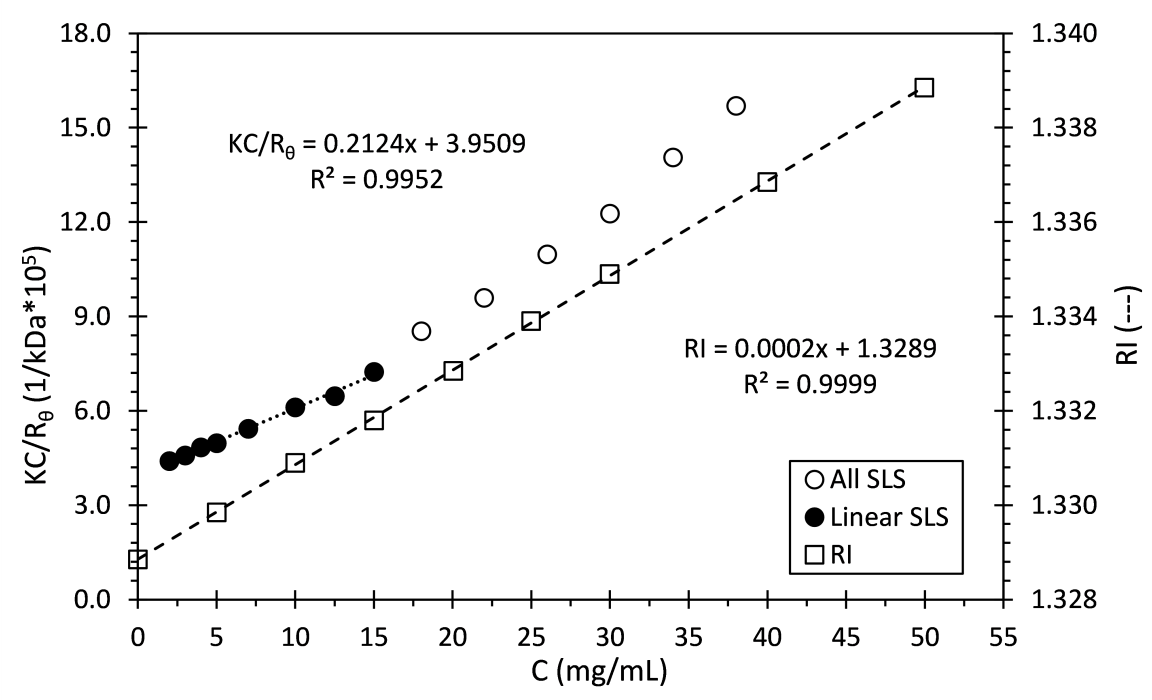

Figure 2.10: Example SLS and DRI (□) plots vs PVP concentration in methanol. SLS parameters are extracted from the dilute linear region (•) prior to onset of nonlinear behavior (○) attributable to higher order virial terms.

These results are extended to all solvent mixtures explored and captured in 2.11. Per figure 2.11, the apparent M_w^* and B_{22}^* behavior as a function of θ_{ACE} does not follow an obvious trend, similarly rising and falling at various acetone amounts with a surprisingly greater M_w^* when in the presence of naproxen. These deviations from the

true M_w are related to the extent of preferential solvation and the DRI for acetone ($\approx 0.02 - 0.04 \pm 0.00068$) and naproxen ($0.286 \pm 0.0038$) in methanol respectively, per equation (2.10). As the DRI of naproxen is much greater compared to acetone, this can result in a substantial shift of M_w^* even for comparatively smaller preferential solvation effects. This impact of a large cosolute DRI on the observed M_w gives rise to questions about the validity of equation (2.11) in the determination of the true B_{22}. This relation implies that even in conditions of minor preferential solvation, a substantial change in solvent quality would result, which does not seem an appropriate conclusion.

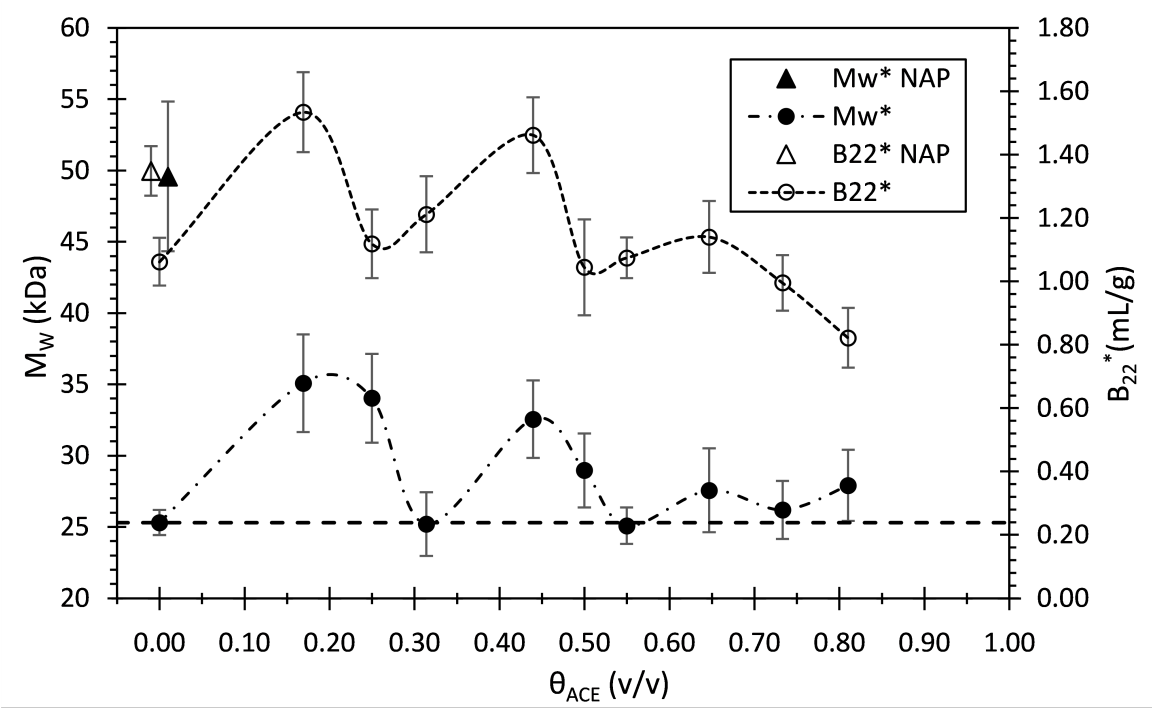

Figure 2.11: Summary B_{22}^* (∘ w/o, △ w/ NAP) and M_w^* (• w/o, ▲ w/ NAP) results vs θ_{ACE}. The horizontal dashed line represents true M_w determined from pure methanol solvent that serves as a reference of the extent of preferential solvation. Remaining dashed lines are a trace included as an aid to the eye. Solvent quality trends lower with increasing acetone except for maxima located at 17 and 44% θ_{ACE}. It also rises substantially in the presence of NAP, in contrast to DLS and DSV observations. Strong preferential solvation effects are indicated at 17, 25, 44, and 50% θ_{ACE} as well as in the presence of NAP as evidenced by M_w^* observations that differ significantly from the true M_w.

Furthermore, if the addition of a cosolute to a binary polymer-solvent system

results in the preferential exclusion of the solute, as demonstrated here by the positive λ for NAP when added to PVP in methanol, one would expect that the addition of such a cosolute would reduce the solvent quality - otherwise, it would not be excluded. It is clear that in cases where the DRI of the cosolute of interest is very large, the shift in M_w^* (per 2.10) may be more attributable to the rate of the refractive index changes of the bulk composition rather than to the magnitude of change in solvent quality arising from preferential solvation. This implies that for large DRI of cosolute in the absence of the macromolecule, this relationship may no longer be appropriate and may be worth further investigation to resolve, which is beyond the scope of this work.

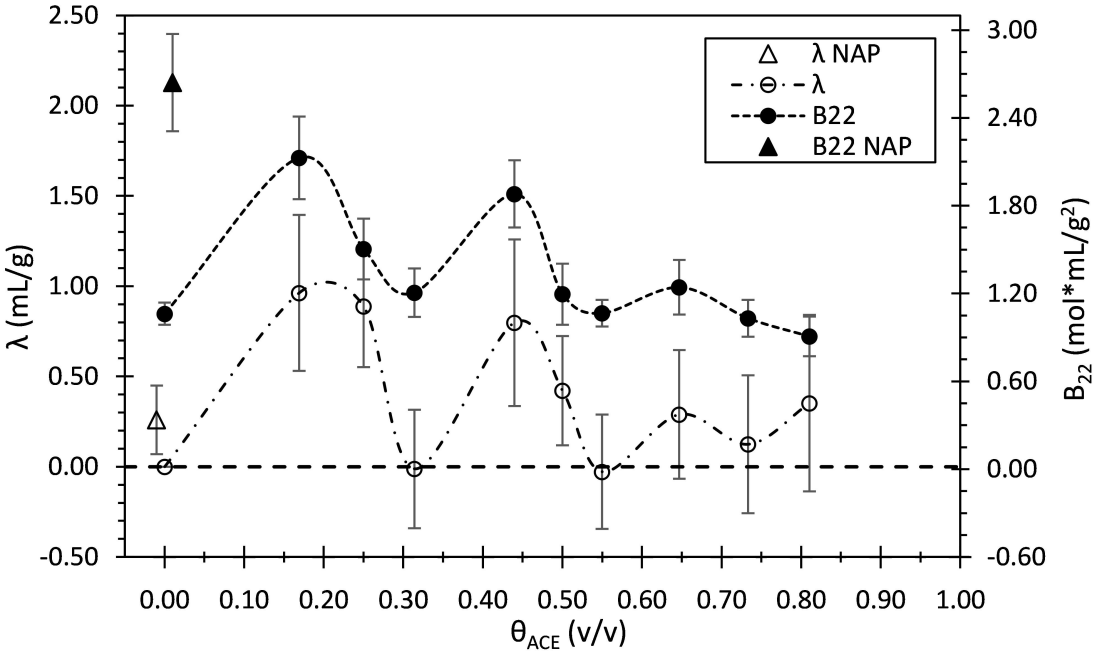

Figure 2.12: Summary B_{22} (• w/o, ▲ w/ NAP) and λ (∘ w/o, △ w/ NAP) results vs θ_{ACE}. The general trend of loss in solvent quality with increasing acetone is observed, except for those conditions which exhibit strong preferential solvation. Naproxen is excluded from the local polymer environment when co-dissolved in methanol. Horizontal dashed line is the condition $\lambda = 0$, from which deviation demonstrates the extent of preferential solvation effects. $\lambda \geq 0$ indicates exclusion, ≤ 0 indicates solvation. Other dashed lines are a trace included as an aid to the eye.

From the measured DRI and M_w, λ and true B_{22} values were calculated per equations (2.11) and (2.10) and plotted in figure 2.12, where the two parameters track the behavior of the apparent results closely. Acetone is either excluded from the local polymer environment, as indicated by positive preferential solvation coefficients at varying θ_{ACE}, or the compositions of the bulk solution and pervaded volumes are near equivalent for conditions where λ is not significantly different from zero. Interestingly, both λ and B_{22} were found to have local minima at $\approx 30\%$ and 55 % volume fractions (or $\approx$ 4:1 and 3:2 moles of methanol to acetone respectively) which corresponds with the prior conditions of sharp changes with collapsing polymer conformation and/or reduction in solvent quality per the DLS results. Similarly those conditions with positive λ at 17, 25, 44 and 50% volume fractions are generally consistent with greater or increasing size and solvent quality observed by DLS. As PVP and acetone are well known to have unfavorable interactions, the exclusion of acetone in favor of excess methanol improves the relative solvation of the polymer. These results demonstrate the explanatory power of preferential exclusion in understanding the non-intuitive changes of polymer-solution interactions identified initially by DLS.

Naproxen is likewise excluded in the presence of methanol, though not as strongly as acetone at some conditions, despite the large M_w shift previously described. This is an important finding as it provides an additional mechanistic reasoning for the reduced stability of spray dried naproxen-PVP dispersions arising from solutions containing methanol as demonstrated previously in the literature [15]. Ideally, knowledge of naproxen preferential solvation/exclusion would be known as a function of θ_{ACE} in quaternary solutions as well. Unfortunately this SLS technique is not suitable for the discernment of preferential solvation for solutions containing more than three components due to the inability to determine which components, either in whole or in part, are responsible for the shift on molecular weight arising from changes in polymer solution DRIs, per equation (2.8).

However, as the literature [15] observed improved physical stability of those dis-

persions prepared with increasing acetone content, this may imply that the drug becomes less excluded or even preferentially solvated as the volume fraction of acetone increases. The role of solvent interactions in driving such behavior may be understood due to the ability of the solvent systems to either maintain or disrupt strong self-associations of naproxen. Naproxen has been found to preferentially form dimers in proton donating solvents (i.e. methanol), while proton accepting solvents (i.e. acetone) substantially reduces the prevalence of these dimers in solution [147] - these observations may also help explain why naproxen exhibits a 2-3x greater solubility in acetone than methanol [142]. Naproxen dimer formation in the presence of high methanol content may likely prevent the ability to develop strong interactions with the hydrogen-bond accepting groups of the polymer. If such self-association behavior is the source of naproxen preferential exclusion, it may be likewise appropriate to frame this interaction instead as the exclusion of the polymer from the local environment of the API in favor of naproxen-naproxen contacts. As the solvent system is modified with increasing acetone to disrupt this behavior, then naproxen may be more readily available to maximize drug-polymer contacts within the pervaded volume, which can then aid in the development of a more homogeneous and stable spray dried dispersion.

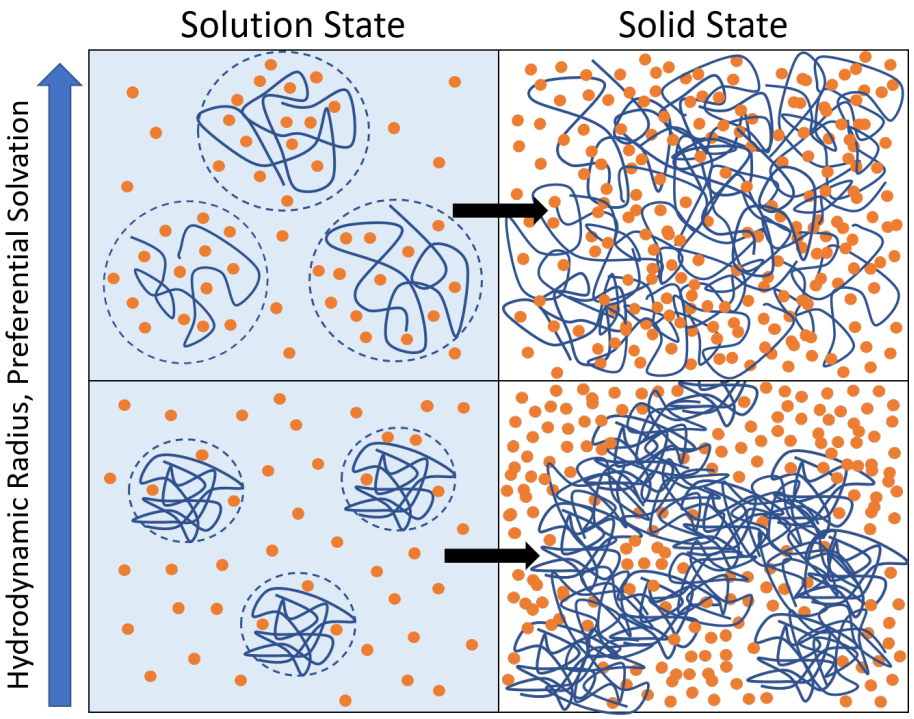

Figure 2.13: Illustration of potential effects of R_H and λ on post-processing SDD solid-state homogeneity. Polymer swelling and preferential inclusion of drug in the local polymer environment may lead to improved product uniformity and stability.

Per figure 2.13, a qualitative illustration has been constructed to describe the potential combined roles that both polymer conformation (i.e. hydrodynamic size) and drug preferential solvation may play in controlling the homogeneity and physical stability of spray dried dispersions. This image shows that polymer conformation alone may not tell a sufficiently detailed story of solution state behavior, while the consideration of preferential solvation can help add rich context in understanding the prevalence and strength of drug-polymer interactions in solution. One can imagine solvent conditions where even though solubility of drug and polymer might be maximized in support of processing needs, poor dispersion stability may result - either by drug-solvent interactions dominating drug-polymer interactions such that the polymer may be excluded and therefore collapse, or by polymer-solvent interactions which dominate drug-polymer interactions such that the drug is instead excluded from the local polymer environment; or from some combination of these effects that either way

reduces the strength of net drug-polymer interactions and places a risk on the critical quality and performance attributes of the drug product.

2.5 Conclusions

In this work we have demonstrated that the evaluation of dilution series and conducting accurate viscometry measurements are important to ensuring the appropriate interpretation of DLS studies. The diffusion interaction parameter, k_D, has been highlighted as a readily accessible and potentially sensitive solvent quality indicator useful for understanding drug-polymer-solvent interactions in spray dried dispersion solutions.

Strong preferential solvation was found to correlate with conditions of unexpected and out-of-trend behavior that were observed in the DLS studies. The solvent ratios where acetone was found to be preferentially excluded were consistent with outcomes indicating improved solvent quality and polymer size, revealing its potential utility as a mechanistic explanation for understanding solution-state properties in complex media. Importantly, naproxen was likewise found to be preferentially excluded in pvp-methanol solutions, in agreement with DLS outcomes and aligning with a prior report in the literature [15] of poor naproxen-PVP dispersion stability when sprayed out of methanol.

Overall, PVP is found to consistently exhibit complex non-intuitive behavior in mixed solvent and solvent-solute systems across a variety of light scattering techniques. These findings underscore the need for a greater understanding of the implications of preferential solvation and related solution-state parameters in the design of multi-component systems that are inherent to spray-dried and solvent-based dispersion processing.

2.6 Future Work

Extension to systems of four or more components

Notably, recent work by Calero-Rubio et al. [148] provides an experimental technique capable of overcoming the short comings of light scattering with respect to preferential solvation, which is limited in the characterization of systems of no more than three components. Their method leverages the application of inverse Kirkwood-Buff solution theory combined with highly precise density measurements in order to describe the preferential interactions of specific cosolutes with macromolecules in solutions containing any arbitrary number of constituents. This approach should be similarly applicable to spray drying feed solutions and other solvent based processing methods, offering a promising future for the exploration of solution state properties in amorphous dispersions.

Assessing the translation to the solid-state

Once drug-polymer interactions in the solution state are well understood, preparation of the solid state dispersion can be conducted via the spray drying process. By varying the solvents used, droplet size distributions, evaporation rates, and phase behavior will be impacted during the drying process as previously described in chapter 1. As such, each solvent system should be well understood and characterized to allow for standardization of these effects as best as possible, to support the meaningful comparison when spraying out of different solvent conditions. Droplet size distributions can be measured by laser diffraction and atomization parameters tuned until systems produce equivalent distributions. Evaporation rates can be controlled by varying process gas temperature and flow rates. Phase behavior can not be well controlled due to the material and composition dependence nature of these effects. However, the effects of varying phase behavior can either be quantified by the development of multi-component phase diagrams and/or operating at very rapid evaporation rates to

minimize the extent of phase effects during the drying process. It is likely useful to explore a range of evaporation rates for each solvent system to better understand interactions between evaporation and homogeneity of resulting dispersions as a function of solvent composition.

Characterization of the nano-scale miscibility of solid state dispersions is no simple task. However recent progress in the fields of solid-state NMR techniques offer promise in better understanding miscibility limits of solid dispersions [149, 150]. Furthermore, the use of solution calorimetry in solid dispersions pioneered by the Marsac lab, has been utilized to directly measure the strength of drug-polymer enthalpic interactions in the solid state which can be used to assess relative interactions between dispersions prepared out of different solvents or process conditions [151]. Lastly, additional techniques holding great promise for the detailed characterization includes scattering technologies such as small angle neutron and x-ray scattering (SANS, SAXS). Both techniques offer sub nanometer resolution of material properties including polymer conformation and drug preferential solvation in the solid-state by SANS through analogous measures as to those conducted by light scattering or density (i.e. compositional) uniformity by SAXS [152, 153]. SANS is a niche technique that requires a synchrotron radiation source for operation which limits its broader utility as well as required deuteration and/or carbon-13 labeling of system components to provide scattering contrast for analysis [153].

CHAPTER 3: APPLICATION OF VISCOMETRY TO ASSESS DRUG-POLYMER-SOLVENT INTERACTIONS IN SDDS LIQUID FEEDS

This chapter is a modified reproduction of a portion of the paper by Defrese et al. (2020), reprinted (adapted) with permission [30]. Copyright (2020) American Chemical Society.

3.1 Introduction

Analysis of polymer solutions by dilute solute viscometry (DSV) is a classical technique originating from the early days of macromolecular science. Viscometry produces data that is both complimentary and orthogonal to light scattering measurements, and is commonly utilized in tandem for the comprehensive characterization of polymer solutions. In conjunction with a concentration detector (UV or RI detector) and size exclusion chromatography (known as triple detection SEC), the combination of these techniques are still among the state of the art for the characterization of industrial polymers. DSV allows for the determination of parameters such as the intrinsic viscosity ($[\eta]$) and Huggins' coefficient (k_H), which are analogous to the hydrodynamic radius (R_H) and solvent quality parameters (k_D , B_{22}) identified by light scattering.

Relative to light scattering, viscometry approaches offer some practical upsides. Notably, light scattering equipment can be cost prohibitive for many labs (typically ranging from $30-100k) and sample preparation is often very tedious due to the need for stringent removal of particulate impurities and thorough cleaning protocols. Light scattering samples are ideally prepared in a clean room environment to minimize risk for additional contamination of particles introduced from the laboratory environment.

In comparison, viscometry samples are much more forgiving, and quality instrumentation for the purpose of intrinsic viscosity measurements ranges from the low hundreds to low tens of thousands of dollars. While the highest quality rheometers can easily approach or exceed light scattering costs, there are not necessary for most applications. A major drawback for rheometry is that molecular weights of samples are determined on a relative basis rather than on an absolute basis as is the case with light scattering [75]; which can limit the value of some measurements and/or require additional measurements for the development of robust calibration curves.

This purpose of this chapter is to establish the preferred methods for the viscometric analysis of spray dried dispersion solutions and compare these outcomes to those found by light scattering. As such, we have evaluated the systems previously explored in chapter 2 by DSV to validate the findings from light scattering as well as explored additional systems of PVP in dichloromethane-acetone solvent mixtures which have been of interest in the literature [15].

3.2 Theoretical Background

Intrinsic viscosity is classically determined from viscosity measurements conducted on a dilution series that are treated according to the truncated empirical Huggins and/or Kraemer functions with extrapolation to zero concentration and shear rates[75]:

$$[\eta]_{red} = \frac{\eta - \eta_s}{\eta_s c} = [\eta] + k_H[\eta]^2 c + ... \tag{3.1}$$

$$[\eta]_{inh} = \frac{ln(\eta/\eta_s)}{c} = [\eta] + k_K[\eta]^2 c + ... \tag{3.2}$$

$$k_K = k_H - \frac{1}{2} \tag{3.3}$$

where $[\eta]_{red}$ is the reduced viscosity, η is the viscosity of the solution, η_s is the viscosity of the pure solvent or reference solution without dissolved macromolecule viscosity, $[\eta]_{inh}$ is the inherent viscosity and k_K is the Kraemer's coefficient.

Physically, the intrinsic viscosity captures the contribution of a solute to the viscosity of a solution and is related to the shape and size of the solute in solution [75, 130]; while the Huggins' coefficient is the second virial coefficient arising from the virial expansion of the solution viscosity under low concentrations, just as was done with respect to the DLS and SLS analysis for k_D and B_{22}, respectively. The Kraemer function is derived from the Huggins' equation, through the rearrangement of viscosity terms, then taking the natural logarithm of the entire function and substituting an expansion of the logarithm on the right side of the equation, which produces an analogous structure to the Huggins' treatment [75]. Traditionally, $[\eta]$ and k_H are determined using both equations as a form of quality control, such that if they agree - then the results are valid; otherwise lower polymer concentrations should be used and the analysis repeated until the results are consistent across both approaches [75].

An additional concern with DSV measurements is understanding and mitigating the effects of shear experienced by the particles during the course of the measurement. Polymer solutions are well known to exhibit a range of possible non-Newtonian behaviors (i.e. non-linear change in viscosity with variable shear rates), including most prominently shear-thinning (negative deviation with increasing shear) and shear-thickening (positive deviation with increasing shear) phenomena. Ideally, determination of $[\eta]$ and k_H should be conducted at multiple shear rates to rule out non-Newtonian behavior and/or extrapolated to the zero shear rate to prevent these affects on the DSV analysis.

With $[\eta]$ reliably known, we can then calculate a viscometric analog of the hydrodynamic radius, R_η for direct comparison to the DLS results [130]:

$$R_\eta = (\frac{3[\eta]M_w}{10\pi N_A})^{(1/3)} \tag{3.4}$$

Where M_w is the polymer molecular weight and N_A is Avogadro's constant. It should be noted that R_η is not derived from an absolute measure of polymer size, but is relative to the thermodynamic quality of the solvent in which it is measured. This results in the expectation of the viscometric radius to be less than or equal to the

hydrodynamic radius R_H determined by light scattering, i.e. $R_\eta \leq R_H$. R_η will increase in similarity to R_H as the Mark-Houwink-Sakurada (MHS) solvent factor approaches unity, which is generally a rare occurrence [130, 154].

Wolf's Intrinsic Viscosity

A limitation of the Huggins and Kraemer approaches for measuring intrinsic viscosities is that for strongly electrostatic self-interactions, these traditional treatments are not appropriate. To address this limitation, B.A. Wolf derived a relationship for the intrinsic viscosity starting from the condition that the solution viscosity is a function of state and incorporating additional parameters to describe the behavior of charged macromolecules in solution [155]:

$$ln(\eta/\eta_s) = \frac{c[\eta] + Bc^2[\eta][\eta]^\bullet}{1 + Bc[\eta]} \tag{3.5}$$

$$B = \frac{0.5 - k_H}{1 - ([\eta]^\bullet/[\eta])} \tag{3.6}$$

where B is a system specific constant and $[\eta]^\bullet$ a parameter which accounts for electrostatic effects on hydrodynamic parameters with varying ionic strength, which is further assumed to be zero for uncharged solutes. This equation is a generalized solution that has been shown to correctly determine the intrinsic viscosity for both uncharged and charged polymers under a variety of ionic strength conditions [155, 156, 157, 74].

Xiong et al. then demonstrated that the Wolf plot produces reduced error in comparison to the traditional Huggins approach and is also more suitable for a wider range of polymer types including uncharged polymers, polyelectrolytes with and without salt cosolutes, copolymer blends, and star-branched polymers. In order to probe whether the Wolf plot maintains improved precision of parameter estimates under mixed solvent conditions, we have likewise analyzed our viscometry data with both the Huggins and Wolf techniques for comparison. The linearized Wolf plot as simplified for uncharged polymers (adapted from [155]) follows:

$$\frac{1}{ln(\eta/\eta_s)} = \frac{1}{c[\eta]} + B \tag{3.7}$$

$$B = 0.5 - k_H \tag{3.8}$$

Lastly, just as preferential solvation of the cosolvent/solute (λ_i) impacts static light scattering results as discussed in chapter 2, so also are the apparent intrinsic viscosities $[\eta]^*$ and Huggins coefficients k_H^* likewise affected. Caparros and Bohdanecky derived corrections for preferential solvation of ternary systems as revealed through the changing viscosity of the bulk reference solution with varying macromolecule concentration (adapted from [132]):

$$[\eta] = [\eta]^* - \frac{\lambda_i (d\eta_s/d\theta_i)_0}{\eta_s} \tag{3.9}$$

$$k_H = k_H^* \frac{([\eta]\eta_s + \lambda_i)^2 - \lambda_i \eta_s [(d[\eta]/d\theta_i) + [\eta](d\eta_s/d\theta_i)_0]}{[\eta]^2 \eta_s} \tag{3.10}$$

where $(d\eta_s/d\theta_i)_0$ and $(d[\eta]/d\theta_i)_0$ are the differentials of the reference solvent mixture or solution viscosity in the absence of the macromolecule and the intrinsic viscosity with respect to the i^{th} (i.e. cosolvent/solute) volume fraction respectively. It should be noted that to determine the true Huggins coefficient in multi-component solutions within any reasonable confidence requires highly precise measures of preferential solvation as well as the $(d\eta_s/d\theta_i)_0$ and $(d[\eta]/d\theta_i)_0$ terms, which may often be experimentally challenging.

3.3 Materials and Methods

Polyvinylpyrrolidone K25 (PVP) was gifted from Ashland Global Specialty Chemicals Inc. (Covington, KY). The polymer was held at 40 °C under vacuum for at least 24 hours prior to use for removal of residual water content. (S)-(+)-2-(6-Methoxy-2-naphthyl)propionic Acid (i.e. Naproxen (NAP)), $\geq$ 99.0% purity was sourced from TCI America (Portland, OR) and purchased through VWR International (Radnor, PA) and used as received. HPLC grade Dichloromethane (DCM), Methanol (MeOH), and Acetone (ACE) with maximum specifications of 0.05, 0.03, and 0.2 % (w/w) water content were purchased from VWR International and used as received. 0.02

um Whatman Anotop Syringe Filters were sourced from GE Healthcare (Chicago, IL), purchased though VWR International and used as received. The chemical structures of PVPK25 and Naproxen are shown in Figure 2.1.

Solution Preparation

All solvent mixtures and solutions were prepared by mass under room temperature conditions. Concentration series of polymer solutions were prepared independently in volumetric flasks using a previously prepared reference solvent mixture or drug solution for each selected cosolute/solvent composition. Each solution was allowed to equilibrate a minimum of 12 hours and sealed with parafilm to minimize evaporation. Solutions were then filtered 3-6 times as necessary to remove impurities prior to characterization. All samples were visually transparent and uniform, and no analyte was observed to be lost due to the filtration process.

Viscometry

The viscosity of all solvent mixtures and solutions were measured using a Rheosense microVisc Viscometer with A05 chip and temperature controller, conducted at 25.00 (+/- 0.04) °C with an equilibration time of at least 3 minutes for each new pipette, with 150 uL prime and 60 uL measurement volumes. Each solvent mixture and solution viscosity was averaged across at least 6 measurements using 2 disposable pipettes, with at least 3 measures per pipette. If large differences between averaged pipette measures were observed (> 0.015 cP), a third pipette with at least 3 additional measures was conducted and averaged to reduce variance attributable to deviations in pipette dimensions.

Non-Newtonian behavior was investigated at variable shear rates of 2500, 5000, and 7500 reciprocal seconds (1/s) for the methanol solvent system. As only shear insensitive typical Newtonian behavior was observed, extrapolation to zero shear for all solutions was considered unnecessary. Regardless, for each solution shear rates

were adjusted to the minimum suitable shear rate necessary to keep the pressures generated during measurements within the rated performance limits of the instrument to minimize any potential for shear thinning effects as possible.

Data Analysis and Presentation

Statistical analysis and graphs prepared in excel with visualization aided by Daniel's XL Toolbox addin for Excel, version 7.3.2 [138]. All error bars represent 95% confidence intervals as determined by regression analysis unless stated otherwise. Data Thief was used for the extraction of data from graphs in the literature for comparison and analysis [139].

3.4 Results and Discussion

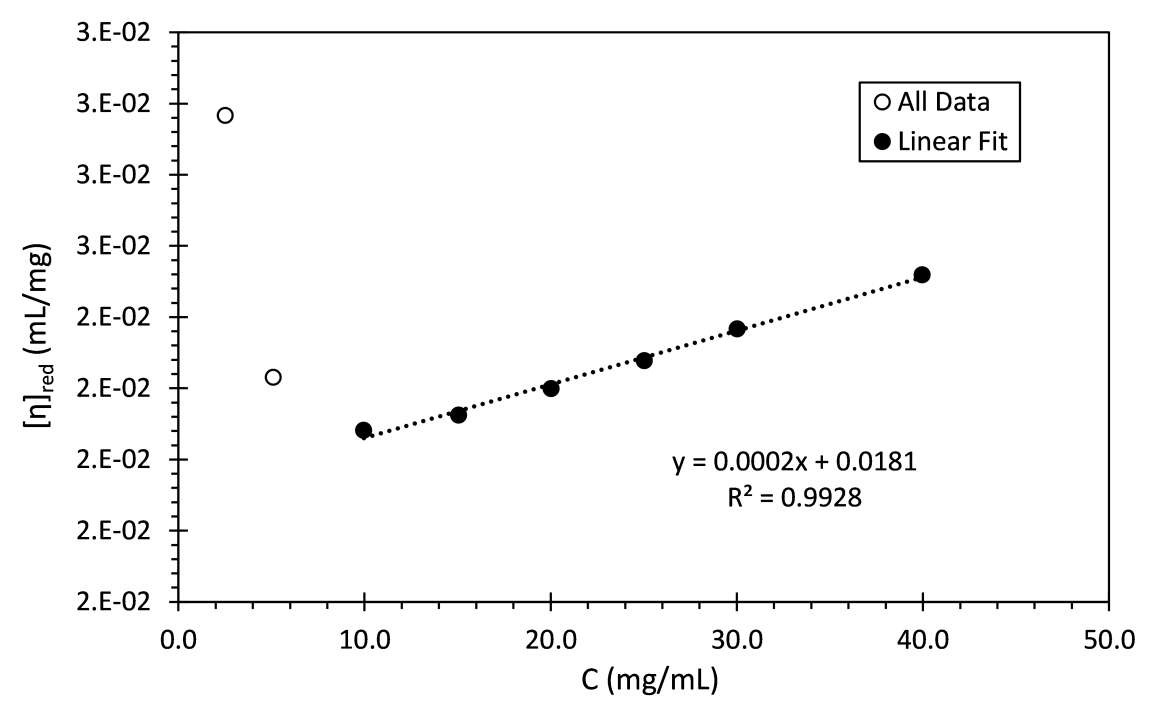

Figure 3.1: Example DSV plot of PVP in 31% θ_{ACE} solvent mixture, including the nonlinear (○) and linear regions (●) utilized for extrapolation with the Huggins treatment.

In order to characterize intrinsic viscosity and Huggins coefficients for comparison to prior DLS and SLS results, we evaluated the same concentration series of polymer solutions by DSV ranging from 2-50 mg/mL at dispersant compositions of naproxen in methanol at 4.7% θ_{NAP} (i.e. 50 mg/mL) and solvent mixtures of acetone in methanol ranging from 0-88% θ_{ACE}. Additional systems of DCM-ACE solvent mixtures were also evaluated by DSV at polymer concentrations of 2-50 mg/mL with acetone volume fractions up to 73%, as the precipitation point was found to occur at 82% acetone content in DCM (compared with 88% for the MeOH system as previously noted in chapter 2). The DCM-ACE systems were found to be unsuitable for the light scattering measurements and as such, only the DSV data for the DCM-ACE systems are presented in this dissertation.

Notably, at lowest polymer concentrations, typically occurring from 2-10 mg/mL, non-linear behavior was observed when using equation (3.1) (figure 3.1). This is attributed to the inability of the rheometer to detect meaningful viscosity differences at low absolute viscosities relative to the rate of reduction in polymer concentration when calculating the reduced viscosity (i.e. the denominator gets smaller as the numerator does not change due to lack of sensitivity). This effect results in the observation of rapidly rising $[\eta]_{red}$ values, though this is only an artifact of insufficient experimental sensitivity for these conditions. As such, those low concentrations exhibiting non-linear behavior were excluded from further analysis. Example DSV results can be seen in figure 3.2.

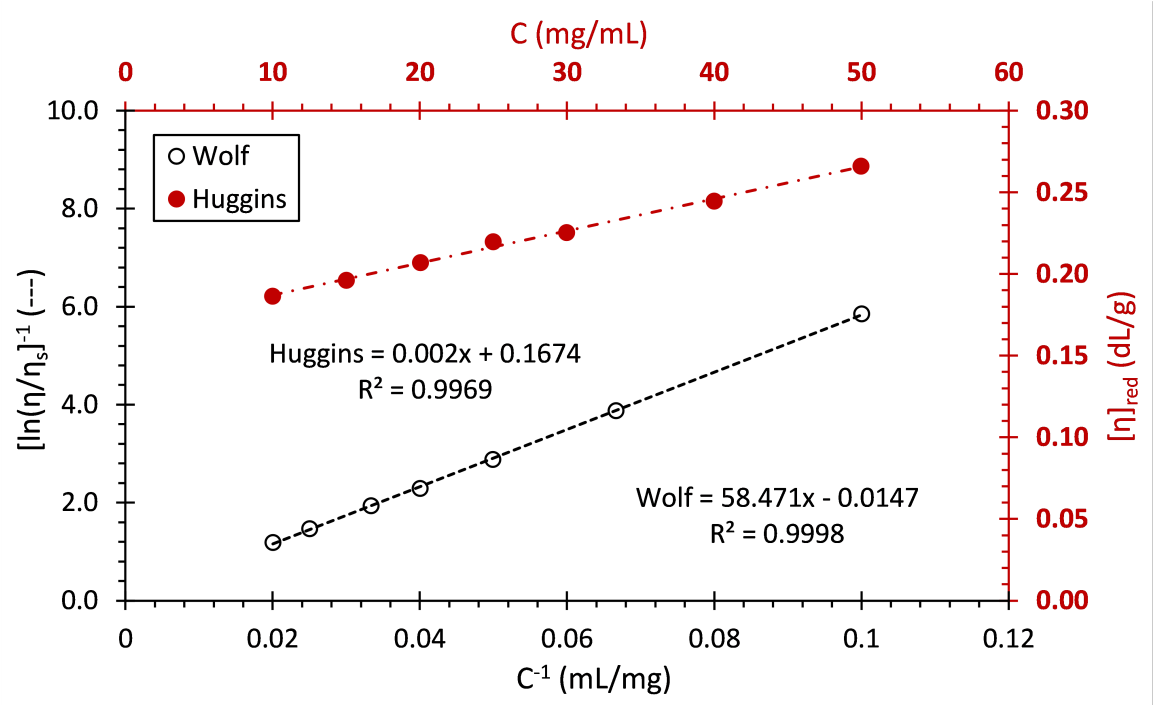

Figure 3.2: Example of viscometry functions vs concentration (or C^{-1}) for PVP in methanol with linear regression fits.

For each solvent or reference solution condition, the viscometry functions were plotted vs the polymer concentration for the Huggins treatment or the inverse concentration for the Wolf treatment, respectively per figure 3.2. Determination of the extrapolated linear intercepts and slopes were used to find the apparent $[\eta]^*$ and k_H^* according to equations (3.1), (3.7), and (3.8). To assess for the presence of shear sensitivity on the intrinsic viscosity, determination of intrinsic viscosity at shear rates of 2,500, 5,000, and 7,500 1/s were conducted for PVP in methanol solutions (figure 3.3). No meaningful effect of shear on $[\eta]$ was observed by either analysis method; and as such, only single shear rate measurements were conducted for remaining solutions.

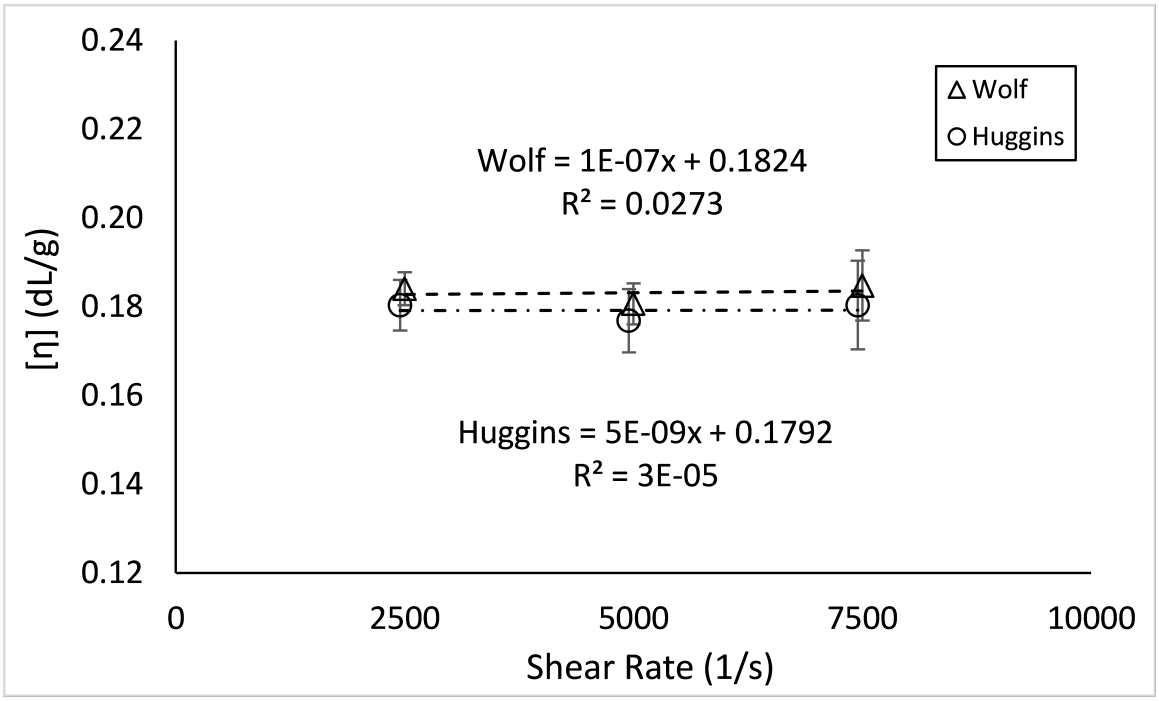

Figure 3.3: Intrinsic viscosities of PVPK25 in methanol measured at variable shear rates of 2,500, 5,000, 7,500 1/s and evaluated by Wolf (△) and Huggins (○) methods. No meaningful effect of shear is observed, demonstrating expected Newtonian behavior of dilute PVP solutions for this study.

True $[\eta]$ was then calculated from equation (3.9) to correct for preferential solvation effects observed in chapter 2 for the MeOH-ACE and MeOH-NAP systems. Only apparent $[\eta]^*$ values are presented for the DCM-ACE systems due to lack of preferential solvation parameters to correct for these conditions. Unfortunately, due to the large relative error observed for the $\frac{d[\eta]}{d\theta_{ACE}}$ terms, similar corrections to the Huggins coefficient per equation (3.10) are not experimentally meaningful and thus only k_H^* is presented for all data sets. Summary DSV results can be seen in figures 3.4 and 3.5 for the MeOH systems and figures for the DCM systems. Tables 3.1 and 3.2 contain the numerical results and quantification of analytical differences by method for the MeOH and DCM systems, respectively.

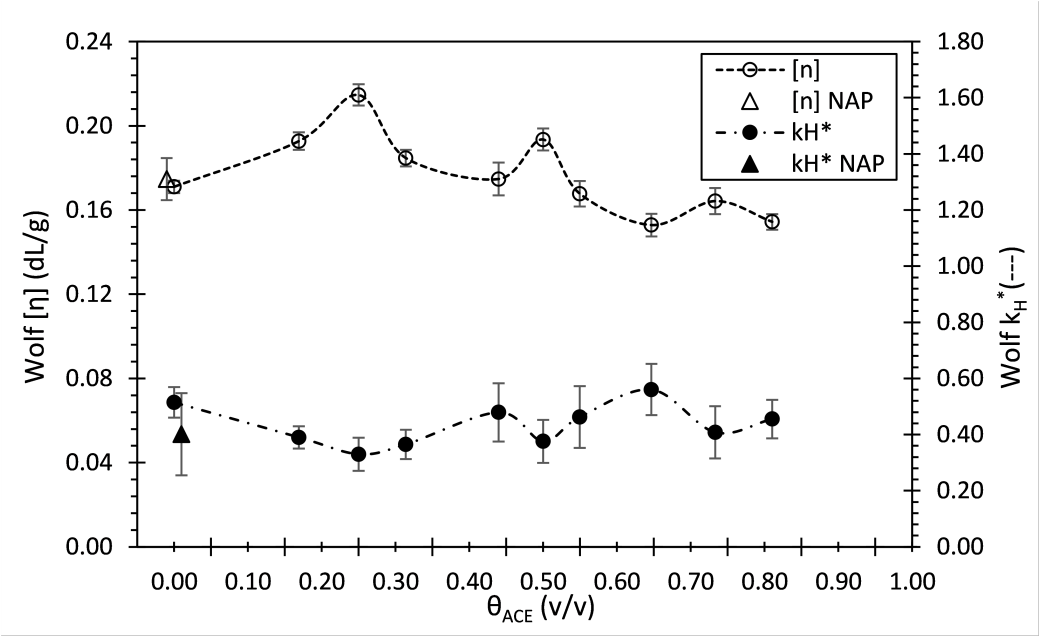

Figure 3.4: True Wolf [η] ($\circ$) and apparent k_H^* ($\bullet$) vs θ_{ACE} for PVP in MeOH-ACE and MeOH-NAP systems. $\triangle$ and $\blacktriangle$ are results in the presence of 50 mg/mL NAP in methanol. Trace lines are included as an aid to the eye. Error bars are 95% confidence intervals.

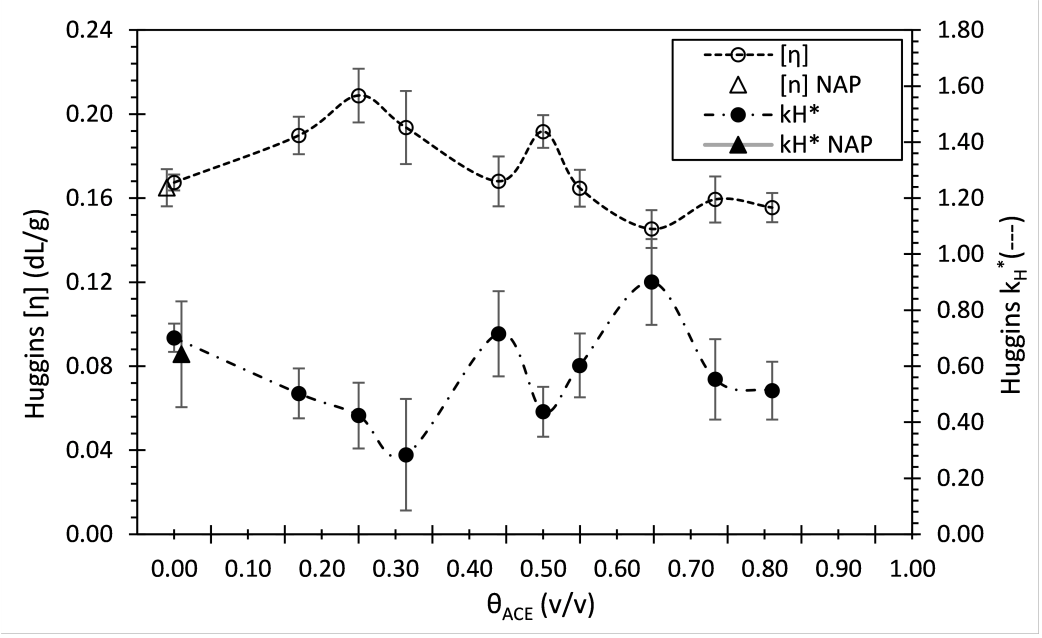

Figure 3.5: True Huggins [η] ($\circ$) and apparent k_H^* ($\bullet$) vs θ_{ACE} for PVP in MeOH-ACE and MeOH-NAP systems. $\triangle$ and $\blacktriangle$ are results in the presence of 50 mg/mL NAP in methanol for PVP in MeOH-ACE and MeOH-NAP systems. Trace lines are included as an aid to the eye. Error bars are 95% confidence intervals.

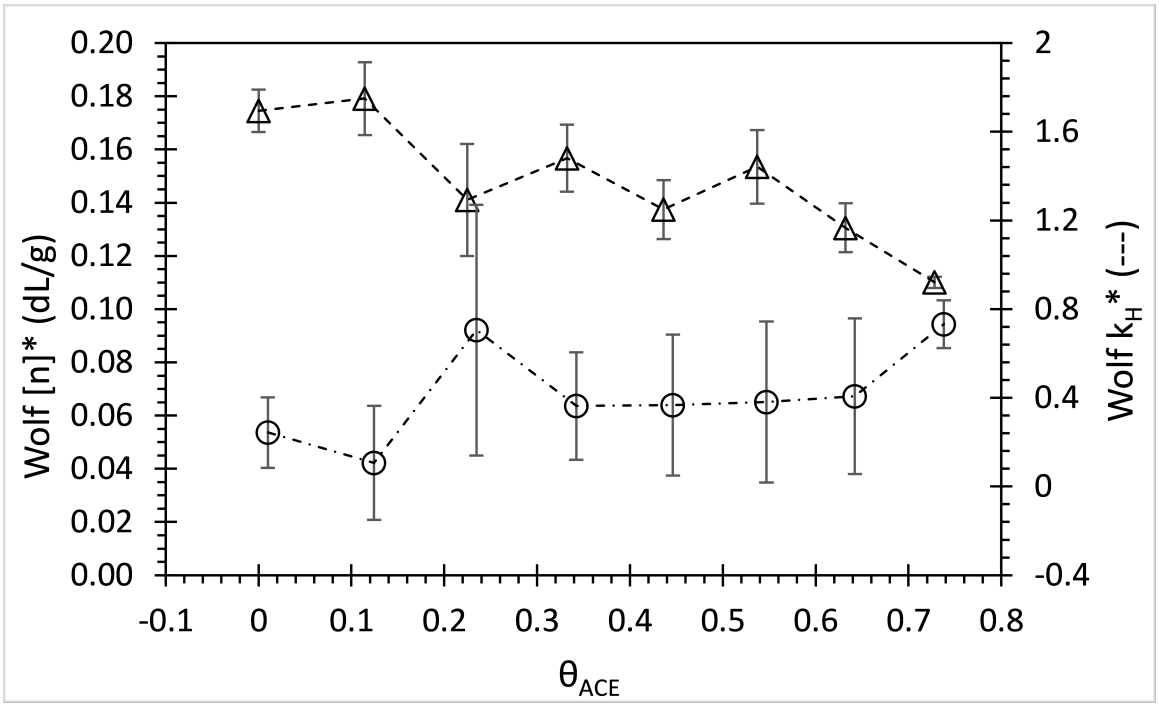

Figure 3.6: Apparent Wolf $[\eta]^*$ ($\circ$) and apparent k_H^* ($\bullet$) vs θ_{ACE} for PVP in DCM-ACE systems. Trace lines are included as an aid to the eye. Error bars are 95% confidence intervals.

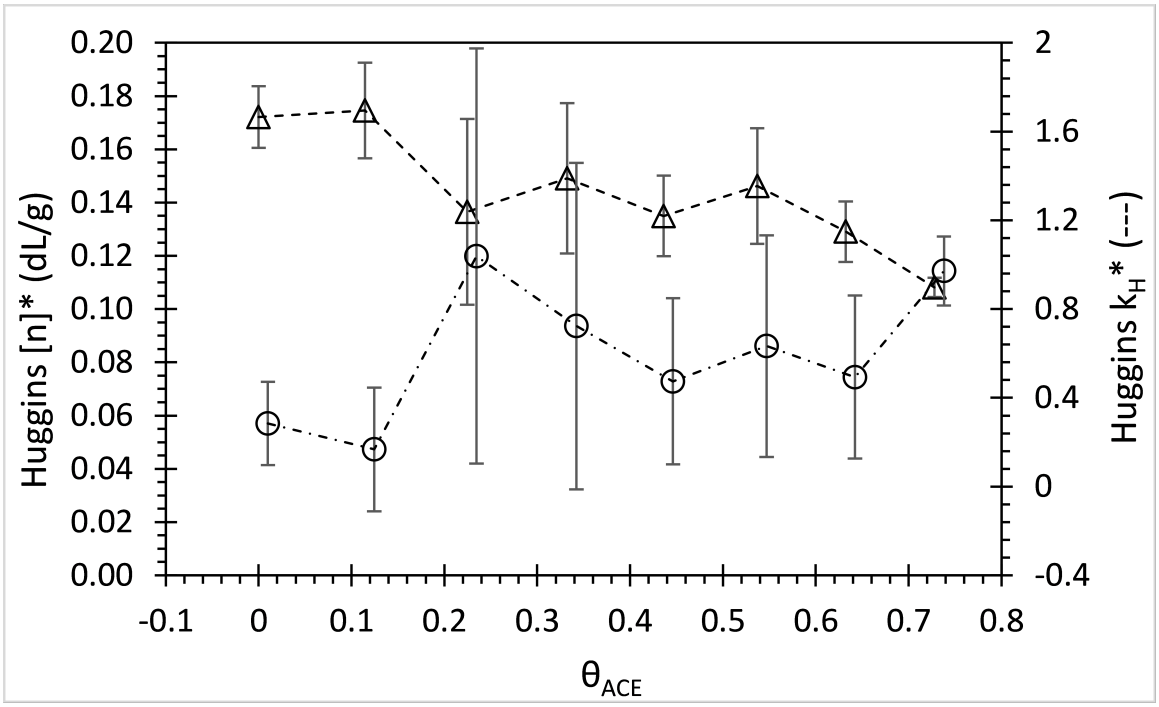

Figure 3.7: Apparent Huggins $[\eta]^*$ ($\circ$) and apparent k_H^* ($\bullet$) vs θ_{ACE} for PVP in DCM-ACE systems. Trace lines are included as an aid to the eye. Error bars are 95% confidence intervals.

In figures 3.4, 3.5, 3.6 and 3.7, it can be seen that both techniques produce similar results and trends, with two important distinctions. First, it can be visually assessed that the 95% confidence intervals for both $[\eta]$, $[\eta]^*$ and k_H^* are generally larger for the Huggins treatment in comparison with the Wolf treatment across all systems. Second, it is also clear that the Huggins values for k_H^* demonstrate a greater variation with respect to θ_{ACE}, encompassing a range of values of 0.284-0.901 compared with 0.330-0.560 for the Wolf data for the MeOH systems, while the DCM systems range from 0.167-1.039 compared with 0.107-0.732 for the Wolf data. Typically, it is expected that the k_H^* of flexible chains such as PVP should fall within 0.2-0.4 for good solvents and within 0.4-0.7 for theta and poor solvents [158] - implying that the Wolf treatment provides outcomes more consistent with theoretical expectations, even for these mixed solvent and cosolute systems. Additionally, greater error is observed in the DCM systems compared with the MeOH systems - this can be attributed to the 20-30%

Table 3.1: Wolf vs. Huggins DSV Analysis for ACE/NAP-MeOH systems

Wolf							Huggins					
θ_{ACE}	$[\eta]^*$	**±95%CI**	**%ERR**	k_H^*	**± 95%CI**	**%ERR**	$[\eta]^*$	**±95%CI**	**%ERR**	k_H^*	**±95%CI**	**%ERR**
(v/v)	(dL/g)	(dL/g)	%	(—)	(—)	%	(dL/g)	(dL/g)	%	(—)	(—)	%
0.000	0.171	0.003	1.73	0.515	0.055	10.67	0.167	0.004	2.26	0.701	0.050	7.15
0.169	0.185	.002	1.28	0.390	0.039	10.10	0.182	0.008	4.55	0.503	0.089	17.72
0.250	0.208	0.004	2.13	0.330	0.059	17.87	0.202	0.013	6.18	0.424	0.118	27.78
0.314	0.185	0.003	1.65	0.365	0.052	14.28	0.194	0.017	8.91	0.284	0.199	70.04
0.440	0.169	0.007	4.19	0.479	0.104	21.69	0.163	0.011	7.06	0.716	0.152	21.24
0.500	0.191	0.005	2.51	0.376	0.076	20.32	0.189	0.008	3.98	0.437	0.089	20.34
0.550	0.168	0.006	3.40	0.463	0.110	23.79	0.165	0.009	5.20	0.603	0.114	18.85
0.647	0.151	0.005	3.29	0.560	0.091	16.31	0.144	0.009	6.12	0.901	0.153	16.97
0.733	0.164	0.006	3.63	0.408	0.093	22.89	0.159	0.011	6.84	0.553	0.144	26.00
0.810	0.153	0.003	1.95	0.455	0.069	15.12	0.154	0.007	4.31	0.513	0.103	20.07
0 w/ NAP	0.181	0.009	4.88	0.401	0.147	36.58	0.171	0.006	3.43	0.643	0.189	29.35

	$[\eta]^*$	**±95% CI**	**%ERR**	k_H^*	**±95% CI**	**%ERR**
$\overline{\Delta(W-H)}$	0.003	-0.004	-2.56	-0.140	-0.046	-5.99
$\overline{\Delta(W-H)\%}$	2.03	-40.1	-41.8	-20.5	-31.8	-8.79

	$[\eta]$ **vs** k_H^*	$[R_\eta]$ vs R_H	k_H^* vs k_D
Wolf R^2	0.620	0.752	0.071
Huggins R^2	0.582	0.569	0.019

±95% CI are the 95% confidence intervals

%ERR values are the relative % errors of the 95% confidence intervals to the observed parameter estimates

$\overline{\Delta(W-H)}$ and $\overline{\Delta(W-H)\%}$ are the average difference and % average difference between the Wolf and Huggins treatments, respectively

lower relative viscosities of the DCM systems as these measurements are operating nearer to the sensitivity limits of the rheometer.

Per the results of the MeOH (DCM) systems listed in table(s) 3.1 (3.2), the Wolf method yielded 2 (3)% larger $[\eta]^*$ values relative to the Huggins with reduced absolute errors of $\approx$ 40 (57)%, while producing smaller k_H^* values by about 20 (46)%, with exhibits greater internal consistency with a slightly higher linear correlation R^2 between $[\eta]^*$ and k_H^* of 0.620 (0.684) vs 0.582 (0.554), per the bottom right section of the table . Importantly, the MeOH system Wolf results also align more closely with the prior DLS results, with a sharp polymer collapse and loss of solvent quality observed at 30% and >50% θ_{ACE}, as indicated by a drop in the intrinsic viscosities and rise in the Huggins coefficients, respectively. As such, it becomes apparent that the Wolf method is the better technique for understanding the systems studied in this work and offers support that it may be better suited for the study of other multi-component systems in general.

Table 3.2: Wolf vs. Huggins DSV Analysis for DCM systems

Wolf							Huggins					
θ_{ACE}	$[\eta]^*$	**±95%CI**	**%ERR**	k_H^*	**± 95%CI**	**%ERR**	$[\eta]^*$	**±95%CI**	**%ERR**	k_H^*	**±95%CI**	**%ERR**
(v/v)	(dL/g)	(dL/g)	%	(—)	(—)	%	(dL/g)	(dL/g)	%	(—)	(—)	%
0.000	0.175	0.008	4.53	0.243	0.159	65.43	0.172	0.012	6.75	0.285	0.188	66.03
0.114	0.179	.014	7.65	0.107	0.257	241.8	0.175	0.018	10.29	0.167	0.278	166.18
0.225	0.141	0.021	14.93	0.706	0.565	80.10	0.136	0.035	25.55	1.039	0.935	89.97
0.332	0.157	0.013	8.07	0.363	0.243	66.89	0.149	0.028	18.93	0.723	0.736	101.72
0.436	0.137	0.011	8.03	0.367	0.317	86.44	0.135	0.015	11.20	0.474	0.374	78.93
0.537	0.153	0.014	8.98	0.381	0.407	95.47	0.146	0.022	14.89	0.633	0.499	78.81
0.632	0.131	0.009	6.99	0.407	0.351	86.24	0.129	0.011	8.84	0.493	0.367	74.43
0.728	0.110	0.002	1.92	0.732	0.107	14.61	0.108	0.004	3.39	0.972	0.155	15.97
	$[\eta]^*$	**±95% CI**	**%ERR**	k_H^*	**±95% CI**	**%ERR**				$[\eta]$ **vs** k_H^*	$[R_\eta]$ vs R_H	k_H^* vs k_D
$\overline{\Delta(W-H)}$	0.004	-0.007	-4.84	-0.185	-0.146	8.04			**Wolf** R^2	0.684	N/A	N/A
$\overline{\Delta(W-H)\%}$	2.69	-57.5	-62.2	-46.3	-50.0	-0.466			**Huggins** R^2	0.554	N/A	N/A

±95% CI are the 95% confidence intervals

%ERR values are the relative % errors of the 95% confidence intervals to the observed parameter estimates

$\overline{\Delta(W-H)}$ and $\overline{\Delta(W-H)\%}$ are the average difference and % average difference between the Wolf and Huggins treatments, respectively

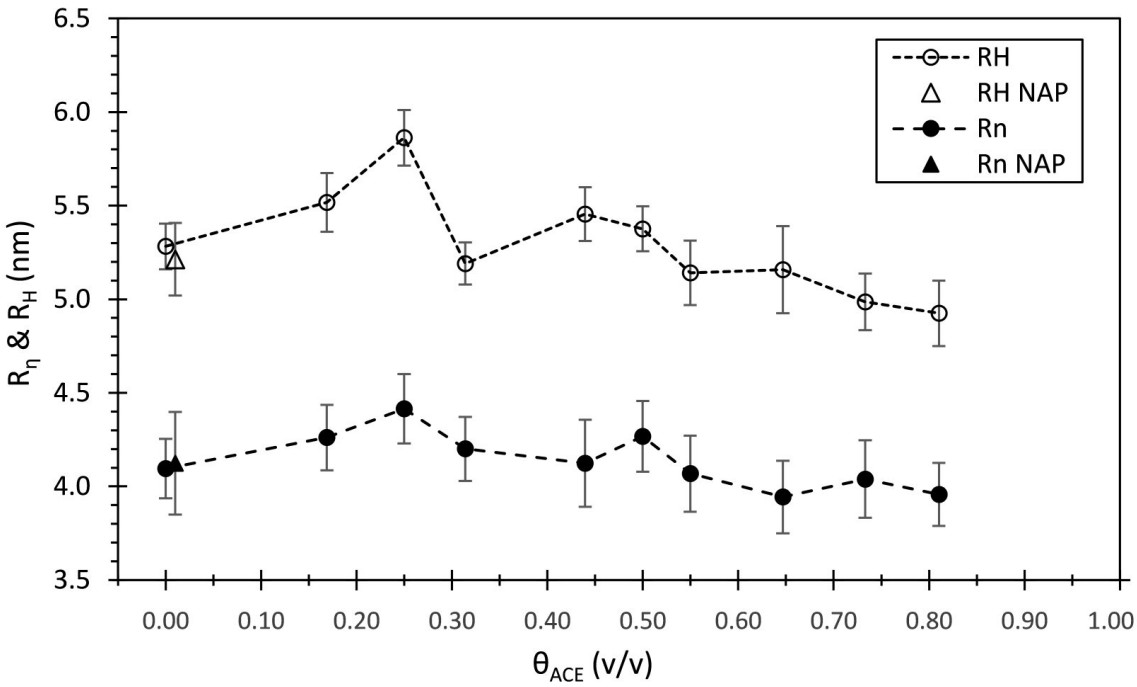

Figure 3.8: R_H (○) and R_η (●) vs θ_{ACE}. △ and ▲ are results in the presence of 50 mg/mL NAP in methanol. Viscometric radii demonstrate similar behavior to hydrodynamic radii, though on average ≈ 28% smaller in value. Trace lines are included as an aid to the eye. Error bars are 95% confidence intervals.

When we next compare the MeOH DSV results to the DLS outcomes from chapter 2, the Wolf treatment also correlates more strongly with respect to both the hydrodynamic (R_H) and viscometric radii (R_η), as well as between the DLS interaction parameter (k_D) and the apparent Huggins coefficient (k_H^*). It is worth noting how well the MeOH DSV behavior captured in figures 3.4 and mirrors the DLS outcomes presented in figures 2.3 and 2.4. $[\eta]$ demonstrates swelling of the polymer coils up to 25% acetone fraction, then contracting at 30% before swelling again near 40-50%, with further polymer collapse upon increasing acetone; with consistent inverse behavior observed for k_H^*. Similar trending behavior is observed when comparing the R_H with R_η, though increased error in R_η is observed due to uncertainty in the M_w determination (figre 3.8). No difference is observed in $[\eta]$ in the presence vs absence of co-dissolved naproxen, just as no difference was observed in R_H for the same. Notably, an apparent minor *improvement* in solvent quality is observed in the presence

of the drug cosolute with respect to k_H^* - though the difference with respect to the pure methanol solution is not statistically significant. In contrast, k_D was able to distinguish a significant loss of solvent quality when in the presence of drug, and it was similarly found to be preferentially excluded by SLS techniques. This disagreement may be due to the inability to correct k_H^* for preferential solvation effects due to limitations in sensitivity of the rheometer. Taken together, the MeOH DSV and light scattering are in good agreement and tell a story of non-obvious complex polymer behavior in the methanol-acetone and methanol-naproxen systems; though light scattering may be more sensitive to solvent quality changes for these systems.

Interestingly, the DCM systems appear to exhibit more predictable behavior in comparison to the MeOH systems, with steadily decreasing $[\eta]^*$ as θ_{ACE} increases until precipitation was observed. There does not appear to be strong instances of out of trend behavior as for the MeOH systems as observed with swelling at 25% and 40-50% acetone content. It is unfortunate that light scattering data was unable to be completed for the DCM systems, as the strong background scattering of the DCM solvent precluded the generation of high quality light scattering data at this time. Should the absence of strong preferential solvation effects be found in the DCM systems, this may help bolster the argument that such effects are responsible for the out of trend swelling behaviors found in the MeOH systems, as they correlate well with λ. For the most part, PVP appears to be in a more collapsed state in the DCM system as indicated by the generally smaller $[\eta]^*$ values measured at comparable acetone content. This suggests that DCM is not as capable of over coming the poor ACE-PVP interactions as MeOH may be for PVP and/or that DCM-ACE interactions are relatively stronger than for MeOH-ACE such that the polymer is excluded from those solvents. Per [15], the DCM-ACE systems demonstrated improved physical stability of NAP-PVP dispersions relative to those prepared out of MeOH-ACE systems. From these perspectives, we may speculate the possibility that strong DCM-ACE interactions may similarly exclude naproxen, such that polymer-drug interactions are more

favorable overall, which may then lead to more homogeneous dispersions.

3.5 Conclusions

In this chapter we have evaluated the Wolf method against traditional Huggins treatments for DSV data across a range of mixed cosolvent/cosolute compositions for PVPK25 solutions. The wolf method was found to be superior compared to the Huggins approach in terms of both relative and absolute errors while demonstrating greater internal consistency across all systems studied. The results from the Wolf method also correlated most strongly with the prior light scattering results explored in chapter 2, further supporting its likely greater accuracy and precision. We conclude that the wolf method is the preferred tool for the analysis of DSV data of mixed cosolvent/cosolute systems.

The DCM system exhibited more predictable behavior in comparison to the MeOH systems with increasing acetone content, as the polymer steadily collapsed in size as the precipitation point was reached near 82% acetone content. MeOH appears to mitigate the loss in solvent quality better than DCM for PVP with added acetone, as demonstrated by larger polymer size at similar acetone levels. The DCM data was more variable and less precise than the MeOH system, attributed to lower absolute viscosities measured near the sensitivity limits of the rheometer. Overall, the MeOH system viscometry data agreed well with the light scattering data from chapter 2, with the polymer swelling and increasing in size at the same acetone concentrations as identified by DLS results. Importantly however, the presence of naproxen was not found to have an impact on the DSV results in comparison to its absence - highlighting light scattering as a potentially more sensitive and useful technique for understanding drug-polymer interactions and/or the need for a more sensitive rheometer.

3.6 Future Work

Quantifying of drug-polymer-solvent thermodynamic parameters by viscometry

An understanding of drug-polymer-solvent interactions is often desired when studying amorphous dispersions, with important applications to both the solution and solid-state as previously discussed. In particular to spray dry processing, knowledge of all binary and ternary Flory-Huggins (FH) interaction parameters in solution would be ideal, though these parameters are often experimentally difficult to determine using classical approaches such as static light scattering, osmometry, refractive index, or head-space gas chromatography. These methods typically necessitate highly specialized knowledge and training, expensive instrumentation, tedious sampling requirements, and/or substantial material quantities. In contrast, alternative viscometric techniques are generally simple to perform and interpret, and can be executed with inexpensive equipment using relatively small sample sizes. Notably, glass viscometers offer little control over shear effects and can be quite tedious in practice, though modern instrumentation exists which are available at moderate costs (such as the Rheosense microVisc utilized in this work) to address most of these concerns.

Analytically, the connections between viscometry and FH interaction parameters have been mostly solved, though they are little appreciated or applied in the field of spray dried dispersions. Approximately 40 years ago, Kok and Rudin developed a method to relate intrinsic viscosity measurements to second virial coefficients and polymer-solvent FH interaction parameters[]. However, a major limitation of their approach is knowledge of the intrinsic viscosity of the polymer under theta solvent conditions which can add substantial experimentation if this parameter is unknown. This value can be determined using either the classical Mark-Houwink method using several fractions of varying molecular weight polymer or through the Gundiah and Kapur method, by measuring the intrinsic viscosity with increasing anti-solvent

content until the polymer phase separates, and then extrapolating $[\eta]$ with respect to the antisolvent composition to the observed precipitation point as $[\eta]_\theta$ [159, 160]. If the M_w of the polymer and the Mark-Houwink constant at theta conditions K_θ are already known, then $[\eta]_\theta$ can be easily calculated []. Unfortunately, these parameters are often unknown or unavailable to many pharmaceutical practitioners. Qian et al developed an analytical method to estimate $[\eta]_\theta$ from the intrinsic viscosity determined at a typical non-theta condition [161], though is reliability and veracity has been questioned [162]. Lastly, Xu and Qiu utilized cloud points extracted from simple titration measurements in combination with groups of candidate antisolvent-polymer and solvent-antisolvent interaction parameters derived from viscometric measurements, which were then best fit to the observed binodal curves for the accurate determination of all ternary FH interaction parameters. It is quite possible that this same approach will be applicable to drug-polymer-solvent systems and is worth further investigation.

With reliable knowledge of the theta and non-theta intrinsic viscosities, second virial coefficients and the ternary system FH parameters, a range of critical material properties can be explored in spray dried dispersions. For example, the polymer membrane literature is well aware of the relationship of the strength and compositional dependence of the solvent-cosolvent interaction parameter and resulting varieties of microstructures that develop during precipitation events. Specifically, as the polymer-solvent and/or polymer-cosolvent interaction parameters increase in favorability, the expected miscibility gap during concentration reduces and larger macrovoid structures are expected to form; in contrast where solvent-cosolvent interactions are increasing in favorability, then a more porous sponge-like structure is expected as the miscibility gap increases with precipitation [163]. This offers the opportunity to engineer SDD microstructures by varying solvent and drug solute compositions in spray drying processes which can affect properties such as particle density and surface area available to enhance dissolution performance. Additionally, and most strongly relevant to the

prior light scattering work in this dissertation, Campos et al derived a relationship between the FH interaction parameters and the inversion point for preferential solvation - that is the cosolvent and/or drug concentration in the feed solution the controls its preference for residing with or external to the pervaded volume of the polymer [164]. This knowledge allows the formulator to potentially tailor the extent of local interactions in solution prior to forming the spray dried dispersion using relatively simple measurements. Clearly the opportunities for leveraging viscometric approaches in SDDs is a rich environment ripe for further investigation.

CHAPTER 4: EFFECT OF FORM AND ENVIRONMENTAL MOISTURE ON THE HYDROLYTIC STABILITY OF A HP-API IN A CONTROLLED-RELEASE WET GRANULATION

4.1 Introduction

The United States continues to battle an opioid epidemic that has been so costly, in terms of both human lives and dollars, that it was declared a public health emergency in 2017 [165, 166, 167, 168]. The onset of the epidemic is generally attributed to the over prescription of opioids beginning in the 1990s, eventually giving way to increasing utilization of illicit heroin and fentanyl by the early 2010s and leading to the widespread prevalence of overdose deaths and addiction (i.e. opioid use disorder (OUD)) [169, 168]. At its 2017 peak, the crisis resulted in the loss of more than 47,000 lives and 2.3 million cases of OUD [170]. Federally funded research studies into comprehensive community approaches to curb overdose death rates have recently been initiated; however, significant work remains to understand and apply effective treatment strategies on a national scale.

As these efforts continue, it is critical that practitioners and patients have options to navigate the environmental, behavioral, and physiological factors that can influence recovery treatment success. One such physiological factor that can create barriers to initiating recovery treatment is opioid withdrawal syndrome (OWS) [171, 172, 173]. OWS manifests as a constellation of intense flu-like symptoms including nausea, vomiting, diarrhea, sweating, rhinorrhea, lacrimation, and muscle cramps as well as anxiety and insomnia [174, 175]. When not adequately treated, the intensity of withdrawal symptoms can drive patients to return to opioid use [176, 177].

Pharmacological intervention for OWS occurs with two primary drug classes, opioid agonists and α2-adrenergic agonists. Medications in the α2 agonist class for OWS, primarily clonidine and lofexidine, are the favored management strategy for patients and communities with preferences or contraindications that limit the therapeutic use of opioid agonists. Additional pharmacodynamic effects resulting from this mechanism of action include reduced blood pressure (consistent with clonidine indicated uses) and heart rate, somnolence, and dry mouth [178]. Comparative trials of lofexidine and clonidine, summarized in a Cochrane review, generally concluded that the agents were equally effective but that lofexidine was associated with better tolerability [179, 180, 181, 182]. Lofexidine has been approved in the United Kingdom (U.K.) since the 1990s, and recently gained US FDA approval for the treatment of OWS in 2018 as an immediate release (IR) branded product, LUCEMYRA™ [183, 184].

LUCEMYRA is a highly potent compound and is currently dosed as a 0.18 mg lofexidine (0.2 mg HCl salt) tablet that is usually administered as 3-4 tablets (0.525 to 0.700 mg) QID (i.e. four times daily) for up to 14 days. Although the QID regimen does support successful treatment, the requirement for such frequent administration is not ideal, particularly given the labeled opportunity for the outpatient use of LUCEMYRA. Adherence to the lofexidine dosing regimen is important to maintain exposures associated with efficacy as missed doses and the resulting subtherapeutic exposure in the opioid-withdrawing patient can have significant consequences. Several studies have demonstrated significant improvement in patient compliance/adherence for prescribed medications when fewer daily doses are required in the outpatient setting [185, 186, 187, 188, 189]. Modified or controlled-release systems are commonly employed solutions which offer multiple clinical benefits including modification of pharmacokinetic (PK) parameters, enhanced control of pharmacokinetic/pharmacodynamic (PK/PD) effects, and reduction of dosing frequency. As such, the development of an extended release (XR) lofexidine tablet was initiated to reduce patient pill burden and explore opportunities to improve adherence and

PK/PD effects.

Lofexidine contains a 2-imidazoline ring which is generally understood to be susceptible to alkaline hydrolysis via a specific base catalysis ring opening mechanism [190, 191, 192, 193]. However, the rate of degradation is much reduced under neutral and mildly acidic conditions. As such, citric acid was utilized in both the IR and XR formulations to act as an organic acid stabilizer to facilitate a reduced solid-state pH. However, during the development of the XR product, increased degradation due to hydrolysis was observed relative to the IR formulation despite prior successful application of the citric acid stabilizer. This necessitated reformulation investigations to understand and improve the stability of the XR product.

The XR formulation utilizes a wet granulation process to ensure adequate uniformity of the low dose API within the final blend. The acid and API are both dissolved in ethanol which is then sprayed into the granulation powder bed to distribute the acid and API in intimate contact to control the local pH. A consequence of this approach is that the co-dissolved API and acid may precipitate in a variety of physical states including amorphous, co-crystal(s), hydrates, solvates, and/or polymorphic forms which will likewise exhibit a range of chemical stability and moisture sensitivity. For example, amorphous materials are well known to be more chemically reactive while also sorbing excess moisture relative to crystalline forms [194].

As such, the purpose of this study is to characterize the presence/absence of the API crystalline or amorphous form, moisture sensitivity, and chemical stability under a variety of temperature and relative humidity conditions using several organic acid stabilizers at varying amounts to identify a reformulation which exhibits acceptable stability performance. It is hypothesized that the organic acid conditions which allow the API to precipitate as a stable crystal after wet granulation and exhibit low pKa(s) and hygroscopicity will be best suited to ensuring a stable and robust formulation. The effects of temperature and environmental moisture on degradation rates will be assessed through a modified Arrhenius equation to better elucidate differences in acid

formulations. Additionally, we aim to propose a formulation strategy for continued development that is able to prevent 3% formation of the hydrolysis product over the course of a projected two year shelf life at 25 °C / 60 %RH.

4.2 Background

Imidazoline hydrolysis

Literature review of imidazoline hydrolysis indicates that under basic media, the rate of reaction is expected to be greatest when the neutral form approaches its maximum and demonstrates an apparent 1st order reaction with respect to the hydroxide ion as pH increases beyond this point [195, 193]. Alkaline hydrolysis has been found to be first order with respect to both hydroxide and imidazoline concentrations, and overall is a bimolecular second-order reaction [191]. The evidence appears to favor that the rate determining step in basic media (where the protonated form is negligible) is due to the attack of the hydroxide ion on the neutral molecule at the imine carbon, though there is some argument that the ring opening step may be the rate limiting step as well [191, 195, 193]. Steric hindrance at the α-carbon has been shown to substantially reduce hydrolysis rates in basic media [195] supporting the hydroxide attack as rate limiting. As pH increases such that the fraction of protonated form is minuscule, ring-opening would become the rate limiting step as protonation is likely required to facilitate the amine as a stable leaving group. Overall, the literature supports the hydroxide ion attack on the neutral form as the rate limiting step in strongly basic media.

In a study of antazoline hydrolysis, a distinct mechanism in semi-alkaline media (pH 6.0-7.4) with a slower rate limiting step attributed to attack by the hydroxide ion at the α-carbon on the protonated form, when compared to the neutral molecule [193]. This is consistent with work done on imidazolines by S.O. Bondareva et al where the protonated form is associated with reduced hydrolysis rates observed for

pH $\approx$ 6-10 which was attributed to a reduction in the partial positive at the α-carbon thereby destabilizing the carbo-cation resonance form with the imine nitrogen [195]. This demonstrates the protective effects of increasingly acidic media on hydrolysis when the rate limiting step is attributed to nucleophilic attack at the α-carbon. For pH near 5, antazoline was found to demonstrate a non-catalyzed mechanism with a proposed rate limiting step attributed due to the ring opening step and had the lowest degradation rates observed from pH 0-7.4 (i.e. pH of maximum stability), [193]. At pH 3-4, antazoline was found to exhibit an increased rate of hydrolysis relative to pH 5 and the rate limiting step was now attributed to the nucleophilic attack of water on the protonated molecule. The ring opening step is no longer rate limiting as the protonated amine consistently behaves as a strong leaving group [193]. This implies the possibility of an optimal pH to inhibit hydrolysis of some imidazolines rather than simply always increasing the acidity. Under acidic media, the rates of hydrolysis for imidazolines are found to be substantially reduced relative to basic conditions [191, 195], consistent with our internal results.

Notably, there are much less studies exploring the degradation mechanism and kinetics under acidic conditions. S.O. Bondareva et al. argued that in acidic conditions, the rate is expected to be greatest when both protonated forms of the imine and secondary amine within the ring are at their maximum, as this allows for the development of a partial positive charge at the α-carbon [195], though this is not supported across the remaining literature observed. Similar to basic conditions, the rate limiting step is proposed to be the attack of water at the α-carbon, though there is little direct evidence to support this assumption [191, 195]. This is expected to be most prevalent at strongly acidic conditions, i.e. $<$ 2 pH [191, 195]. In contrast, K. Berzins et al found that additional complex mechanisms of hydrolysis with additional intermediates and increased rates were observed under highly acidic conditions for antazoline [193]. A study by S. Limatibul and J.W. Watson on the degradation kinetics of 2-(m-Nitrophenyl)-imidazoline under highly acidic conditions found increasing rates of

hydrolysis under increasing molarity of H2SO4 from 4-14 molarity. The rate limiting step is again attributed to nucleophilic attack by water at the α-carbon, though attenuation of the rate kinetics was observed and attributed to reducing water activity with increasing acid molarity [196].

A review of the literature was unable to unearth much evidence regarding the specific vs. general catalysis behavior of imidazoline hydrolysis. S. Limatibul and J.W. Watson did note that acid type can affect rates of hydrolysis in highly acidic media with sulfuric and hydrochloric acids being $\approx 3x$ greater than perchloric acid [196], though these environments may not be relevant to mild solid-state conditions. Notably, LADP is an amide that is known to hydrolyze further to LDPA, and amides are known to exhibit general catalysis indicating that buffer may influence LDPA formation rates [197]. D. Drake et al demonstrated that amides undergo general acid and base catalysis in the decomposition step after hydroxide ion or water attack at the α-carbon through stabilization of the charged intermediate [198]. Aside from amide hydrolysis, elucidation of the specific vs. general catalysis of imidazolines was unable to be found in the literature and is likely worthy of future investigation. Likewise, no studies on the stability of imidazolines in organic solvents were found.

Degradation modeling

It is often difficult to identify a suitable reaction mechanism for modeling purposes in drug product degradation owing to a myriad of complexities that can be introduced due to the presence of multiple phases, crystal habit, surface area, excipient interactions, and more [194]; in addition to the incomplete understanding of the solution state hydrolysis of LFX previously discussed. As such, stability studies are executed with degradation behavior modeled empirically by fitting determining the rate constant at initial conditions. Per ICH Q1E, evaluation of stability data guidance, shelf life estimations can be extrapolated from the observed linear degradation rate to the maximum potency loss &/or degradant limits. ICH Q1A (R2) stability

guidelines allow no more than a 5% change in drug potency within the shelf life of a drug product [199]. This approach generally yields a reliable and conservative shelf life as degradation rates are typically expected to be at their highest at initial conditions. In particular for the lofexidine tablet, the maximum acceptable upper limit of the first hydrolysis degradant product has been previously established to be 3%, and hydrolysis is the primary mode of degradation of the API.

With the initial rate constants determined at multiple temperatures and humidity conditions, a greater understanding of the hydrolysis behavior can be explored with the linear form of the humidity-corrected Arrhenius expression below [200]:

$$ln(k) = ln(A) - \frac{E_a}{RT} + B * RH \tag{4.1}$$

Where k is the initial linear rate constant in %/day, A the pre-exponential factor in %/day, E_a the energy of activation in kJ/mol, R the gas constant in kJ/(mol*K), T is temperature in Kelvin, B represents the moisture sensitivity factor, and RH is the % relative humidity.

The pre-exponential or frequency factor, A, can generally be understood as an empirically defined entropic component of the rate function, which reflects the frequency of molecular collisions which contribute to the reaction [201]. It is expected to exhibit a weak relationship with temperature which is typically overshadowed by the temperature effects of the exponential activation energy term in addition to the long extrapolation to 0 K temperature such that A is often difficult to assess accurately. A can be determined theoretically from collision theory and then be compared from the empirical result for a qualitative interpretation of the empirical results. Lower empirical results than collision theory indicates the potential for geometric or steric constraints that hinder reaction progression while larger values imply strongly favorable entropic contributions [201]. The E_a term may be considered a measure of thermal sensitivity of the reaction rate - the larger the activation energy, the less sensitive the rate is to changes in temperature and vice versa. At higher E_a, a larger thermal energy is required to overcome the barrier to reaction progression and as

such the rate will slow down. Similarly, the B parameter represents sensitivity of the reaction to water activity, where larger values indicate greater reactivity with water. This parameter might be interpreted as the ability of the reactive substrate to encourage or hinder interactions with water.

4.3 Materials and Methods

API, lofexidine hydrochloride (LFX), was provided by US WorldMeds, LLC (USWM, Louisville, KY). Organic acid stabilizers comprising DL-malic (Alfa Aesar, Ward Hill, MA), glutaric (Acros Organics, Fair Lawn, NJ), monohydrate citric, anhydrous citric, tartaric, maleic, fumaric, oxalic, and adipic (TCI America, Portland, OR) acids were purchased through VWR International (Radnor, PA). Succinic and pimelic acids were purchased from Sigma-Aldrich (St. Louis, MO). Chemical structures of organic acids and API are captured in figure 4.1.

Hydroxypropylmethylcellulose (HPMC K200) was used as the controlled release polymer (CR) and ordered from XXX. Microcrystalline cellulose (MCC 50μm) was used as both the intra-granular diluent and extra-granular binder, calcium stearate (CaSt) as the lubricant, and povidone (PVP, $M_w \approx 40$ kDa) as the intra-granular binder, were all purchased from Sigma Aldrich.

HPLC grade methanol, ethanol, acetonitrile, sodium phosphate, and 85% phosphoric acid were purchased from VWR International and used as received. 0.2 μm hydrophobic PTFE syringe filters were sourced from Tisch Scientific (Northbend, OH) and purchased though VWR International. All materials were used as received. Ultra pure water was freshly prepared from a MilliQ XXX system and passed through a 0.2 um filter.

Film Preparation

Films were produced by first mixing LFX with the organic acids at a 1:1.13 (w/w) ratio per the initial formulation composition, with 150 mg of LFX and 170 mg of

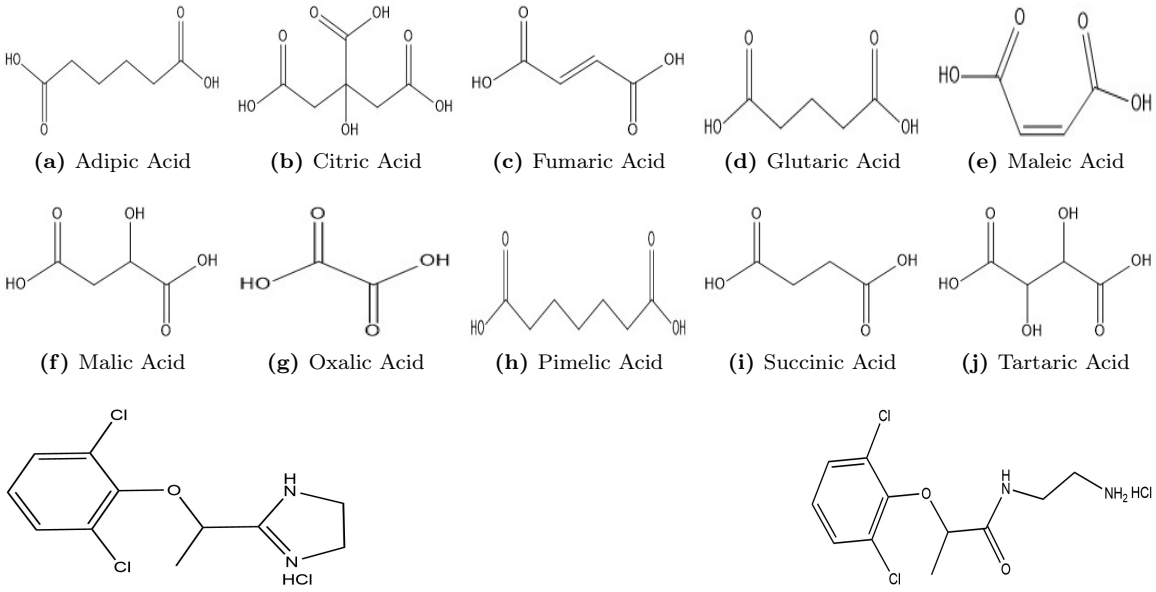

(a) Adipic Acid **(b)** Citric Acid **(c)** Fumaric Acid **(d)** Glutaric Acid **(e)** Maleic Acid

(f) Malic Acid **(g)** Oxalic Acid **(h)** Pimelic Acid **(i)** Succinic Acid **(j)** Tartaric Acid

(k) Lofexidine HCl **(l)** Hydrolysis Product 1 (LADP HCl)

Figure 4.1: Structures of organic acids, LFX, and hydrolysis product, LADP

acid. This was followed by dissolving the mixture in either ethanol or water with approximately 5 minutes of sonication. The solution was then placed under a gentle nitrogen stream at room temperature, evaporating the solvent to produce a film; this process ranged from 24-48 hours. The films were then characterized by a combination of differential scanning calorimetry (DSC), dynamic vapor sorption (DVS), and powder X-ray diffraction (XRD).

X-Ray Diffraction

Samples of 5-10 mg were placed on a low mass mirrored sample plate before being compressed into a flat horizontal plane. Once planar, the sample was then transferred to a mini flex powder x-ray diffractometer sample chamber (Rigaku Americas Corporation, TX, USA). Scanning was performed between 2-40°2θ using Cu Kα radiation at 45 kV and 40 mA. The step size was set to 0.025°at a scanning speed of 1.00°min.

Differential Scanning Calorimetry

Samples of 5-10 mg were placed within a T-Zero pan and hermetically sealed. The lid was punctured, creating a pinhole to allow for evaporation of residual vapors. Once sealed, the samples were transferred to a Q2000 DSC (TA Instruments, New Castle, DE). All samples were evaluated with the DSC operating in ramp mode, equilibrated first at 0°C before heating at a rate of 10°C/min up to 250°C. Reported thermal values were determined from the resultant heat flow curves vs. temperature thermograms.

Dynamic Vapor Sorption

Moisture sorption isotherms were generated from dynamic vapor sorption (DVS) data acquired from a Resolution instrument (Surface Measurement Systems, Allentown, PA). Film samples were placed within the DVS sample chamber and dried at 40°C and 0% relative humidity (RH) for 40 hours, then thermally equilibrated at 25°C and 0% RH for four hours, then the sample was held until the percent mass change of the sample was equal to or less than 0.002% for a period of at least 5 minutes. Once this criterion was met, % RH was increased in step sizes of 10% RH up to 90% RH, and then back down from 90% RH to 0% RH. At each step, the sample was held until the mass stability criteria of percent mass changes equal or less than 0.002% for 2 minutes was met, or a period of four hours had elapsed - whichever occurred first. Total dry nitrogen gas flow rates used to ensure % RH was 200 sccm. Equilibrium moisture content was determined from the initial dry sample mass and the final sample mass weights from each step condition.

Formulation & Process

Formulations were prepared according to the materials and process flow chart in figure 4.2. Granulation solutions were prepared at room temperature with a stir bar spinning at 200 rpm until fully dissolved. The relative amount of dissolved solids were varied

from $\approx$ 18-30% as necessary to ensure complete dissolution of the organic acids, as they exhibited a large range of solubility in ethanol. Primary granulations were prepared with mortar and pestle while slowly spraying the granulation solution from a syringe onto the pre-mixed powder bed. The granulation solution container was rinsed with an additional 5 mL of ethanol which was then added to the granulation to aid in the recovery of any residual API from the container. The wet granulation was wet-milled and dried in a vacuum oven at 40°C for two hours, then dry-milled. Percent mass loss on drying (%LOD) after drying was found to be less than 5% for all primary granulations. Diluent/binder was added along with the primary granulation into a 0.5L media bottle which was then blended on a Turbula blender (Glen Mills Inc, Clifton, NJ) for 5 minutes, resulting in the pre-blend. Lubricant was then added and blended for an additional 1 minute on the Turbula to complete the final blend. The intragranular MCC diluent amount was adjusted as necessary to account for variation in the intragranular acid content. These adjusted amounts are called out at their respective locations within figure 4.2. The initial acid screening stability study included all 10 acids at 0.565 (1x) total w/w % (8.54 % intragranular MCC), while the second stability study only included the top 5 performing acids at 10 times the increased amount at 5.654 (10x) total w/w % (3.45 % intragranular MCC).

Stability Study

Initial stability screening was conducted by preparation of all acid formulations at 0.565 w/w % which were placed in open 20 mL vials and stored at conditions of 58% RH at 25°C, controlled by placing the vials within a sealed glass desiccator containing a saturated salt solution of sodium bromide stored in an incubator set to 25°C. After two weeks, the powders in the vials were mixed with a spatula to ensure homogeneity before sampling for solid-phase extraction (SPE) and HPLC analysis. The bottom five performing acids were removed from further study and the remaining acids were evaluated at additional times points and storage conditions of 43% RH,

25°C (potassium carbonate salt solution, KCO3) and 75% RH, 40°C (sodium chloride salt solution, NaCl) to further explore moisture and temperature stability. Formulations of the top five performing acids were prepared at higher acid concentrations of 5.654 w/w % to assess the effects of increased acid amounts on stability and analyzed at one and two weeks after exposure to conditions of 75% RH, 40°C (i.e saturated NaCl solution).

High Pressure Liquid Chromatography

HPLC analyses were conducted on a Dionex Ultimate 3000 HPLC System (Thermo Scientific, Waltham ,MA) with degasser, binary pump, autosampler set to 4°C, column oven set to 30°C, and UV detector set to a detection wavelength of 214 nm. Separation was achieved with a Waters Sunfire C18 Column (250 mm length, 4.6 mm diameter, 5 um particle size) and Phenomenex KrudKatcher Ultra In-Line Filter (0.5 um x 0.004 in.) using a gradient with mobile phase A consisting of a mixture of acetonitrile (MeCN) and 0.06 M KH_2PO_4 buffer (20:80 v/v), pH 3.0 (adjusted with 85% phosphoric acid), and mobile phase B consisting of pure MeCN, as captured in Table 4.1. SPE of samples was conducted by weighing out 50 mg formulation powder into 5 mL of methanol, which was vortexed for 30 seconds, sonicated for 5 minutes, then vortexed for an additional 30 seconds. Samples were then centrifuged at 13k RPM for 10 minutes. The supernatant was filtered and diluted 5x with mobile phase A into an HPLC vial to a target LFX concentration of 20 μg/mL, and stored at 4°C until analysis. The assay results are reported with respect to the % LADP formation relative to the remaining LFX, taken as the ratio of the peak areas after adjusting for the relative response factor of 0.778 for LADP/LFX as previously established by USWM (data not shown). No unknown peaks were observed in this course of this study.

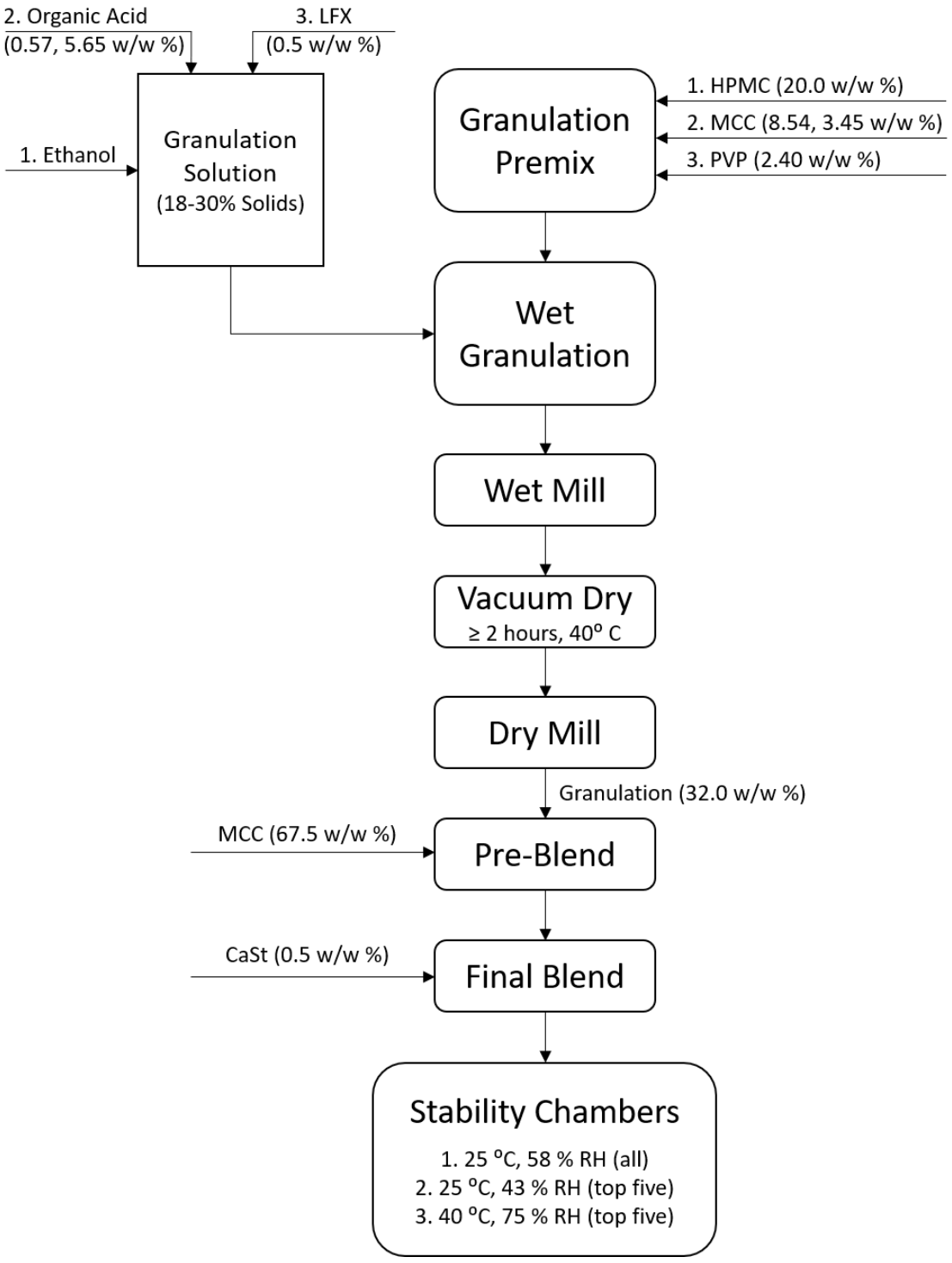

Figure 4.2: Materials and process flow chart of the wet granulated controlled-release lofexidine formulations

Table 4.1: HPLC Gradient Method

Time (minutes)	% Mobile Phase A	% Mobile Phase B
0.0	100	0
7.0	100	0
30.0	56	44
35.0	56	44
45.0	100	0

Data Analysis and Presentation

Chemical structure figures were prepared in ChemDraw Professional, version 19.1.1.21 (PerkinElmer, Waltham, MA). DVS and XRD graphs and formulation stability statistical analysis were prepared in Microsoft Excel for Microsoft 365 32-bit (Microsoft, Redmond, WA) with visualization aided by Daniel's XL Toolbox addin for Excel, version 7.3.2 [138]. DSC figures were prepared in Thermal Advantage Software version 5.5.24 (TA Instruments, New Castle, DE). All errors presented are 95% confidence intervals as determined by regression analysis unless stated otherwise. OPLS multivariate analysis was conducted using SIMCA 16 (Sartorius Stedim Data Analytics AB, Umeå, Sweden)

4.4 Results and Discussion

Solid-State Characterization

In order to understand the solid-state behavior of the organic acid-LFX films prepared out of ethanol, it is necessary to compile and develop an overall picture of the data as extracted from the various XRD, DSC, and DVS techniques. It is also worth noting that each film was also visually assessed for opacity or clarity. Samples which are opaque imply the presence of crystalline forms while clear samples indicate a glassy, isotropic phase. All films were found to be opaque with the exception of the citric acid film, indicating the formation of a glass between the drug and citric acid, and

crystalline forms in all other cases. In agreement with the visual observations, all films are found to be crystalline by XRD per the observation of sharp peaks characteristic of ordered structures in crystalline materials, with the exception of the citric acid film which exhibits the unmistakable amorphous 'halo' consistent with amorphous forms per figure 4.3. For the crystallized films (panels c & d), the presence of new peaks or loss of previous peaks at θ values relative to those observed in the initial pure components (panels a & b) implies the potential for new polymorphic, salt, &/or co-crystal forms. Those films which appear to potentially exhibit new forms due to the presence of additional or loss of prior peaks include the fumaric, maleic, oxalic and tartaric films. The remaining crystalline films, adipic, glutaric, malic, pimelic and succinic appear to indicate a mixture of the initial acid and API forms rather than new structures.

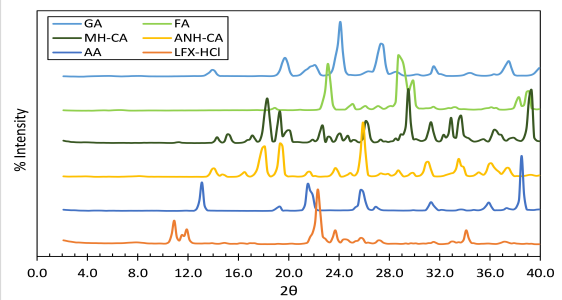

(a) As Received LFX-HCl, Adipic, Citric (monohydrate, anhydrous), Fumaric, & Glutaric acids

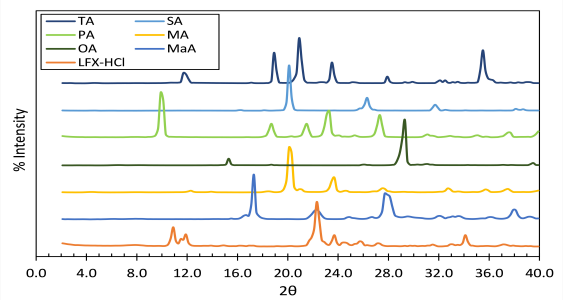

(b) As Received LFX-HCl, Maleic, Malic, Oxalic, Pimelic, Succinic, & Tartaric acids

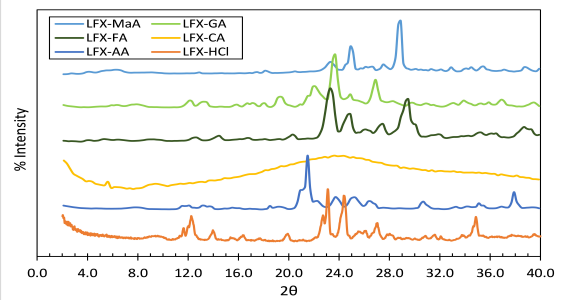

(c) Ethanolic films of pure LFX-HCl & LFX-Acid mixtures (Adipic, Citric, Fumaric, Glutaric, & Maleic acids)

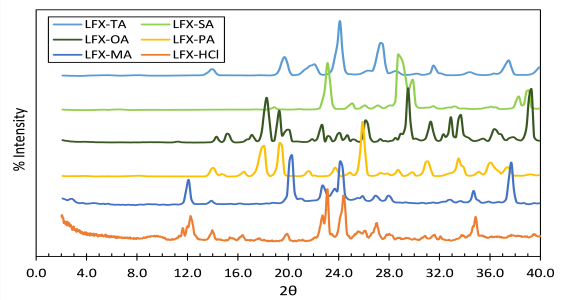

(d) Ethanolic films of pure LFX-HCl & LFX-Acid mixtures (Malic, Oxalic, Pimelic, Succinic, & Tartaric acids)

Figure 4.3: X-ray diffractograms of API and Organic acids: As received (a, b) and film precipitates out of ethanolic solutions (c,d). Notably, all films exhibit crystalline behavior with the exception of the amorphous 'halo' observed for the LFX-CA film.

The DSC data can describe the presence of crystalline and/or amorphous forms through the observation of glass transition temperatures and enthalpic melting events. Per figure 4.4, parts a) and b) we can observe the summary DSC thermograms of the as-received organic acids and API for comparison to the DSC results for the films in parts c) and d). The majority of the as-received acids as well as the API all demonstrate a pronounced sharp endothermic event which indicates their respective melting points, and some broad deviations from the baseline following the melt, that can generally be attributed to the onset of chemical degradation experienced within the range of the temperature scan of the DSC experiments; all of which agree well with the literature. A more detailed review of the as-received DSC data follows for those acids which exhibit more complex behavior (i.e. citric, fumaric, glutaric, pimelic, and oxalic acids).

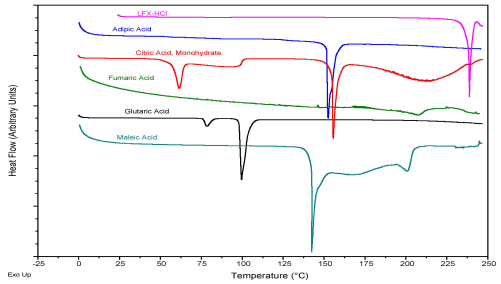

(a) As Received LFX-HCl, Adipic, Citric (monohydrate), Fumaric, Glutaric & Maleic acids

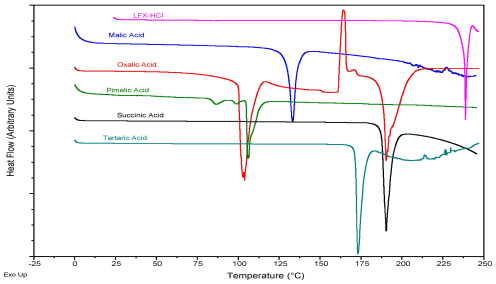

(b) As Received LFX-HCl, Malic, Oxalic, Pimelic, Succinic, & Tartaric acids

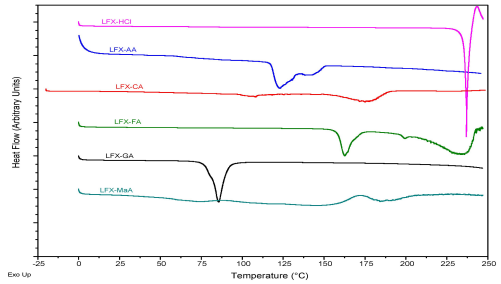

(c) Ethanolic films of pure LFX-HCl & LFX-Acid mixtures (Adipic, Citric, Fumaric, Glutaric, & Maleic acids)

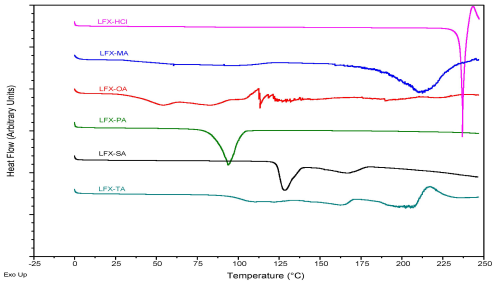

(d) Ethanolic films of pure LFX-HCl & LFX-Acid mixtures (Malic, Oxalic, Pimelic, Succinic, & Tartaric acids)

Figure 4.4: DSC thermograms of LFX and organic acids: As received (a, b) and film precipitates out of ethanolic solutions (c,d).

Per the as received citric acid monohydrate thermogram in 4.4 part a), we can see a series of endothermic events which indicate various phenomena with respect to temperature. The first event beginning at $\approx$ 37 °C up to 100 °C represents the dehydration of the monohydrate form (sharp peak) and evaporation of entrained moisture (broad slope) as it converts to the anhydrous form [202], which then melts per the sharp peak near $\approx$ 152 °C [203], before the onset of chemical degradation (broad hill) at $\approx$ 175 °C and higher temperatures [204]. Notably, as fumaric acid melts at temperatures higher than those explored in this study, no strong melting event is observed, though a small endothermic event near 205 °C is observed that is due to a polymorphic transition [205]. Glutaric acid has a minor endothermic peak prior to its primary melting point, which is attributed to the polymorphic conversion from

the room temperature stable β form to the α form which is more stable at elevated temperatures [205]. In panel b) we can observe that pimelic acid has two small endothermic events prior to its expected melting point which are likewise attributed to polymorphic transitions of form $3 \rightarrow 2 \rightarrow 1$, with its melting point observed near 104 °C [206]. The as-received oxalic acid was in a dihydrate from and as such its behavior is most similar to that observed in the monohydrate citric acid, though with an additional exothermic peak observed between the dehydration event and melting temperature which can be attributed to crystallization into the stable form before melting [207].

When reviewing panels c) and d), the films behave in substantially different ways than the as received materials and can be partitioned into three groups of outcomes. The first group of films (containing adipic, glutaric, pimelic, and succinic acids) are those which exhibit essentially single endothermic peaks (either sharp, broad, or shallow) that occur below the melting points of both the initial acid and API forms and are characteristic of a eutectic melting process [205]. The films imply that forms similar to the as-received materials exists after precipitation out of ethanol. In the second group (fumaric, maleic, malic, oxalic, and tartaric acids), either single, broad/shallow and or multiple endothermic events are observed, with or without additional exothermic events that occur after the endothermic peaks which together indicate the possible formation of salts &/or co-crystals consisting of both the acid and API [205]. Lastly, the third group contains only the citric acid film, which displayed a glass transition near 100 °C and a small endothermic event near 175 °C. Due to the visually transparent nature of this film and the glass transition event, we can be confident that the majority of this sample is in the amorphous state and distinct from all other films. This is an important finding as amorphous materials tend to be more chemically reactive and sorb excess moisture relative to crystal forms [194], which may exacerbate the hydrolysis of the API. Overall, the DSC data agrees well with the XRD results with the possible exception of the malic acid film, which has greater ambiguity as

to whether a new form is present or not. The DSC results indicate large potential variability in the API form after precipitation, including possible salt/co-crystal formation with the acids in group 1, preservation of the initial crystal form with acids in group 2, and stabilization in the amorphous state with citric acid.

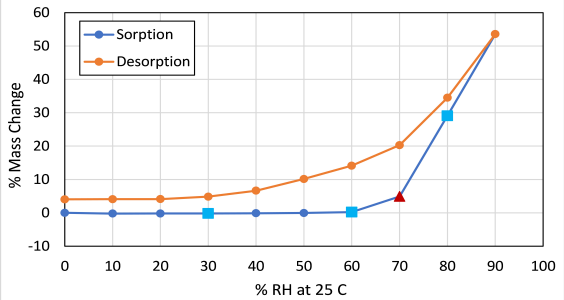

(a) Example DVS Isotherm for LFX-GA film.

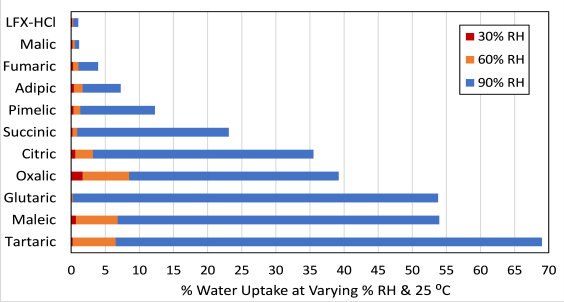

(b) As Received LFX-HCl, Maleic, Malic, Oxalic, Pimelic, Succinic, & Tartaric acids

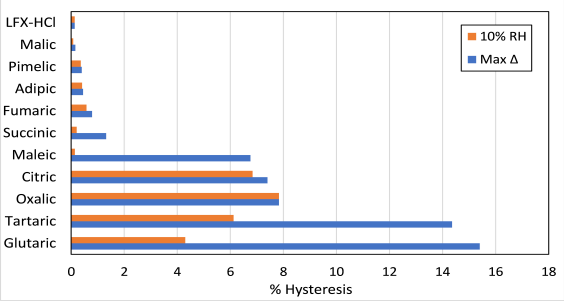

(c) Ethanolic films of pure LFX-HCl & LFX-Acid mixtures (Adipic, Citric, Fumaric, Glutaric, & Maleic acids)

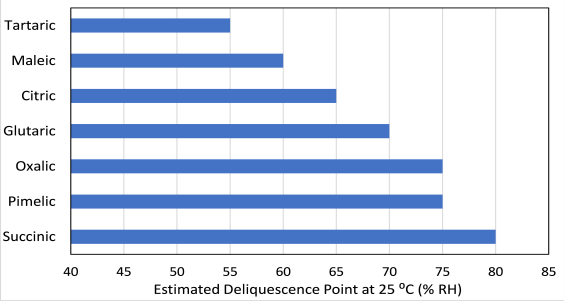

(d) Ethanolic films of pure LFX-HCl & LFX-Acid mixtures (Malic, Oxalic, Pimelic, Succinic, & Tartaric acids)

Figure 4.5: Example LFX-GA DVS isotherm (a) and summary DVS results of hygroscopicity (b), hysteresis (c), and estimated deliquescent/ critical RH % (d) of LFX-Acid 1:1 films

Moving on to the DVS results in figure 4.5, we can explore relative interactions with environmental moisture of the film precipitates. In panel a), we can see an example equilibrium sorption and desorption isotherms at 25 °C of the glutaric acid-LFX film. From these isotherms, information to explore the film interactions with moisture were extracted for comparison across all acids. The square symbols (□) are the relative humidity (% RH) conditions at which the hygrosopicity (i.e. the extent of water uptake) was compiled as representative low (30 %), medium (60 %), and high (90 %) % RH conditions as displayed in panel b) for comparison. Hysteresis

assessments, taken as the difference in moisture uptake between the sorption and desorption isotherms, were recorded at 10% RH as well as the % RH which exhibited the maximum difference for each acid film and is compiled in panel c). Lastly, an estimated deliquescent point or critical RH % is recorded for the % RH condition at which the water uptake increased rapidly with increasing humidity (identified by the red triangle for an estimate of 70% for the glutaric acid film), which is presented for comparison in panel d).

Per the hygroscopicity data, we can observe substantial differences in water uptake by the acid used and also that most of the acids took up very large amounts of moisture at 90% RH conditions. Notably, the malic acid film is very resistant to moisture uptake at all conditions and exhibits behavior most similar to the pure LFX film. This highlights malic acid as a leading contender to minimize water interactions in the solid state, which may be robust to even very high water activity. If the 90% condition is neglected as a properly manufactured and packaged drug product is not expected to experience such conditions, then fumaric, adipic, pimelic. succinic, citric, and glutaric acids all appears to be reasonably resistant to water uptake at 60% RH or less. Glutaric acid does show a striking increase at higher RH which may imply a high risk /lower robustness to varying RH conditions. Oxalic, maleic, and tartaric demonstrate greater moisture uptake than the other acids at lower RH which may increase LFX exposure to water. In panel c) we can observe the hysteresis results where the LFX, malic, pimelic, adipic, fumaric, and succinic acid films demonstrate the least difference between the soprtion/desorption isotherms. This implies that the solid state forms of these acids may be resistant to change in the presence of moisture regardless of moisture uptake, which is a good indication of physical stability such that we might expect the precipitate form to stay consistent and predictable throughout a range of humidity exposures. It is worth noting that those acids which had the lowest hygroscopicity from panel a) also had the least hysteresis. In panel d) we can find the estimate deliquescent or critical RH % for all acid films except for the LFX, adipic,

malic, fumaric, and tartaric films which did not appear to exhibit a rapid change in moisture uptake with increasing humidity. Those films which may deliquesce at lower humidities are likely at the highest risk of extensive hydrolysis and expressing sensitivity to variation in environmental moisture. Taken together, the malic acid film demonstrates the most preferred solid-state behavior across all techniques due to the confirmed crystal form by XRD, possible favorable interactions by DSC co-crystal behavior, and lowest exhibited water interactions per DVS results.

We must also consider the physical and chemical acid properties that may govern potential stabilizing interactions as captured in table 4.2. These include molecular weight, melting temperature, acidity (i.e. pKas), solubility in both ethanol and water, hydrophobicity/philicity (per log P), the number of hydrogen bond donors and acceptors (in total and by mass), topological polar surface area, crystalline density, enthalpy, and entropy parameters. As we know that the API is better stabilized in increasingly acidic media in the solution state, we likewise expect such behavior to apply in the solid state as well. The acids with the lowest pKas, specifically oxalic, maleic, and tartaric acids, would be expected to best reduce the solid-state pH to reduce the hydrolysis rate. Furthermore, as the active site of hydrolysis is an strong hydrogen-bond acceptor, it is anticipated that those acids with greater and stronger hydrogen-bond donating (HBDs) groups will be best suited to stabilize LFX - those acids with the most potential to accept strong hydrogen bonds are citric, tartaric and malic acids.

Table 4.2: Organic Acid Properties

Acid	M_w	T_m	1^{st} pKa	2^{nd} pKa	Log P	$[S]_{EtOH}$	$[S]_{H_2O}$	HBDs	HBAs	HBAs/g Acid	RBs	TPSA	ρ	ΔH_{fus}	ΔS_{fus}	Sources
—	g/mol	C	—	—	—	mg/mL	mg/mL	—	—	mol/g	—	Å^2	g/cm^3	kJ/mol	J/molK	—
Adipic	146.1	152	4.42	5.41	0.08	95	20	2	4	0.0137	5	74.6	1.36	36.3	81.92	[208, 209]
Citric	192.1	153	3.13	4.76	-1.64	1159	615	4	7	0.0208	5	132	1.67	40.32	94.26	[210, 203]
Fumaric	116.1	289	3.02	4.38	0.46	37.7	8.09	2	4	0.0172	2	74.6	1.64	117.84	210.43	[211, 205]
Glutaric	132.1	97.9	4.32	5.42	-0.29	715	693	2	4	0.0151	4	74.6	1.43	20.3	56.33	[212, 209]
Maleic	116.1	143	1.92	6.23	-0.48	414	441	2	4	0.0172	2	74.6	1.59	26.9	66.58	[213, 214, 209]
Malic	134.1	132	3.4	5.11	-1.26	281	425	3	5	0.0224	3	94.8	1.6	34.5	85.3	[215, 216]
Oxalic	90	190	1.25	3.81	-0.81	186	105	2	4	0.0222	1	74.6	1.9	51.19	110.53	[217, 218]
Pimelic	160.2	104	4.71	5.58	0.61	377	64	2	4	0.0125	6	74.6	1.33	30.3	79.9	[219, 220]
Succinic	118.1	185	4.21	5.64	-0.59	117	21	2	4	0.0169	3	74.6	1.57	32.4	69.4	[221, 205]
Tartaric	150.1	174	2.98	4.34	-0.76	175	583	4	6	0.0266	3	115	1.98	36.31	81.59	[203, 222]

Data sourced from a combination of [223] in addition to acid specific references

[S]: Solubility in ethanol or water, HBDs: # of Hydrogen Bond Donors per molecule, HBAs: # of Hydrogen Bond Acceptors per molecule

HBAs/ g Acid:# of moles of Hydrogen Bond Acceptors per gram of acid, TPSA: Topological Polar Surface Area per molecule, ρ : acid density

$\Delta H_f°$: enthalpy of fusion, $\Delta S_f°$: entropy of fusion

Hydrophobicity/philicity as explored by water solubility and log P can describe the relative extent of interactions with water - more strongly hydrophobic materials (low solubility, high log P) may allow the acid to repel moisture from the local environment of the API or in contrast, while more strongly hydrophilic materials (high solubility, low log P) may bind moisture more tightly such that it is less available to react with the drug. The most hydrophobic acids appear to be adipic, fumaric, and pimelic acids while the more hydrophilic acids appears to be citric, malic, tartaric and maleic. Glutaric, oxalic, and succinic acids appear to be more centered between these extremes.

Additionally, ethanol solubility may help describe the propensity for phase separation during the precipitation process from the API and may dictate the relative homogeneity between the API and acid. It is expected that having the API in close proximity to the acid will be beneficial for reduction in the local environment solid state pH. Notably, those acids which are the least soluble in water likewise appear to be less soluble in ethanol. Based on these considerations from the physical-chemical property data, it may be anticipated that oxalic, maleic, tartaric, citric and malic would be top performers due to low pKas and multiple HBDs; provided that the potential hydrophilicity is not detrimental.

Degradation Rate Analysis

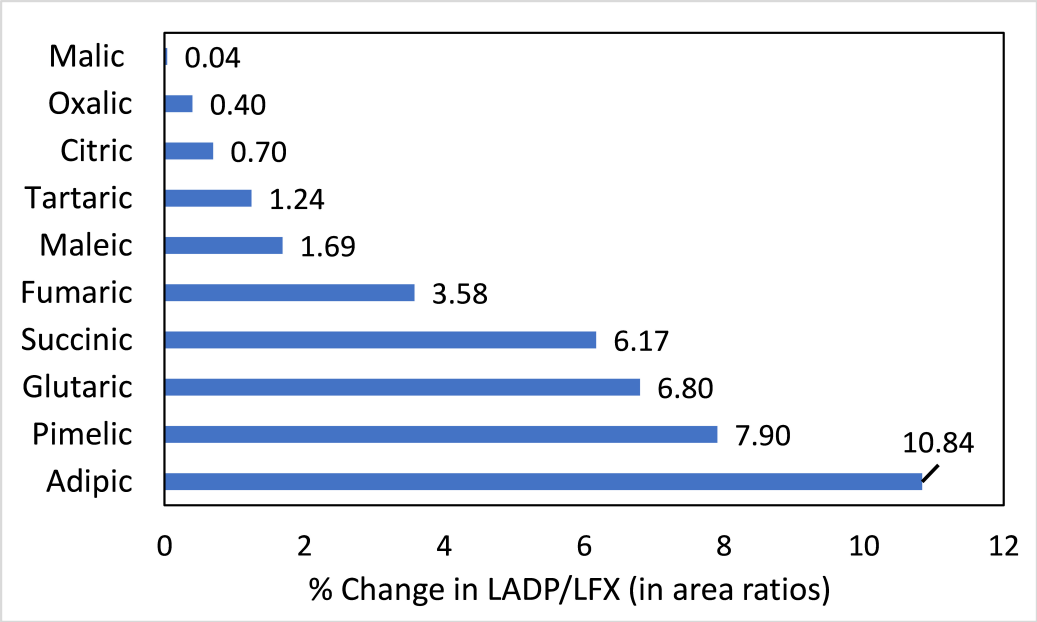

Figure 4.6: The change in hydrolysis product (LADP) amount relative to LFX by HPLC area ratios for all ten acid formulations at 0.565 w/w % (1x) after two weeks exposure to accelerated stability conditions (i.e. 40°C/75% RH. The top five performing acids (malic, oxalic, citric, tartaric, and maleic) were selected for additional study.

Initial stability screening results conducted for two weeks at 25 °C/ 58% RH found the top five performers to be the malic, oxalic, citric, tartaric and maleic acid formulations. These results align well with the solid state expectations in terms of favorable API-acid interactions indicated per the previously discussed XRD and DSC results. Interestingly, these acids are also those that exhibit more hydrophilic properties as demonstrated in figure 4.5 and table 4.2; with the exception of very low moisture interaction of malic acid per the DVS results. The continued stability studies, rate constant, and projected shelf life results for the top five formulations can be found in figure 4.7 and table 4.3, respectively. From these results, it is clearly observed that the malic acid formulation consistently outperforms all other formulations regardless of storage condition; while the citric acid formulation relative performance varies sub-

stantially in comparison to the other acids. This also appears to highlight the greater sensitivity of the citric acid formulations to changing humidity exposure.

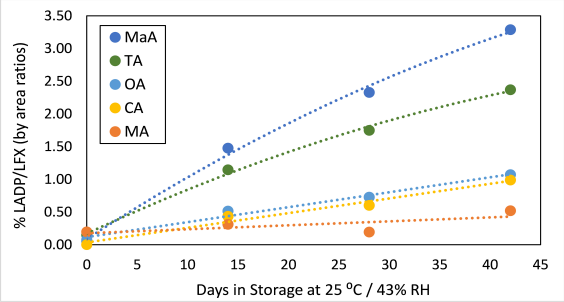

(a) 0.565 w/w % (1x) acid amount with six weeks exposure time at 25 °C/43 %RH storage conditions

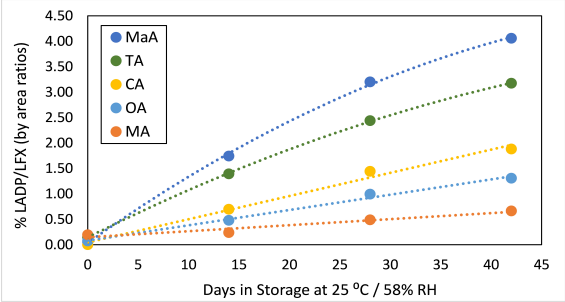

(b) 0.565 w/w % (1x) acid amount with six weeks exposure time at 25 °C/58 %RH storage conditions

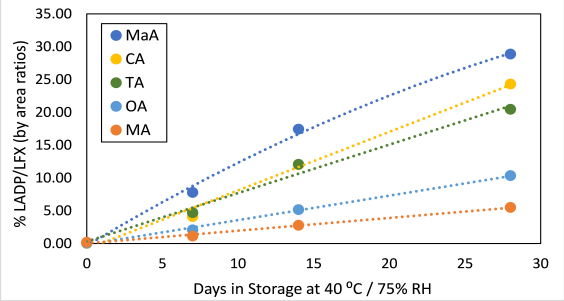

(c) 0.565 w/w % (1x) acid amount with four weeks exposure time at 40 °C/75 %RH storage conditions

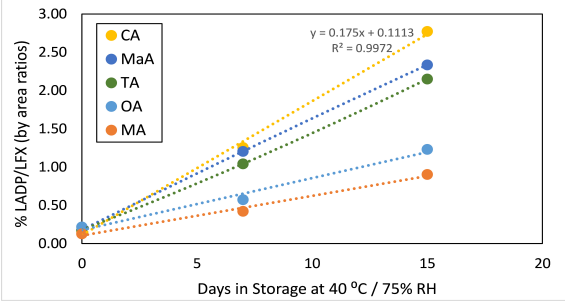

(d) 5.654 w/w % (10x) acid amount with two weeks exposure time at 40 °C/75 %RH storage conditions

Figure 4.7: Summary stability results for top five acids formulations at varying acid amounts (0.565 w/w % - 1x (a,b,c), 5.654 w/w % - 10x (d)), exposure time (six (a,b), four (c), and two (d) weeks) and storage conditions (25 °C/43 %RH (a), 25 °C/58 %RH (b), and 40 °C/75 %RH (c, d)). Malic acid is consistently the top performer at all conditions, while citric acid varied the most with respect to humidity.

To quantitatively understand the effects of temperature and environmental moisture on the degradation rates, the data from the top 5 acids at the 1x acid amounts were fit to the model described in equation 4.1, with the results listed in table 4.4. Ideally, stability data would have been collected at more temperatures and stability conditions (n≥5) to provide better parameter estimates and confidence intervals, but there is still value in using the existing data to generate an understanding of the underlying effects diving differences in stability performance. From the modified Arrhenius model, we would expect that reduced temperature and moisture sensitivity would be expressed by large E_a values and smaller B values, and would be most

favorable for drug product stability. The pre-exponential term is typically considered temperature independent relative to the other parameters within the temperature ranges explored in drug stability studies, and instead represents the relative entropic favorability for the reaction to proceed.

Interestingly, oxalic acid had the greatest resistance to temperature and humidity effects, but the high pre-exponential factor overrode these benefits relative to the malic performance. This may be attributed to the small molecular weight of the acid which implies greater mobility in the solid-state that allows greater frequency of favorable collisions to occur. Alternatively, the smaller size of the acid may provide reduced steric hindrance and/or greater access of water molecules to the active site of the API to initiate the hydrolysis mechanism. In contrast, citric acid had the greatest temperature and moisture sensitivity, but had the smallest pre-exponential factor. This aligns with its larger molecular weight and greater number of sites available for hydrogen-bonding which my restrict the mobility of moisture in the formulation near the API. However, the enhanced sensitivity to moisture may be due to the plasticization effects of sorbed moisture on amorphous solids, such that free volume and molecular mobility is rapidly increased in the presence of increasing moisture content. At low temperature and humidity conditions, citric acid may be the best performing acid due to its order of magnitude or more lower A value, but it implies poor robustness against varying environmental exposure which is not desired for a drug product that may experience multiple such conditions across the shelf life and particularly once the packaged product is open for patient use.

Malic acid was found to be the best candidate acid per its consistently lowest degradation rates, with the median A value, 2^{nd} highest E_a and B values respectively. It is interesting that the malic acid formulation was found to be relatively high in water sensitivity given that the opposite of these results were implied from the DVS data. It is worth reiterating that the data fit to equation 4.1 is limited and may help explain some of this discrepancy. However, even with the higher B value and

at high relative humidities, the high E_a term helps to attenuate these effects. For example, even at 100% RH conditions, the moisture contribution to the sum of the malic acid exponential terms (i.e -$E_a/RT + B * RH$), is equivalent to an E_a of 101.5 kJ/mol which is still larger (i.e higher net energy barrier for the reaction to overcome) than the citric, maleic, and tartaric acid exponential sums at 0% RH (96.6, 98.9, and 94.9 kJ/mol, respectively). Likewise, the two orders of magnitude difference in the pre-exponential factors for oxalic and malic is sufficient to explain how malic can be more stable even with greater temperature and humidity sensitivity. These findings demonstrates the greater importance of a high E_a and low A values in the mitigation of the hydrolysis of LFX.

Table 4.3: Initial degradation rate constants (k) for top five acid formulations

Acid	**Amount**	**Condition**	**Rate +/- 95% CI**	Shelf Life
—	w/w %	°C / % RH	(% LADP/LFX)/DAY	days
Citric	1x	25 / 43	0.0224 +/- 0.0109	134
		25 / 58†	0.0596 +/- 0.1121	50
		40 / 75	0.8915 +/- 0.2326	3
	10x	40 / 75	0.1750 +/- 0.1175	17
Maleic	1x	25 / 43†	0.1002 +/- 0.2140	30
		25 / 58†	0.1407 +/- 0.1178	21
		40 / 75†	1.3830 +/- 2.8741	2
	10x	40 / 75	0.1436 +/- 0.0204	21
Malic	1x	25 / 43	0.0061 +/- 0.0180	492
		25 / 58	0.0118 +/- 0.0089	254
		40 / 75	0.1938 +/- 0.0432	15
	10x	40 / 75	0.0519 +/- 0.0665	58
Oxalic	1x	25 / 43	0.0229 +/- 0.0091	131
		25 / 58	0.0301 +/- 0.0080	100
		40 / 75	0.3730 +/- 0.0643	8
	10x	40 / 75	0.0679 +/- 0.1132	44
Tartaric	1x	25 / 43†	0.0720 +/- 0.1318	42
		25 / 58†	0.0996 +/- 0.0357	30
		40 / 75†	0.9019 +/- 3.1176	3
	10x	40 / 75	0.1316 +/- 0.0551	23

† : Rate constants extracted from 2^{nd} order polynomial fit at t = 0 ;
otherwise linear fit used for all other conditions

Table 4.4: Modified Arrhenius Factors for the top five acid formulations

Acid	A	E_a	B
—	%/day	kJ/mol	—
Citric	$1.87 * 10^{14}$	96.6	0.0553
Maleic	$8.20 * 10^{15}$	98.9	0.0223
Malic	$5.35 * 10^{15}$	107	0.0434
Oxalic	$9.82 * 10^{17}$	114	0.0183
Tartaric	$1.22 * 10^{15}$	94.9	0.0217

In addition to understanding the factors which drive hydrolysis rate, the other

primary goal of this work is to identify an acceptable formulation for continued development that can be expected to meet the shelf life requirements of less than 3% LADP formation over two years (730 days) when held at 25 °C / 60 %RH. A comparison of the stability results for the citric and malic formulations are explored in greater detail (table 4.5) to meet this target, as citric acid was used in the initial formulation and malic acid is the clear leading acid from those explored in this study. Notably, the malic acid formulation demonstrates expected shelf lives 3-5x greater (or conversely degradation rates 3-5x smaller) than citric acid, though they are still well below the target 730 days. However, this data is still encouraging for a multitude of reasons. The higher 10x acid content is found to improve rate constants 3-5x under accelerated stability conditions relative to the low acid contents. If similar improvement can be translated to the long term stability conditions (i.e. 25 °C / 60 %RH), then we can readily expect the malic formulation to meet the desired shelf life. These findings also suggest that further increases in acid content may continue to increase stability to provide additional assurances. Lastly and most importantly, these stability studies are conducted on open powder formulations that are not sealed in appropriate packaging conditions or otherwise protected from environmental moisture. For example, tablets made from these formulations could be coated with a moisture protective barrier and/or stored in a low moisture vapor diffusion packaging condition with desiccant to scavenge excess moisture - all of which would be expected to drastically improve hydrolysis stability. As such, identifying a powder formulation under these storage conditions that is able to improve stability from the reference formulation by 3-5 fold by the simple exchange of acid, and and additional 3-5 fold by increasing the amount of acid - allowing for a potential 9-25 fold improvement overall, if these effects are found to be additive.

Table 4.5: Comparison of Citric and Malic Acid Formulations

Comparison of Citric vs. Malic Degradation Rates

Amount	Condition	p-value	k Ratios (CA/MA)
w/w %	°C / % RH	—	—
1x	25 / 43	0.0286	3.696 +/- 2.5806
	25 / 58	0.0133	5.046 +/- 1.1600
	40 / 75	0.0002	4.599 +/- 0.3666
10x	40 / 75	0.0074	3.371 +/- 0.3837

Comparison of 1x vs 10x w/w % Degradation Rates

Acid	Condition	p-value	k Ratios (1x/10x)
—	°C / % RH	—	—
Citric	40 / 75	0.0010	5.093 +/- 0.4096
Malic	40 / 75	0.0011	3.733 +/- 0.4230

4.5 Conclusions

In this chapter we have found that the citric acid formulation is likely to form an amorphous phase with the drug when sprayed out of ethanol onto the granulation powder bed, while all other acids resulted in various crystal forms. The prevalence of co-crystal/salt formations appears likely with a number of the evaluated acids per DSC and XRD results. The malic acid formulation clearly exhibited the most beneficial water interactions per the DVS studies which is promising for the reduction of hydrolysis reactions in particular. Overall, the solid-state characterization data indicated that the malic acid formulation demonstrated the most favorable properties for drug stability.

The initial screening stability study identified citric, maleic, malic, oxalic, and tartaric acids as the top five contenders for further investigation. These top performing acids agreed well with the expectations from the solid state characterization and acid physical-chemical property data, where greater acidity and hydrophilicity were

correlated with improved performance. These top acid formulations were evaluated at multiple temperature and humidity conditions for the determination of reaction rate parameters from the modified Arrhenius equation, such as the pre-exponential factor A, energy of activation E_a, and humidity factor B. Of these, it was found that the most important outcomes for better stability performance were a large E_a with a small A, which can make the humidity factor less pertinent. Citric acid was found to have the greatest moisture sensitivity which is consistent with plasticization effects that would be expected of amorphous forms.

The malic acid formulation at the higher acid content has been identified as the best acid choice for the stabilization of this LFX controlled-release tablet with a potentially improved shelf life of 9-25 fold that of the reference citric formulation, with greater resistance to temperature and humidity effects. Overall, the data consistently highlights malic acid as the best stabilizing material for LFX against hydrolysis and offers promised of the continued successful development of a controlled release drug product.

4.6 Future Work

Additional hydrolysis mitigation strategies

Protective coatings on tablets or capsules can add an additional moisture barrier such that hydrolysis can be slowed by reducing the rate of moisture accumulation in the drug product [224]. Investigations of coating types, amounts/thickness, and processing methods could further mitigate the formation of the LADP hydrolysis product. Packaging considerations such as foil pouches, blister packs, and/or HDPE (high density polyethylene) bottles inhibit moisture uptake in the local environment of the drug product to help reduce the hydrolysis rate by minim zing the relative humidity. Adding silicon dioxide desiccant is also frequently utilized as a moisture scavenger to reduce relative humidity. There are many additional approaches that

can be utilzied in addition to acid optimization to improve the hydrolytic stability of LFX.

BIBLIOGRAPHY

[1] C. A. Lipinski, F. Lombardo, B. W. Dominy, and P. J. Feeney, "Experimental and computational approaches to estimate solubility and permeability in drug discovery and development settings," *Advanced drug delivery reviews*, vol. 23, no. 1-3, pp. 3–25, 1997.

[2] C. A. Lipinski, "Drug-like properties and the causes of poor solubility and poor permeability," *Journal of pharmacological and toxicological methods*, vol. 44, no. 1, pp. 235–249, 2000.

[3] L. Di, P. V. Fish, and T. Mano, "Bridging solubility between drug discovery and development," *Drug discovery today*, vol. 17, no. 9-10, pp. 486–495, 2012.

[4] Y. Shu, T. L. Diamond, J. C. Hershey, S. Huang, B. C. Magliaro, J. A. O'Brien, K.-A. S. Schlegel, V. Puri, V. N. Uebele, J. M. Uslaner, *et al.*, "Discovery of 4-arylquinoline-2-carboxamides, highly potent and selective class of mglur2 negative allosteric modulators: From hts to activity in animal models," *Bioorganic & Medicinal Chemistry Letters*, p. 127066, 2020.

[5] Y. A. Ivanenkov, R. S. Yamidanov, I. A. Osterman, P. V. Sergiev, V. A. Aladinskiy, A. V. Aladinskaya, V. A. Terentiev, M. S. Veselov, A. A. Ayginin, D. A. Skvortsov, *et al.*, "2-pyrazol-1-yl-thiazole derivatives as novel highly potent antibacterials," *The Journal of antibiotics*, vol. 72, no. 11, pp. 827–833, 2019.

[6] H. Lei, M. Guo, X. Li, F. Jia, C. Li, Y. Yang, M. Cao, N. Jiang, E. Ma, and X. Zhai, "Discovery of novel indole-based allosteric highly potent atx inhibitors with great in vivo efficacy in mouse lung fibrosis model," *Journal of Medicinal Chemistry*, 2020.

[7] J. Zheng, *Formulation and analytical development for low-dose oral drug products*. John Wiley & Sons, 2009.

[8] T. Loftsson and M. E. Brewster, "Pharmaceutical applications of cyclodextrins: basic science and product development," *Journal of pharmacy and pharmacology*, vol. 62, no. 11, pp. 1607–1621, 2010.

[9] A. T. Serajuddin and M. Pudipeddi, *Salt selection strategies*. Wiley-VCH, Weinheim, 2002.

[10] S. V. Jermain, C. Brough, and R. O. Williams III, "Amorphous solid dispersions and nanocrystal technologies for poorly water-soluble drug delivery–an update," *International journal of pharmaceutics*, vol. 535, no. 1-2, pp. 379–392, 2018.

[11] L. S. Taylor and G. G. Zhang, "Physical chemistry of supersaturated solutions and implications for oral absorption," *Advanced drug delivery reviews*, vol. 101, pp. 122–142, 2016.

[12] L. H. Fish, H. L. Schwartz, J. Cavanaugh, M. W. Steffes, J. P. Bantle, and J. H. Oppenheimer, "Replacement dose, metabolism, and bioavailability of levothyroxine in the treatment of hypothyroidism," *New England Journal of Medicine*, vol. 316, no. 13, pp. 764–770, 1987.

[13] J. Swarbrick and J. C. Boylan, *Encyclopedia of pharmaceutical technology: volume 20-supplement 3*. CRC Press, 2000.

[14] H. Al-Obaidi, S. Brocchini, and G. Buckton, "Anomalous properties of spray dried solid dispersions," *Journal of pharmaceutical sciences*, vol. 98, no. 12, pp. 4724–4737, 2009.

[15] A. Paudel and G. Van den Mooter, "Influence of solvent composition on the miscibility and physical stability of naproxen/pvp k 25 solid dispersions prepared by cosolvent spray-drying," *Pharmaceutical research*, vol. 29, no. 1, pp. 251–270, 2012.

[16] A. Paudel, E. Nies, and G. Van den Mooter, "Relating hydrogen-bonding interactions with the phase behavior of naproxen/pvp k 25 solid dispersions: evaluation of solution-cast and quench-cooled films," *Molecular pharmaceutics*, vol. 9, no. 11, pp. 3301–3317, 2012.

[17] M. Hugo, K. Kunath, and J. Dressman, "Selection of excipient, solvent and packaging to optimize the performance of spray-dried formulations: case example fenofibrate," *Drug development and industrial pharmacy*, vol. 39, no. 2, pp. 402–412, 2013.

[18] F. Wan, A. Bohr, M. J. Maltesen, S. Bjerregaard, C. Foged, J. Rantanen, and M. Yang, "Critical solvent properties affecting the particle formation process and characteristics of celecoxib-loaded plga microparticles via spray-drying," *Pharmaceutical research*, vol. 30, no. 4, pp. 1065–1076, 2013.

[19] M. T. Davis, D. P. Egan, M. Kuhs, A. B. Albadarin, C. S. Griffin, J. A. Collins, and G. M. Walker, "Amorphous solid dispersions of bcs class ii drugs: a rational approach to solvent and polymer selection," *Chemical Engineering Research and Design*, vol. 110, pp. 192–199, 2016.

[20] H. S. Purohit, J. D. Ormes, S. Saboo, Y. Su, M. S. Lamm, A. K. Mann, and L. S. Taylor, "Insights into nano-and micron-scale phase separation in amorphous solid dispersions using fluorescence-based techniques in combination with

solid state nuclear magnetic resonance spectroscopy," *Pharmaceutical research*, vol. 34, no. 7, pp. 1364–1377, 2017.

[21] Y. Chen, W. Huang, J. Chen, H. Wang, S. Zhang, and S. Xiong, "The synergetic effects of nonpolar and polar protic solvents on the properties of felodipine and soluplus in solutions, casting films, and spray-dried solid dispersions," *Journal of pharmaceutical sciences*, vol. 107, no. 6, pp. 1615–1623, 2018.

[22] C. Luebbert, D. Real, and G. Sadowski, "Choosing appropriate solvents for asd preparation," *Molecular pharmaceutics*, vol. 15, no. 11, pp. 5397–5409, 2018.

[23] M. K. Ghorab and M. C. Adeyeye, "Enhancement of ibuprofen dissolution via wet granulation with β-cyclodextrin," *Pharmaceutical development and technology*, vol. 6, no. 3, pp. 305–314, 2001.

[24] H. Wikström, P. J. Marsac, and L. S. Taylor, "In-line monitoring of hydrate formation during wet granulation using raman spectroscopy," *Journal of pharmaceutical sciences*, vol. 94, no. 1, pp. 209–219, 2005.

[25] F. Kato, M. Otsuka, and Y. Matsuda, "Kinetic study of the transformation of mefenamic acid polymorphs in various solvents and under high humidity conditions," *International journal of pharmaceutics*, vol. 321, no. 1-2, pp. 18–26, 2006.

[26] D. Tank, K. Karan, B. Y. Gajera, and R. H. Dave, "Investigate the effect of solvents on wet granulation of microcrystalline cellulose using hydroxypropyl methylcellulose as a binder and evaluation of rheological and thermal characteristics of granules," *Saudi pharmaceutical journal*, vol. 26, no. 4, pp. 593–602, 2018.

[27] J. P. Reddy, J. W. Jones, P. S. Wray, A. B. Dennis, J. Brown, and P. Timmins, "Monitoring of multiple solvent induced form changes during high shear wet

granulation and drying processes using online raman spectroscopy," *International journal of pharmaceutics*, vol. 541, no. 1-2, pp. 253–260, 2018.

[28] N. S. Trasi, S. Bhujbal, Q. T. Zhou, and L. S. Taylor, "Amorphous solid dispersion formation via solvent granulation–a case study with ritonavir and lopinavir," *International journal of pharmaceutics: X*, vol. 1, p. 100035, 2019.

[29] N. S. Trasi, S. V. Bhujbal, D. Y. Zemlyanov, Q. Zhou, and L. S. Taylor, "Physical stability and release properties of lumefantrine amorphous solid dispersion granules prepared by a simple solvent evaporation approach," *International Journal of Pharmaceutics: X*, p. 100052, 2020.

[30] M. Defrese, M. A. Farmer, Y. Long, L. Timmerman, Y. Bae, and P. J. Marsac, "Approaches to understand the solution state organization of spray dried dispersion feed solutions and its translation to the solid state," *Molecular Pharmaceutics*, 2020.

[31] S. Percy, "Improvement in drying and concentrating liquid substances by atomizing," 1872. US Patent 125,406A.

[32] R. Vehring, W. R. Foss, and D. Lechuga-Ballesteros, "Particle formation in spray drying," *Journal of Aerosol Science*, vol. 38, no. 7, pp. 728–746, 2007.

[33] R. Vehring, "Pharmaceutical particle engineering via spray drying," *Pharmaceutical research*, vol. 25, no. 5, pp. 999–1022, 2008.

[34] A. Paudel, Z. A. Worku, J. Meeus, S. Guns, and G. Van den Mooter, "Manufacturing of solid dispersions of poorly water soluble drugs by spray drying: formulation and process considerations," *International journal of pharmaceutics*, vol. 453, no. 1, pp. 253–284, 2013.

[35] T. Vasconcelos, S. Marques, J. das Neves, and B. Sarmento, "Amorphous solid dispersions: Rational selection of a manufacturing process," *Advanced drug delivery reviews*, vol. 100, pp. 85–101, 2016.

[36] A. Singh and G. Van den Mooter, "Spray drying formulation of amorphous solid dispersions," *Advanced drug delivery reviews*, vol. 100, pp. 27–50, 2016.

[37] M. Davis and G. Walker, "Recent strategies in spray drying for the enhanced bioavailability of poorly water-soluble drugs," *Journal of Controlled Release*, vol. 269, pp. 110–127, 2018.

[38] S. Poozesh, N. Setiawan, F. Arce, P. Sundararajan, J. Della Rocca, A. Rumondor, D. Wei, R. Wenslow, H. Xi, S. Zhang, *et al.*, "Understanding the process-product-performance interplay of spray dried drug-polymer systems through complete structural and chemical characterization of single spray dried particles," *Powder technology*, vol. 320, pp. 685–695, 2017.

[39] N. Shah, H. Sandhu, D. S. Choi, H. Chokshi, and A. W. Malick, "Amorphous solid dispersions," *Theory and Practice; Springer: Berlin, Germany*, 2014.

[40] J. J. O'Sullivan, E.-A. Norwood, J. A. O'Mahony, and A. L. Kelly, "Atomisation technologies used in spray drying in the dairy industry: A review," *Journal of food engineering*, vol. 243, pp. 57–69, 2019.

[41] L. X. Huang, K. Kumar, and A. Mujumdar, "A comparative study of a spray dryer with rotary disc atomizer and pressure nozzle using computational fluid dynamic simulations," *Chemical Engineering and Processing: Process Intensification*, vol. 45, no. 6, pp. 461–470, 2006.

[42] K. Masters, *Spray drying in practice*. SprayDryConsult, 2002.

[43] N. Ashgriz, *Handbook of atomization and sprays: theory and applications*. Springer Science & Business Media, 2011.

[44] Z. Chen, K. Yang, C. Huang, A. Zhu, L. Yu, and F. Qian, "Surface enrichment and depletion of the active ingredient in spray dried amorphous solid dispersions," *Pharmaceutical research*, vol. 35, no. 2, p. 38, 2018.

[45] S. Poozesh and E. Bilgili, "Scale-up of pharmaceutical spray drying using scale-up rules: A review," *International Journal of Pharmaceutics*, vol. 562, pp. 271–292, 2019.

[46] M. B. Albro, V. Rajan, R. Li, C. T. Hung, and G. A. Ateshian, "Characterization of the concentration-dependence of solute diffusivity and partitioning in a model dextran–agarose transport system," *Cellular and molecular bioengineering*, vol. 2, no. 3, pp. 295–305, 2009.

[47] J. Wang, M. de Wit, R. M. Boom, and M. A. Schutyser, "Charging and separation behavior of gluten–starch mixtures assessed with a custom-built electrostatic separator," *Separation and Purification Technology*, vol. 152, pp. 164–171, 2015.

[48] S. Poozesh, S. M. Jafari, and N. K. Akafuah, "Interrogation of a new inline multi-bin cyclone for sorting of produced powders of a lab-scale spray dryer," *Powder Technology*, vol. 373, pp. 590–598, 2020.

[49] K. B. Shepard, A. M. Dower, A. M. Ekdahl, M. M. Morgen, J. M. Baumann, and D. T. Vodak, "Solvent-assisted secondary drying of spray-dried polymers," *Pharmaceutical research*, vol. 37, no. 8, pp. 1–11, 2020.

[50] B. C. Hancock and M. Parks, "What is the true solubility advantage for amorphous pharmaceuticals?," *Pharmaceutical research*, vol. 17, no. 4, pp. 397–404, 2000.

[51] S. B. Murdande, M. J. Pikal, R. M. Shanker, and R. H. Bogner, "Solubility advantage of amorphous pharmaceuticals: I. a thermodynamic analysis," *Journal of pharmaceutical sciences*, vol. 99, no. 3, pp. 1254–1264, 2010.

[52] R. Paus, Y. Ji, L. Vahle, and G. Sadowski, "Predicting the solubility advantage of amorphous pharmaceuticals: a novel thermodynamic approach," *Molecular pharmaceutics*, vol. 12, no. 8, pp. 2823–2833, 2015.

[53] C. Bhugra and M. J. Pikal, "Role of thermodynamic, molecular, and kinetic factors in crystallization from the amorphous state," *Journal of pharmaceutical sciences*, vol. 97, no. 4, pp. 1329–1349, 2008.

[54] G. B. Winkelman, C. Dwyer, C. Marsh, T. S. Hudson, D. Nguyen-Manh, M. Döblinger, and D. J. Cockayne, "The crystal/glass interface in doped si3n4," *Materials Science and Engineering: A*, vol. 422, no. 1-2, pp. 77–84, 2006.

[55] M. D. Ediger, "Perspective: Highly stable vapor-deposited glasses," *The Journal of chemical physics*, vol. 147, no. 21, p. 210901, 2017.

[56] P. J. Marsac, T. Li, and L. S. Taylor, "Estimation of drug–polymer miscibility and solubility in amorphous solid dispersions using experimentally determined interaction parameters," *Pharmaceutical research*, vol. 26, no. 1, p. 139, 2009.

[57] K. Lehmkemper, S. O. Kyerematen, M. Bartels, M. Degenhardt, and G. Sadowski, "Physical stability of api/polymer-blend amorphous solid dispersions," *European Journal of Pharmaceutics and Biopharmaceutics*, vol. 124, pp. 147–157, 2018.

[58] X. Lin, Y. Hu, L. Liu, L. Su, N. Li, J. Yu, B. Tang, and Z. Yang, "Physical stability of amorphous solid dispersions: A physicochemical perspective with thermodynamic, kinetic and environmental aspects," *Pharmaceutical research*, vol. 35, no. 6, p. 125, 2018.

[59] N. Shetty, L. Zeng, S. Mangal, H. Nie, M. R. Rowles, R. Guo, Y. Han, J. H. Park, and Q. T. Zhou, "Effects of moisture-induced crystallization on the aerosol performance of spray dried amorphous ciprofloxacin powder formulations," *Pharmaceutical research*, vol. 35, no. 1, p. 7, 2018.

[60] N. S. Trasi, H. S. Purohit, and L. S. Taylor, "Evaluation of the crystallization tendency of commercially available amorphous tacrolimus formulations exposed to different stress conditions," *Pharmaceutical research*, vol. 34, no. 10, pp. 2142–2155, 2017.

[61] H. S. Purohit and L. S. Taylor, "Phase behavior of ritonavir amorphous solid dispersions during hydration and dissolution," *Pharmaceutical research*, vol. 34, no. 12, pp. 2842–2861, 2017.

[62] H. Chen, Y. Pui, C. Liu, Z. Chen, C.-C. Su, M. Hageman, M. Hussain, R. Haskell, K. Stefanski, K. Foster, *et al.*, "Moisture-induced amorphous phase separation of amorphous solid dispersions: molecular mechanism, microstructure, and its impact on dissolution performance," *Journal of pharmaceutical sciences*, vol. 107, no. 1, pp. 317–326, 2018.

[63] M. C. Dalsin, S. Tale, and T. M. Reineke, "Solution-state polymer assemblies influence bcs class ii drug dissolution and supersaturation maintenance," *Biomacromolecules*, vol. 15, no. 2, pp. 500–511, 2014.

[64] S. V. Bhujbal, D. Y. Zemlyanov, A. Cavallaro, S. Mangal, L. S. Taylor, and Q. T. Zhou, "Qualitative and quantitative characterization of composition heterogeneity on the surface of spray dried amorphous solid dispersion particles by an advanced surface analysis platform with high surface sensitivity and superior spatial resolution," *Molecular pharmaceutics*, vol. 15, no. 5, pp. 2045–2053, 2018.

[65] Y. Chen, H. Chen, S. Wang, C. Liu, and F. Qian, "A single hydrogen to fluorine substitution reverses the trend of surface composition enrichment of sorafenib amorphous solid dispersion upon moisture exposure," *Pharmaceutical research*, vol. 36, no. 7, p. 105, 2019.

[66] M. Li, F. Meng, Y. Tsutsumi, J.-P. Amoureux, W. Xu, X. Lu, F. Zhang, and Y. Su, "Understanding molecular interactions in rafoxanide-povidone amorphous solid dispersions from ultrafast magic angle spinning nmr," *Molecular Pharmaceutics*, 2020.

[67] S. Poozesh, N. Setiawan, N. K. Akafuah, K. Saito, and P. J. Marsac, "Assessment of predictive models for characterizing the atomization process in a spray dryer bi-fluid nozzle," *Chemical Engineering Science*, vol. 180, pp. 42–51, 2018.

[68] J. R. Dorgan and D. Yan, "Kinetics of spinodal decomposition in liquid crystalline polymers: processing effects on the phase separation morphology," *Macromolecules*, vol. 31, no. 1, pp. 193–200, 1998.

[69] J. Kim, S. Lee, Y. Choi, S.-M. Lee, and D. Jeong, "Basic principles and practical applications of the cahn–hilliard equation," *Mathematical Problems in Engineering*, vol. 2016, 2016.

[70] K. Fischer and M. Schmidt, "Pitfalls and novel applications of particle sizing by dynamic light scattering," *Biomaterials*, vol. 98, pp. 79–91, 2016.

[71] J. Stetefeld, S. A. McKenna, and T. R. Patel, "Dynamic light scattering: a practical guide and applications in biomedical sciences," *Biophysical reviews*, vol. 8, no. 4, pp. 409–427, 2016.

[72] M. Koziol, K. Fischer, and S. Seiffert, "Origin of the low-frequency plateau and the light-scattering slow mode in semidilute poly (ethylene glycol) solutions," *Soft matter*, vol. 15, no. 12, pp. 2666–2676, 2019.

[73] K. Franks, V. Kestens, A. Braun, G. Roebben, and T. P. Linsinger, "Non-equivalence of different evaluation algorithms to derive mean particle size from dynamic light scattering data," *Journal of Nanoparticle Research*, vol. 21, no. 9, p. 195, 2019.

[74] X.-p. Xiong, Q.-r. Ke, and S.-q. Zhu, "Introduction of a reliable method for determination of intrinsic viscosity for any polymer with high precision," *Chinese Journal of Polymer Science*, vol. 32, no. 2, pp. 209–217, 2014.

[75] M. Rubinstein, R. H. Colby, *et al.*, *Polymer physics*, vol. 23. Oxford university press New York, 2003.

[76] L. Gargallo and D. Radic, *Physicochemical behavior and supramolecular organization of polymers*. Springer Science & Business Media, 2009.

[77] D. Shukla, C. P. Schneider, and B. L. Trout, "Molecular level insight into intrasolvent interaction effects on protein stability and aggregation," *Advanced drug delivery reviews*, vol. 63, no. 13, pp. 1074–1085, 2011.

[78] T. J. Kamerzell, R. Esfandiary, S. B. Joshi, C. R. Middaugh, and D. B. Volkin, "Protein–excipient interactions: Mechanisms and biophysical characterization applied to protein formulation development," *Advanced drug delivery reviews*, vol. 63, no. 13, pp. 1118–1159, 2011.

[79] D. M. Parikh, *Handbook of pharmaceutical granulation technology*. CRC Press, 2016.

[80] A. M. Ruiz, M. Jimenez-Castellanos, J. Cunningham, and A. Katdare, "Theoretical estimation of dwell and consolidation times in rotary tablet machines," *Drug development and industrial pharmacy*, vol. 18, no. 19, pp. 2011–2028, 1992.

[81] E. Chevalier, M. Viana, S. Cazalbou, and D. Chulia, "Comparison of low-shear and high-shear granulation processes: effect on implantable calcium phosphate granule properties," *Drug development and industrial pharmacy*, vol. 35, no. 10, pp. 1255–1263, 2009.

[82] S. M. Iveson, J. D. Litster, K. Hapgood, and B. J. Ennis, "Nucleation, growth and breakage phenomena in agitated wet granulation processes: a review," *Powder technology*, vol. 117, no. 1-2, pp. 3–39, 2001.

[83] D. J. A. Ende, *Chemical Engineering in the Pharmaceutical Industry: R & D to Manufacturing*. John Wiley & Sons, 2011.

[84] Z. Mirza, J. Liu, Y. Glocheux, A. B. Albadarin, G. M. Walker, and C. Mangwandi, "Effect of impeller design on homogeneity, size and strength of pharmaceutical granules produced by high-shear wet granulation," *Particuology*, vol. 23, pp. 31–39, 2015.

[85] S. Oka, H. Emady, O. Kašpar, V. Tokárová, F. Muzzio, F. Štěpánek, and R. Ramachandran, "The effects of improper mixing and preferential wetting of active and excipient ingredients on content uniformity in high shear wet granulation," *Powder Technology*, vol. 278, pp. 266–277, 2015.

[86] S. Oka, D. Smrčka, A. Kataria, H. Emady, F. Muzzio, F. Štěpánek, and R. Ramachandran, "Analysis of the origins of content non-uniformity in high-shear wet granulation," *International Journal of Pharmaceutics*, vol. 528, no. 1-2, pp. 578–585, 2017.

[87] S. Gupta, P. Thool, S. Meruva, J. Li, J. Patel, A. Agrawal, S. Karki, W. Bowen, and B. Mitra, "Development of low dose micro-tablets by high shear wet granulation process," *International Journal of Pharmaceutics*, vol. 587, p. 119571, 2020.

[88] B. B. Alsulays, M. H. Fayed, A. Alalaiwe, S. M. Alshahrani, A. S. Alshetaili, S. M. Alshehri, and F. K. Alanazi, "Mixing of low-dose cohesive drug and overcoming of pre-blending step using a new gentle-wing high-shear mixer granulator," *Drug Development and Industrial Pharmacy*, vol. 44, no. 9, pp. 1520–1527, 2018.

[89] W.-J. Sun and C. C. Sun, "A microcrystalline cellulose based drug-composite formulation strategy for developing low dose drug tablets," *International Journal of Pharmaceutics*, p. 119517, 2020.

[90] M. B. Mackaplow, "Using a mass balance to determine the potency loss during the production of a pharmaceutical blend," *Aaps Pharmscitech*, vol. 11, no. 3, pp. 1045–1053, 2010.

[91] L.-S. Wu, G. Torosian, K. Sigvardson, C. Gerard, and M. A. Hussain, "Investigation of moricizine hydrochloride polymorphs," *Journal of pharmaceutical sciences*, vol. 83, no. 10, pp. 1404–1406, 1994.

[92] T. D. Davis, "Wet granulation and drying: Monitoring and control," *Purdue e-Pubs*, 2003.

[93] W. Li, G. D. Worosila, W. Wang, and T. Mascaro, "Determination of polymorph conversion of an active pharmaceutical ingredient in wet granulation using nir calibration models generated from the premix blends," *Journal of pharmaceutical sciences*, vol. 94, no. 12, pp. 2800–2806, 2005.

[94] M. W. Wong and A. G. Mitchell, "Physicochemical characterization of a phase change produced during the wet granulation of chlorpromazine hydrochloride and its effects on tableting," *International journal of pharmaceutics*, vol. 88, no. 1-3, pp. 261–273, 1992.

[95] S. Airaksinen, M. Karjalainen, N. Kivikero, S. Westermarck, A. Shevchenko, J. Rantanen, and J. Yliruusi, "Excipient selection can significantly affect solid-state phase transformation in formulation during wet granulation," *Aaps Pharmscitech*, vol. 6, no. 2, pp. E311–E322, 2005.

[96] J. S. Tantry, J. Tank, and R. Suryanarayanan, "Processing-induced phase transitions of theophylline—implications on the dissolution of theophylline tablets," *Journal of pharmaceutical sciences*, vol. 96, no. 5, pp. 1434–1444, 2007.

[97] P. Chakravarty, R. Govindarajan, and R. Suryanarayanan, "Investigation of solution and vapor phase mediated phase transformation in thiamine hydrochloride," *Journal of pharmaceutical sciences*, vol. 99, no. 9, pp. 3941–3952, 2010.

[98] A. C. Williams, V. B. Cooper, L. Thomas, L. J. Griffith, C. R. Petts, and S. W. Booth, "Evaluation of drug physical form during granulation, tabletting and storage," *International journal of pharmaceutics*, vol. 275, no. 1-2, pp. 29–39, 2004.

[99] H. Nie, W. Xu, L. S. Taylor, P. J. Marsac, and S. R. Byrn, "Crystalline solid dispersion-a strategy to slowdown salt disproportionation in solid state formulations during storage and wet granulation," *International journal of pharmaceutics*, vol. 517, no. 1-2, pp. 203–215, 2017.

[100] S. Badawy, A. Narang, K. Lamarche, G. Subramanian, and S. Varia, "Handbook of pharmaceutical wet granulation," 2019.

[101] N. F. da Costa, A. I. Fernandes, and J. F. Pinto, "Measurement of the amorphous fraction of olanzapine incorporated in a co-amorphous formulation," *International Journal of Pharmaceutics*, p. 119716, 2020.

[102] E. Atef, H. Chauhan, D. Prasad, D. Kumari, and C. Pidgeon, "Quantifying solid-state mixtures of crystalline indomethacin by raman spectroscopy comparison with thermal analysis," *ISRN Chromatography*, vol. 2012, 2012.

[103] J. A. Newman, P. D. Schmitt, S. J. Toth, F. Deng, S. Zhang, and G. J. Simpson, "Parts per million powder x-ray diffraction," *Analytical chemistry*, vol. 87, no. 21, pp. 10950–10955, 2015.

[104] A. Paudel, D. Raijada, and J. Rantanen, "Raman spectroscopy in pharmaceutical product design," *Advanced drug delivery reviews*, vol. 89, pp. 3–20, 2015.

[105] J. A. Baird and L. S. Taylor, "Evaluation of amorphous solid dispersion properties using thermal analysis techniques," *Advanced drug delivery reviews*, vol. 64, no. 5, pp. 396–421, 2012.

[106] C. Leyva-Porras, P. Cruz-Alcantar, V. Espinosa-Solís, E. Martínez-Guerra, C. I. Piñón-Balderrama, I. Compean Martínez, and M. Z. Saavedra-Leos, "Application of differential scanning calorimetry (dsc) and modulated differential scanning calorimetry (mdsc) in food and drug industries," *Polymers*, vol. 12, no. 1, p. 5, 2020.

[107] T. Liu and Z. Xiao, "Dynamic light scattering of rigid rods–a universal relationship on the apparent diffusion coefficient as revealed by numerical studies and its use for rod length determination," *Macromolecular Chemistry and Physics*, vol. 213, no. 16, pp. 1697–1705, 2012.

[108] A. Levin, E. Shmytkova, and K. Minkov, "Determination of the geometric parameters of gold nanorods by partially depolarized dynamic light scattering and absorption spectrophotometry," *Measurement Techniques*, vol. 59, no. 7, pp. 709–714, 2016.

[109] A. D. Levin, E. A. Shmytkova, and B. N. Khlebtsov, "Multipolarization dynamic light scattering of nonspherical nanoparticles in solution," *The Journal of Physical Chemistry C*, vol. 121, no. 5, pp. 3070–3077, 2017.

[110] L. F. Guerra, T. W. Muir, and H. Yang, "Single-particle dynamic light scattering: Shapes of individual nanoparticles," *Nano letters*, vol. 19, no. 8, pp. 5530–5536, 2019.

[111] A. Saluja, R. M. Fesinmeyer, S. Hogan, D. N. Brems, and Y. R. Gokarn, "Diffusion and sedimentation interaction parameters for measuring the second virial coefficient and their utility as predictors of protein aggregation," *Biophysical journal*, vol. 99, no. 8, pp. 2657–2665, 2010.

[112] B. D. Connolly, C. Petry, S. Yadav, B. Demeule, N. Ciaccio, J. M. Moore, S. J. Shire, and Y. R. Gokarn, "Weak interactions govern the viscosity of concentrated antibody solutions: high-throughput analysis using the diffusion interaction parameter," *Biophysical journal*, vol. 103, no. 1, pp. 69–78, 2012.

[113] B. J. Dear, J. J. Hung, T. M. Truskett, and K. P. Johnston, "Contrasting the influence of cationic amino acids on the viscosity and stability of a highly concentrated monoclonal antibody," *Pharmaceutical research*, vol. 34, no. 1, pp. 193–207, 2017.

[114] H. Holthoff, S. U. Egelhaaf, M. Borkovec, P. Schurtenberger, and H. Sticher, "Coagulation rate measurements of colloidal particles by simultaneous static and dynamic light scattering," *Langmuir*, vol. 12, no. 23, pp. 5541–5549, 1996.

[115] Y. Adachi, S. Koga, M. Kobayashi, and M. Inada, "Study of colloidal stability of allophane dispersion by dynamic light scattering," *Colloids and Surfaces A: Physicochemical and Engineering Aspects*, vol. 265, no. 1-3, pp. 149–154, 2005.

[116] M. Zembyla, A. Lazidis, B. S. Murray, and A. Sarkar, "Water-in-oil pickering emulsions stabilized by synergistic particle–particle interactions," *Langmuir*, vol. 35, no. 40, pp. 13078–13089, 2019.

[117] Y. Georgalis, E. Starikov, B. Hollenbach, R. Lurz, E. Scherzinger, W. Saenger, H. Lehrach, and E. E. Wanker, "Huntingtin aggregation monitored by dynamic light scattering," *Proceedings of the National Academy of Sciences*, vol. 95, no. 11, pp. 6118–6121, 1998.

[118] A. Atahar, N. N. Mafy, M. M. Rahman, M. Y. A. Mollah, and M. A. B. H. Susan, "Aggregation of urea in water: Dynamic light scattering analyses," *Journal of Molecular Liquids*, vol. 294, p. 111612, 2019.

[119] K. Onuma and N. Kanzaki, "Multi-angle static and dynamic light scattering investigation of lysozyme association: From crystallization to liquid–liquid phase separation," *Journal of crystal growth*, vol. 304, no. 2, pp. 452–459, 2007.

[120] K. Fujita, J. Konishi, K. Nakanishi, and K. Hirao, "Strong light scattering in macroporous tio2 monoliths induced by phase separation," *Applied physics letters*, vol. 85, no. 23, pp. 5595–5597, 2004.

[121] H. Brognaro, S. Falke, C. Nzanzu Mudogo, and C. Betzel, "Multi-step concanavalin a phase separation and early-stage nucleation monitored via dynamic and depolarized light scattering," *Crystals*, vol. 9, no. 12, p. 620, 2019.

[122] D. Lehner, H. Lindner, and O. Glatter, "Determination of the translational and rotational diffusion coefficients of rodlike particles using depolarized dynamic light scattering," *Langmuir*, vol. 16, no. 4, pp. 1689–1695, 2000.

[123] F. E. Berger Bioucas, C. Damm, W. Peukert, M. H. Rausch, T. M. Koller, C. Giraudet, and A. P. Froba, "Translational and rotational diffusion coefficients of gold nanorods dispersed in mixtures of water and glycerol by polarized dynamic light scattering," *The Journal of Physical Chemistry B*, vol. 123, no. 44, pp. 9491–9502, 2019.

[124] R. Nixon-Luke and G. Bryant, "A depolarized dynamic light scattering method to calculate translational and rotational diffusion coefficients of nanorods," *Particle & Particle Systems Characterization*, vol. 36, no. 2, p. 1800388, 2019.

[125] J. Gigault, E. Mignard, H. El Hadri, and B. Grassl, "Measurement bias on nanoparticle size characterization by asymmetric flow field-flow fractionation using dynamic light-scattering detection," *Chromatographia*, vol. 80, no. 2, pp. 287–294, 2017.

[126] A. V. Malm and J. C. Corbett, "Improved dynamic light scattering using an adaptive and statistically driven time resolved treatment of correlation data," *Scientific reports*, vol. 9, no. 1, pp. 1–11, 2019.

[127] I. Teraoka, *Polymer solutions: an introduction to physical properties*. John Wiley & Sons, 2002.

[128] L. H. Sperling, *Introduction to physical polymer science*. John Wiley & Sons, 2005.

[129] R. Borsali and R. Pecora, *Soft matter characterization*, vol. 725. Springer, 2008.

[130] S. Podzimek, *Light scattering, size exclusion chromatography and asymmetric flow field flow fractionation: powerful tools for the characterization of polymers, proteins and nanoparticles*. John Wiley & Sons, 2011.

[131] E. F. Casassa, "Remarks on light scattering from polymers in mixed solvents: Effects of polymer molecular weight, molecular weight distribution, and solvent composition," *Polymer Journal*, vol. 3, no. 4, pp. 517–525, 1972.

[132] A. M. R. Caparros and M. Bohdaneckỳ, "A note on the intrinsic viscosity and huggins coefficient of low-molecular-weight polymers in mixed solvents," *Die Makromolekulare Chemie: Macromolecular Chemistry and Physics*, vol. 186, no. 5, pp. 1005–1013, 1985.

[133] M. A. Blanco, E. Sahin, Y. Li, and C. J. Roberts, "Reexamining protein–protein and protein–solvent interactions from kirkwood-buff analysis of light scattering in multi-component solutions," *The Journal of chemical physics*, vol. 134, no. 22, p. 06B606, 2011.

[134] C. Strazielle and H. Benoit, "N 61.— etude theorique de la diffusion de la lumiere par les systemes ternaires," *Journal de Chimie Physique*, vol. 58, pp. 675–677, 1961.

[135] M. Guettari and A. Gharbi, "A model to study the behavior of a polar polymer in the mixture of polar solvents," *Journal of Macromolecular Science, Part B*, vol. 49, no. 3, pp. 592–601, 2010.

[136] J. Teng, S. Bates, D. A. Engers, K. Leach, P. Schields, and Y. Yang, "Effect of water vapor sorption on local structure of poly (vinylpyrrolidone)," *Journal of pharmaceutical sciences*, vol. 99, no. 9, pp. 3815–3825, 2010.

[137] T. A. Konig, P. A. Ledin, J. Kerszulis, M. A. Mahmoud, M. A. El-Sayed, J. R. Reynolds, and V. V. Tsukruk, "Electrically tunable plasmonic behavior of nanocube–polymer nanomaterials induced by a redox-active electrochromic polymer," *ACS nano*, vol. 8, no. 6, pp. 6182–6192, 2014.

[138] Daniel Kraus, "Daniel's XL Toolbox, v. 7.3.2."

[139] B. Tummers, "DataThief III."

[140] A. Minecka, E. Kaminska, M. Tarnacka, I. Grudzka-Flak, M. Bartoszek, K. Wolnica, M. Dulski, K. Kaminski, and M. Paluch, "Impact of intermolecular interactions, dimeric structures on the glass forming ability of naproxen, and a series of its derivatives," *Molecular pharmaceutics*, vol. 15, no. 10, pp. 4764–4776, 2018.

[141] G. L. Perlovich, S. V. Kurkov, A. N. Kinchin, and A. Bauer-Brandl, "Thermodynamics of solutions iii: Comparison of the solvation of (+)-naproxen with other nsaids," *European Journal of Pharmaceutics and Biopharmaceutics*, vol. 57, no. 2, pp. 411–420, 2004.

[142] W. E. Acree Jr, "Iupac-nist solubility data series. 102. solubility of nonsteroidal anti-inflammatory drugs (nsaids) in neat organic solvents and organic solvent mixtures," *Journal of Physical and Chemical Reference Data*, vol. 43, no. 2, p. 023102, 2014.

[143] I. Tsivintzelis, I. G. Economou, and G. M. Kontogeorgis, "Modeling the phase behavior in mixtures of pharmaceuticals with liquid or supercritical solvents," *The Journal of Physical Chemistry B*, vol. 113, no. 18, pp. 6446–6458, 2009.

[144] K. Noda, M. Ohashi, and K. Ishida, "Viscosities and densities at 298.15 k for mixtures of methanol, acetone, and water," *Journal of Chemical and Engineering Data*, vol. 27, no. 3, pp. 326–328, 1982.

[145] M. Iglesias, B. Orge, and J. Tojo, "Refractive indices, densities and excess properties on mixing of the systems acetone+ methanol+ water and acetone+ methanol+ 1-butanol at 298.15 k," *Fluid Phase Equilibria*, vol. 126, no. 2, pp. 203–223, 1996.

[146] B. Orge, M. Iglesias, J. Tojo, and J. Legido, "Densities and refractive indices of acetone+ methanol+ chlorobenzene at the temperature 298.15 k," *J. Chem. Thermodyn*, vol. 26, pp. 121–127, 1994.

[147] D. L. Tomasko and M. T. Timko, "Tailoring of specific interactions to modify the morphology of naproxen," *Journal of crystal growth*, vol. 205, no. 1-2, pp. 233–243, 1999.

[148] C. Calero-Rubio, C. Strab, G. V. Barnett, and C. J. Roberts, "Protein partial molar volumes in multicomponent solutions from the perspective of inverse kirkwood–buff theory," *The Journal of Physical Chemistry B*, vol. 121, no. 24, pp. 5897–5907, 2017.

[149] X. Yuan, D. Sperger, and E. J. Munson, "Investigating miscibility and molecular mobility of nifedipine-pvp amorphous solid dispersions using solid-state nmr spectroscopy," *Molecular pharmaceutics*, vol. 11, no. 1, pp. 329–337, 2014.

[150] P. Duan, M. S. Lamm, F. Yang, W. Xu, D. Skomski, Y. Su, and K. Schmidt-Rohr, "Quantifying molecular mixing and heterogeneity in pharmaceutical dis-

persions at sub-100 nm resolution by spin diffusion nmr," *Molecular Pharmaceutics*, vol. 17, no. 9, pp. 3567–3580, 2020.

[151] J. Alin, N. Setiawan, M. Defrese, J. DiNunzio, H. Lau, L. Lupton, H. Xi, Y. Su, H. Nie, N. Hesse, *et al.*, "A novel approach for measuring room temperature enthalpy of mixing and associated solubility estimation of a drug in a polymer matrix," *Polymer*, vol. 135, pp. 50–60, 2018.

[152] R.-J. Roe and R. Roe, *Methods of X-ray and neutron scattering in polymer science*, vol. 739. Oxford University Press New York, 2000.

[153] T. Tanaka, *Experimental methods in polymer science: modern methods in polymer research and technology*. Academic Press, 2000.

[154] J. T. Oberlerchner, T. Rosenau, and A. Potthast, "Overview of methods for the direct molar mass determination of cellulose," *Molecules*, vol. 20, no. 6, pp. 10313–10341, 2015.

[155] B. A. Wolf, "Polyelectrolytes revisited: reliable determination of intrinsic viscosities," *Macromolecular rapid communications*, vol. 28, no. 2, pp. 164–170, 2007.

[156] J. Eckelt, A. Knopf, and B. A. Wolf, "Polyelectrolytes: Intrinsic viscosities in the absence and in the presence of salt," *Macromolecules*, vol. 41, no. 3, pp. 912–918, 2008.

[157] C.-E. Brunchi, S. Morariu, and M. Bercea, "Intrinsic viscosity and conformational parameters of xanthan in aqueous solutions: salt addition effect," *Colloids and Surfaces B: Biointerfaces*, vol. 122, pp. 512–519, 2014.

[158] R. Pamies, J. G. H. Cifre, M. d. C. L. Martínez, and J. G. de la Torre, "Determination of intrinsic viscosities of macromolecules and nanoparticles. comparison

of single-point and dilution procedures," *Colloid and Polymer Science*, vol. 286, no. 11, pp. 1223–1231, 2008.

[159] V. R. Gowariker, N. Viswanathan, and J. Sreedhar, *Polymer science*. New Age International, 1986.

[160] L. Xu and F. Qiu, "Simultaneous determination of three flory–huggins interaction parameters in polymer/solvent/nonsolvent systems by viscosity and cloud point measurements," *Polymer*, vol. 55, no. 26, pp. 6795–6802, 2014.

[161] J. Qian, M. Wang, D. Han, and R. Cheng, "A novel method for estimating unperturbed dimension $[\eta]$ θ of polymer from the measurement of its $[\eta]$ in a non-theta solvent," *European polymer journal*, vol. 37, no. 7, pp. 1403–1407, 2001.

[162] S. L. Shmakov, "Comments on the paper "a novel method for estimating unperturbed dimension $[\eta]$ θ of polymer from the measurement of its $[\eta]$ in a non-theta solvent" by jw qian et al., eur. polym. j., 2001; 37: 1403," *European polymer journal*, vol. 6, no. 40, pp. 1255–1256, 2004.

[163] P. Aryanti, D. Ariono, A. Hakim, and I. Wenten, "Flory-huggins based model to determine thermodynamic property of polymeric membrane solution," *J. Phys*, vol. 1090, p. 012074, 2018.

[164] A. Campos, R. Gavara, R. Tejero, C. Gómez, and B. Celda, "A procedure for predicting sorption equilibrium in ternary polymer systems from flory–huggins binary interaction parameters and the inversion point of preferential solvation," *Journal of Polymer Science Part B: Polymer Physics*, vol. 27, no. 8, pp. 1599–1610, 1989.

[165] HHS, "Hhs acting secretary declares public health emergency to address national opioid crisis," *https://www.hhs.gov/about/news/2017/10/26/hhs-acting-*

secretary-declares-public-health-emergency-address-national-opioid-crisis.html,, pp. Accessed July 21, 2020, 2017.

[166] NIDA, "Opioid overdose crisis," *https://www.drugabuse.gov/drugs-abuse/opioids/opioid-overdose-crisis.html,*, pp. Accessed July 21, 2020, 2019.

[167] C. Florence, F. Luo, L. Xu, and C. Zhou, "The economic burden of prescription opioid overdose, abuse and dependence in the united states, 2013," *Medical care*, vol. 54, no. 10, p. 901, 2016.

[168] CDC, "Opioid basics: Understanding the epidemic," *https://www.cdc.gov/drugoverdose/epidemic/index.html#three-waves*, pp. Accessed July 21, 2020, 2020.

[169] W. M. Compton, M. Boyle, and E. Wargo, "Prescription opioid abuse: problems and responses," *Preventive medicine*, vol. 80, pp. 5–9, 2015.

[170] J. F. Kelly and S. E. Wakeman, *Treating Opioid Addiction*. Springer, 2019.

[171] T. R. Kosten and L. E. Baxter, "Effective management of opioid withdrawal symptoms: A gateway to opioid dependence treatment," *The American Journal on Addictions*, vol. 28, no. 2, pp. 55–62, 2019.

[172] T. J. Cicero and M. S. Ellis, "The prescription opioid epidemic: a review of qualitative studies on the progression from initial use to abuse," *Dialogues in clinical neuroscience*, vol. 19, no. 3, p. 259, 2017.

[173] R. D. Weiss, J. S. Potter, M. L. Griffin, R. K. McHugh, D. Haller, P. Jacobs, J. Gardin II, D. Fischer, and K. D. Rosen, "Reasons for opioid use among patients with dependence on prescription opioids: the role of chronic pain," *Journal of substance abuse treatment*, vol. 47, no. 2, pp. 140–145, 2014.

[174] R. Mattick, J. Kimber, C. Breen, and M. Davoli, "Buprenorphine maintenance versus placebo or methadone maintenance for opioid dependence. 2003," *The Cochrane Database of Systematic Reviews. The Cochrane Library*, no. 4, 2008.

[175] B. P. Jarvis, A. F. Holtyn, S. Subramaniam, D. A. Tompkins, E. A. Oga, G. E. Bigelow, and K. Silverman, "Extended-release injectable naltrexone for opioid use disorder: a systematic review," *Addiction*, vol. 113, no. 7, pp. 1188–1209, 2018.

[176] D. R. Wesson and W. Ling, "The clinical opiate withdrawal scale (cows)," *Journal of psychoactive drugs*, vol. 35, no. 2, pp. 253–259, 2003.

[177] M. K. Vernon, S. Reinders, S. Mannix, K. Gullo, C. W. Gorodetzky, and T. Clinch, "Psychometric evaluation of the 10-item short opiate withdrawal scale-gossop (sows-gossop) in patients undergoing opioid detoxification," *Addictive Behaviors*, vol. 60, pp. 109–116, 2016.

[178] M. C. Houston, "Clonidine hydrochloride.," *Southern Medical Journal*, vol. 75, no. 6, pp. 713–719, 1982.

[179] T. Carnwath and J.-a. Hardman, "Randomised double-blind comparison of lofexidine and clonidine in the out-patient treatment of opiate withdrawal," *Drug and Alcohol Dependence*, vol. 50, no. 3, pp. 251–254, 1998.

[180] S.-K. Lin, J. Strang, L.-W. Su, C.-J. Tsai, and W.-H. Hu, "Double-blind randomised controlled trial of lofexidine versus clonidine in the treatment of heroin withdrawal," *Drug and alcohol dependence*, vol. 48, no. 2, pp. 127–133, 1997.

[181] A. Kahn, J. Mumford, G. A. Rogers, and H. Beckford, "Double-blind study of lofexidine and clonidine in the detoxification of opiate addicts in hospital," *Drug and alcohol dependence*, vol. 44, no. 1, pp. 57–61, 1997.

[182] L. Gowing, M. Farrell, R. Ali, and J. M. White, "Alpha 2-adrenergic agonists for the management of opioid withdrawal," *Cochrane Database of Systematic Reviews*, no. 5, 2016.

[183] J. V. Pergolizzi, H. Annabi, C. Gharibo, and J. A. LeQuang, "The role of lofexidine in management of opioid withdrawal," *Pain and Therapy*, vol. 8, no. 1, pp. 67–78, 2019.

[184] USWM, "Lucemyra prescribing information," *https://hcp.lucemyra.com/LUCEMYRA-PI.pdf*, pp. Accessed July 21, 2020, 2018.

[185] W. Kruse, W. Eggert-Kruse, J. Rampmaier, B. Runnebaum, and E. Weber, "Dosage frequency and drug-compliance behaviour—a comparative study on compliance with a medication to be taken twice or four times daily," *European journal of clinical pharmacology*, vol. 41, no. 6, pp. 589–592, 1991.

[186] M. Mann, O. Eliasson, K. Patel, and R. L. ZuWallack, "A comparison of the effects of bid and qid dosing on compliance with inhaled flunisolide," *Chest*, vol. 101, no. 2, pp. 496–499, 1992.

[187] J. Malo, A. Cartier, H. Ghezzo, C. Trudeau, J. Morris, and B. Jennings, "Comparison of four-times-a-day and twice-a-day dosing regimens in subjects requiring 1200 μg or less of budesonide to control mild to moderate asthma," *Respiratory medicine*, vol. 89, no. 8, pp. 537–543, 1995.

[188] P. Kardas, "Comparison of patient compliance with once-daily and twice-daily antibiotic regimens in respiratory tract infections: results of a randomized trial," *Journal of Antimicrobial Chemotherapy*, vol. 59, no. 3, pp. 531–536, 2007.

[189] J.-J. Parienti, D. R. Bangsberg, R. Verdon, and E. M. Gardner, "Better adherence with once-daily antiretroviral regimens: a meta-analysis," *Clinical Infectious Diseases*, vol. 48, no. 4, pp. 484–488, 2009.

[190] A. J. Ross, M.-V. C. Go, D. J. Palling, and D. L. Casey, "Kinetics and mechanism of the hydrolysis of a 2-substituted imidazoline, cibenzoline (cifenline)," *Journal of pharmaceutical sciences*, vol. 76, no. 4, pp. 306–309, 1987.

[191] M. M. Watts, "Imidazoline hydrolysis in alkaline and acidic media—a review," *Journal of the American Oil Chemists' Society*, vol. 67, no. 12, pp. 993–995, 1990.

[192] V. Lisitskii, Z. Akhmetchenko, I. Alekhina, and Y. I. Murinov, "Hydrolysis of 2-substituted and 1, 2-disubstituted imidazolines," *Russian Journal of Applied Chemistry*, vol. 80, no. 5, pp. 761–766, 2007.

[193] K. Bērziņš, I. Grante, I. Nakurte, and A. Actiņš, "The influence of ph on the stability of antazoline: kinetic analysis," *RSC Advances*, vol. 5, no. 83, pp. 68179–68186, 2015.

[194] S. R. Byrn, R. R. Pfeiffer, and J. G. Stowell, *Solid-state chemistry of drugs*. Ssci Inc, 1999.

[195] S. Bondareva, V. Lisitskii, N. Yakovtseva, and Y. I. Murinov, "Hydrolysis of 1, 2-disubstituted imidazolines in aqueous media," *Russian Chemical Bulletin*, vol. 53, no. 4, pp. 803–807, 2004.

[196] S. Limatibul and J. Watson, "Mechanism of acid hydrolysis of imidazolines," *The Journal of Organic Chemistry*, vol. 36, no. 24, pp. 3803–3805, 1971.

[197] R. Kluger and C.-H. Lam, "General base catalysis in acidic solutions. acceleration of intramolecular phosphonate-assisted amide hydrolysis," *Canadian Journal of Chemistry*, vol. 55, no. 4, pp. 640–645, 1977.

[198] D. DRAKE *et al.*, "Diffusion-controlled proton transfer and heavy-atom reorganization in the general acid specific base catalyzed hydrolysis of amides," *Journal of the American Chemical Society*, 1973.

[199] I. C. for Harmonization, "Q1a(r2) stability testing of new drug substances and products," *Q1A(R2)*, 2003.

[200] K. Naveršnik *et al.*, "Humidity-corrected arrhenius equation: The reference condition approach," *International Journal of Pharmaceutics*, vol. 500, no. 1-2, pp. 360–365, 2016.

[201] K. A. Connors, *Chemical kinetics: the study of reaction rates in solution*. Wiley-VCH Verlag GmbH, 1990.

[202] A. Lafontaine, M. Sanselme, Y. Cartigny, P. Cardinael, and G. Coquerel, "Characterization of the transition between the monohydrate and the anhydrous citric acid," *Journal of thermal analysis and calorimetry*, vol. 112, no. 1, pp. 307–315, 2013.

[203] V. Meltzer and E. Pincu, "Thermodynamic study of binary mixture of citric acid and tartaric acid," *Central European Journal of Chemistry*, vol. 10, no. 5, pp. 1584–1589, 2012.

[204] A. D. Barbooti MM, "Thermal decomposition of citric acid," *Thermochimica Acta*, vol. 98, no. 1, pp. 119–126, 1986.

[205] P. Saganowska and M. Wesolowski, "Dsc as a screening tool for rapid co-crystal detection in binary mixtures of benzodiazepines with co-formers," *Journal of Thermal Analysis and Calorimetry*, vol. 133, no. 1, pp. 785–795, 2018.

[206] A. Burger, J.-O. Henck, and M. N. Dünser, "On the polymorphism of dicarboxylic acids: I pimelic acid," *Microchimica Acta*, vol. 122, no. 3-4, pp. 247–257, 1996.

[207] F. Fischer, G. Scholz, L. Batzdorf, M. Wilke, and F. Emmerling, "Synthesis, structure determination, and formation of a theobromine: oxalic acid 2: 1 cocrystal," *CrystEngComm*, vol. 17, no. 4, pp. 824–829, 2015.

[208] A. Gaivoronskii and V. Granzhan, "Solubility of adipic acid in organic solvents and water," *Russian journal of applied chemistry*, vol. 78, no. 3, pp. 404–408, 2005.

[209] P. J. Linstrom and W. G. Mallard, "The nist chemistry webbook: A chemical data resource on the internet," *Journal of Chemical & Engineering Data*, vol. 46, no. 5, pp. 1059–1063, 2001.

[210] M. L. N. Oliveira, R. A. Malagoni, and M. R. Franco Jr, "Solubility of citric acid in water, ethanol, n-propanol and in mixtures of ethanol+ water," *Fluid Phase Equilibria*, vol. 352, pp. 110–113, 2013.

[211] L. Dang, W. Du, S. Black, and H. Wei, "Solubility of fumaric acid in propan-2-ol, ethanol, acetone, propan-1-ol, and water," *Journal of Chemical & Engineering Data*, vol. 54, no. 11, pp. 3112–3113, 2009.

[212] R. Pawar and S. Nahire, "Measurement, correlation and dft study for solubility of glutaric acid in water+ ethanol binary solvents at t=(293.15 to 313.15) k," *Asian Journal of Research in Chemistry*, vol. 13, no. 3, pp. 169–174, 2020.

[213] V. e. a. Kogan, *Handbook on Solubility, Volume 1 Binary Systems*. Academy of the Sciences of the USSR, 1962.

[214] A. Apelblat and E. Manzurola, "Solubility of oxalic, malonic, succinic, adipic, maleic, malic, citric, and tartaric acids in water from 278.15 to 338.15 k," *The Journal of Chemical Thermodynamics*, vol. 19, no. 3, pp. 317–320, 1987.

[215] Y. Yuan, Y. Leng, H. Shao, C. Huang, and K. Shan, "Solubility of dl-malic acid in water, ethanol and in mixtures of ethanol+ water," *Fluid Phase Equilibria*, vol. 377, pp. 27–32, 2014.

[216] H. G. Brittain, *Analytical profiles of drug substances and excipients*. Academic Press, 1994.

[217] S. Gumtya, S. C. Lahiri, and S. Aditya, "Studies on the solubility and dissociation constants of oxalic acid in aquo+ ethanolic mixtures and determination of single-ion gibbs energy of transfer from aqueous to aquo+ ethanolic mixtures," *Zeitschrift für Physikalische Chemie*, vol. 216, no. 8, p. 971, 2002.

[218] N. K. Pandey, H. R. Sehal, V. Garg, T. Gaur, B. Kumar, S. K. Singh, M. Gulati, K. Gowthamarajan, P. Bawa, S. Y. Rajesh, *et al.*, "Stable co-crystals of glipizide with enhanced dissolution profiles: Preparation and characterization," *AAPS PharmSciTech*, vol. 18, no. 7, pp. 2454–2465, 2017.

[219] H. Li, J. Zhu, G. Hu, P. Jiang, L. Zhao, and Y. Zhang, "Measurement and correlation of solubility of pimelic acid in ether, tetrahydrofuran, ethanol, and methanol," *Journal of Chemical & Engineering Data*, vol. 55, no. 3, pp. 1443–1445, 2010.

[220] W. Steele, R. Chirico, A. Cowell, S. Knipmeyer, and A. Nguyen, "Thermodynamic properties and ideal-gas enthalpies of formation for 1, 4-diisopropylbenzene, 1, 2, 4, 5-tetraisopropylbenzene, cyclohexanone oxime, dimethyl malonate, glutaric acid, and pimelic acid," *Journal of Chemical & Engineering Data*, vol. 47, no. 4, pp. 725–739, 2002.

[221] K. Mahali, P. S. Guin, S. Roy, and B. K. Dolui, "Solubility and solute–solvent interaction phenomenon of succinic acid in aqueous ethanol mixtures," *Journal of Molecular Liquids*, vol. 229, pp. 172–177, 2017.

[222] W. Yang, K. Wang, Y. Hu, F. Shen, and J. Feng, "Solubility of l-tartaric acid in ethanol, propanol, isopropanol, n-butanol, acetone and acetonitrile," *Journal of Solution Chemistry*, vol. 42, no. 3, pp. 485–493, 2013.

[223] S. Kim, J. Chen, T. Cheng, A. Gindulyte, J. He, S. He, Q. Li, B. A. Shoemaker, P. A. Thiessen, B. Yu, *et al.*, "Pubchem 2019 update: improved access

to chemical data," *Nucleic acids research*, vol. 47, no. D1, pp. D1102–D1109, 2019.

[224] Q. Yang, F. Yuan, L. Xu, Q. Yan, Y. Yang, D. Wu, F. Guo, and G. Yang, "An update of moisture barrier coating for drug delivery," *Pharmaceutics*, vol. 11, no. 9, p. 436, 2019.

VITA

Matthew Defrese earned his Bachelor of Science in Chemical Engineering from the California State Polytechnic University of Pomona with some additional graduate work completed within the Chemical Engineering department at the University of California, Irvine. He then spent 4+ years working in the nutritional and pharmaceutical industries as a development engineer/scientist prior to returning to academia to earn his Doctor of Philosophy in Pharmaceutical Sciences within the Marsac lab at the College of Pharmacy, University of Kentucky (UKY).

During his tenure as a graduate student, Matt was elected to serve as the Co-Chair of the Gordon Research Seminar (GRS) Preclinical Form and Formulation Group for 2020-2021 as well as the UKY Chapter President of the International Society for Pharmaceutical Engineering (ISPE). He was awarded the Pharmaceutical Research and Manufacturers of America (PhRMA) Foundation Predoctoral Fellowship Award for Pharmaceutics for two years to support the research captured in this dissertation. He was also awarded the Glavinos Travel Award in the spring of 2020 in recognition of his efforts.

After completion of his graduate studies, Matt joined Catalent Pharma Solutions as a Development Scientist to support the design and development of novel and generic drug products and processes. Publications and presentations arising from Matt's graduate research and prior work experience follow.

Publications:

1. Matthew Defrese, Victoria Defrese, Fahd Eisa, Randy Seburg, Nathanael Stocke, Patrick Marsac; "Formulation and Wet Granulation Process Optimization of an

Extended-Release Tablet for the Delivery a Highly Potent API," *In preparation*

2. Matthew Defrese, Heather Campbell, Victoria Defrese, Fahd Eisa, Randy Seburg, Nathanael Stocke, Patrick Marsac; "Understanding and Mitigation of the Hydrolysis of a Highly Potent API Prepared by Wet Granulation," *In preparation*

3. Matthew Defrese, Matthew Farmer, Yuhan Long, Lucas R. Timmerman, Younsoo Bae, Patrick Marsac; "Approaches to understand the solution state organization of spray dried dispersion feed solutions and its translation to the solid state,"*Molecular Pharmaceutics*, Sept. 2020, 17, 12:(4548–4563)

4. Jonas Alin, Nico Setiawan, Matthew Defrese, James DiNunzio, Hang Lau, Lisa Lupton, Hanmi Xi, Yongchao Su, Haichen Nie, Nathan Hesse, Lynne S. Taylor, Patrick Jules Marsac; "A novel approach for measuring room temperature enthalpy of mixing and associated solubility estimation of a drug in a polymer matrix", *Polymer*, Jan 2018, 135:(50-60)

5. Srinivas R. Kamireddy, Christopher Schaefer, Matt Defrese, John Degenstein, Yun Ji; "Pretreatment and enzymatic hydrolysis of sunflower hulls for fermentable sugar production," *International Journal of Agricultural and Biological Engineering*, March 2012, 5(1):62-70

Presentations:

1. Gordon Research Seminar/Conference (GRS/GRC) Preclinical Form and Formulation Group, Waterville Valley, NH, June 2019; "Characterization of Solution State Properties of Model Liquid Feedstocks for Use in Spray Dried Dispersions," Poster

2. Center for Pharmaceutical Development (CPD), Lexington, KY, May 2018; Matt Defrese, Benjamin Burdette, Patrick Marsac; "What is the Role of Solution State Properties in Spray Dried Dispersions?," Poster

3. American Association of Pharmaceutical Scientists (AAPS) Annual Meeting and Exposition, San Diego, CA, November 2017; "Crystalline Solubility and Amorphous Phase Stability of Drugs in Poly(vinylpyrrolidone) (PVP) Dispersions Containing Water – A Solution Calorimetry Based Approach," Poster

4. Center for Pharmaceutical Development (CPD), Lexington, KY, November 2016; Jonas Alin, Matt Defrese, Nico Setiawan, Patrick Marsac; "Towards a Complete Thermodynamic Description of Amorphous Systems," Poster